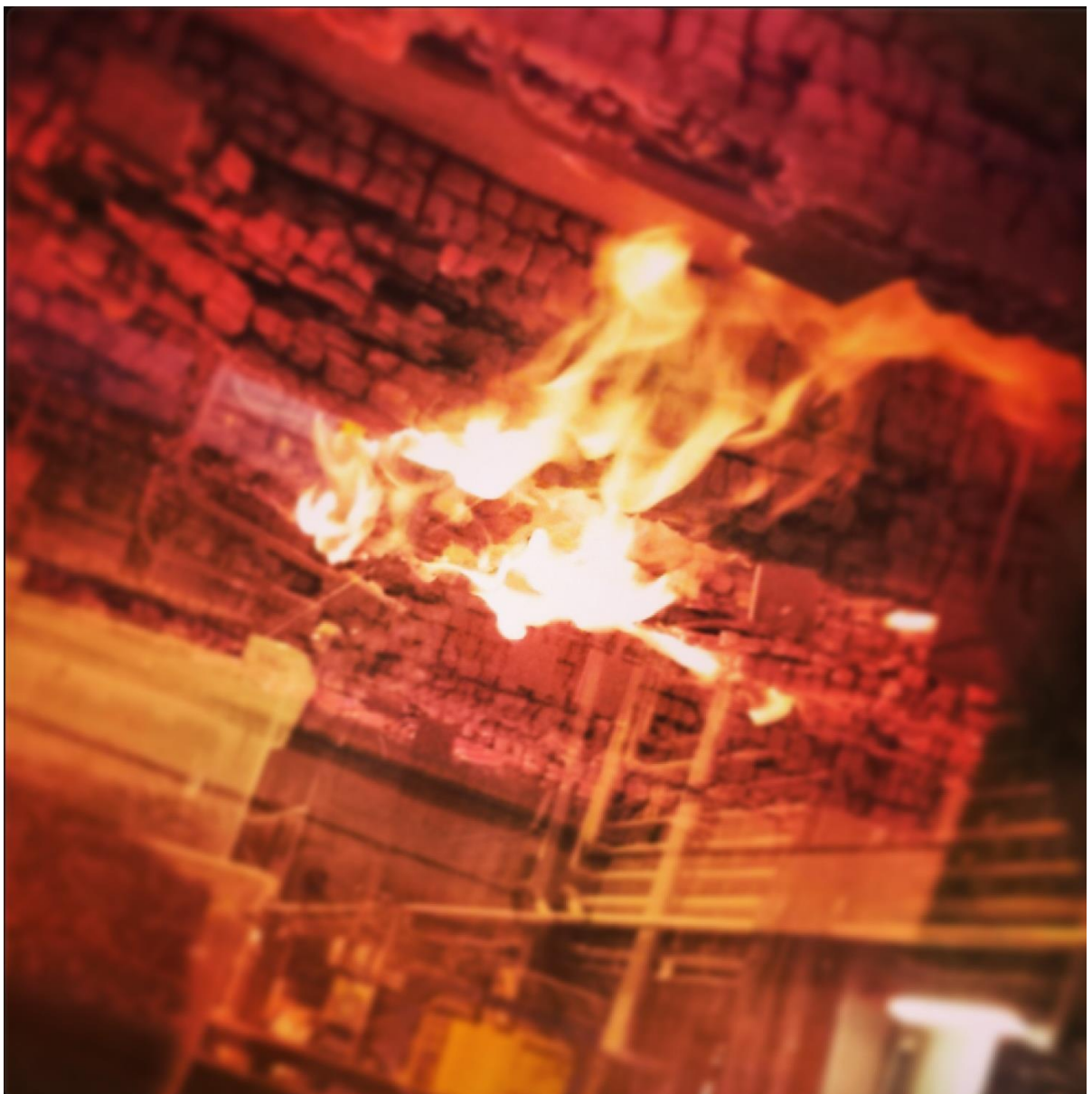


The influence of parametric fire scenarios on structural timber performance and reliability

David Lange, Lars Boström, Joachim Schmid and Joakim Albrektsson



The influence of parametric fire scenarios on structural timber performance and reliability

David Lange, Lars Boström, Joachim Schmid and Joakim Albrektsson

Abstract

This report summarises the results of a project which was conceived to assess the impact of different fires on the level of safety in a timber structure. The means of achieving this was to measure the response of a number of timber elements to a range of fires in a furnace and to identify and quantify the resulting factors which influence the load bearing capacity of timber construction when exposed to the temperature time curves applied during these experiments. In total 32 timber specimens were tested under either standard fire exposure or parametric fire exposure, comprising either a short hot or a long cool parametric fire. 10 specimens were also subjected to destructive reference testing and all specimens were subject to non-destructive reference testing at ambient temperatures in order to ensure uniformity between the different groups used in the different tests.

The reduced cross section method, commonly used for design of timber elements exposed to the standard fire is extended to apply to the parametric fires used in the tests. It is shown that the zero-strength layer is dependent on the temperature time curve to which the timber is exposed in the furnace and that the 7 mm zero strength layer prescribed in EN 1995-1-2 may be un-conservative for members in bending. For the cases studied, the zero strength layer thickness in bending is shown to be around about 15 mm under standard fire exposure and 16 mm under long cool parametric fire exposure but only 8mm under exposure to a short hot parametric fire.

The results of the testing are used to develop analytical and probabilistic models of timber in fire to study the effect that different fires have on the reliability of timber structures. It is seen that timber elements loaded in bending which are exposed to fires which are more aggressive than the standard fire have a reliability which evolves over time and is not dissimilar to the reliability of similar members tested under standard fire conditions. In the tests performed, the reliability of timber exposed to the standard fire reduced to zero after between 23 and 27 minutes, and the reliability of timber exposed to a short hot parametric fire curve reduced to zero at around about 26 minutes. Conversely, timber which is loaded in bending and which is exposed to fire conditions which are less aggressive than standard fire conditions has a significantly longer period (over 50 minutes) under fire exposure before the reliability reduces to zero.

Key words: structural timber, fire, parametric fire, reduced cross section method, reliability

SP Sveriges Tekniska Forskningsinstitut
SP Technical Research Institute of Sweden

SP Report 2014:35
ISBN 978-91-87461-78-1
ISSN 0284-5172
Borås 2014

Contents

1	Introduction	6
1.1	Background	6
1.2	Design of timber structures in fire	7
1.2.1	Charring rates of timber	7
1.2.2	Reduced cross section method	9
1.2.3	Reduced properties method	11
2	Test Specimens	12
2.1	Material characterisation procedure	12
2.2	Dynamic modulus of elasticity measurements	12
2.3	Static modulus of elasticity and bending strength	14
2.4	Density and moisture content measurement	15
3	Fire Tests	17
3.1	Test set-up	17
3.2	Measurement of furnace temperature and pressure	19
3.3	Temperature measurements in the test specimens	21
3.4	Load and deflection measurements	23
3.5	Test procedure	24
4	Fire curves	26
4.1	Overview	26
4.2	Fire curves	26
5	Results from fire tests	27
5.1	Fingerjoint positioning	27
5.2	Fire test 1 – Standard fire	27
5.2.1	Furnace conditions	27
5.2.2	Specimen temperatures	28
5.2.3	Charring rate	31
5.3	Fire test 2 – Standard fire	33
5.3.1	Furnace conditions	33
5.3.2	Specimen temperatures	33
5.3.3	Charring rate	36
5.4	Fire test 3 – Short hot fire	37
5.4.1	Furnace conditions	37
5.4.2	Specimen temperatures	38
5.4.3	Charring rate	41
5.5	Fire test 4 – Long cool fire	42
5.5.1	Furnace conditions	42
5.5.2	Specimen temperatures	42
5.5.3	Charring rate	46
5.6	Summary of average charring rates	46
5.7	Mechanical failure of specimens during the fire tests	48
5.7.1	Failure of specimens in fire test 1	48
5.7.2	Failure of specimens in fire test 2, 3 and 4	48
6	Sectional analysis	51
6.1	Methodology	51
6.2	Statistical analysis	52
6.3	Standard fire tests	54
6.3.1	1-dimensional charring rate	54

6.3.2	Second moment of area	55
6.3.3	Notional charring rate	55
6.4	Short hot fire	56
6.4.1	1-dimensional charring rate	56
6.4.2	Second moment of area	57
6.4.3	Notional charring rate	57
6.5	Long cool fire	58
6.5.1	1-dimensional charring rate	58
6.5.2	Second moment of area	59
6.5.3	Notional charring rate	59
6.6	Comparison of 1-d char rates with char rates based on temperature measurements	60
6.7	Discussion	62
7	Application of measured and estimated charring rates to loading calculations	63
7.1	Notional charring rates	63
7.2	1-dimensional charring rates	68
8	Reliability calculations	71
8.1	Overview of reliability	71
8.2	Margin of safety and reliability index	71
8.3	Reliability of timber structures in fire	72
9	Discussion and conclusions	75
11	References	77
12	Appendix 1 - Material reference testing	79
13	Appendix 2 – Finger joint positioning	83
14	Appendix 3 – cross-sectional analysis	87
15	Appendix 4 – Q-Q plots	112

1 Introduction

1.1 Background

Standard Fire resistance testing has influenced fire protection codes for over a hundred years. The standard fire gives a much simplified estimation of temperatures in a compartment fire [1], based only on a heating phase of effectively unlimited duration. It is only one possible temperature time curve of exposure of a structural element which can represent the variety of fires that can develop in a compartment, however its formulation ignores boundary conditions in the compartment and the available ventilation. It is acknowledged that response to a standard fire test is not the best representation of the response of structures to real fires [2- 4] not only for the reasons listed above, but also because the restraint conditions of elements tested in a standard furnace do not reflect the restraint conditions of elements which are part of a structure. Despite this the response of load bearing structures when exposed to fire is in the vast majority of cases determined with reference to the Standard Fire test.

For many applications however, engineers are turning to the concept of performance based design to demonstrate safety of structures in fire. This requires the comparison of the resistance of the structure when exposed to a fire with the load which is placed upon it. The concept permits the use of non-standard fire curves and even thermal exposures based on CFD or zone models to be used in the design of structures in fire. This may offer a better representation of the thermal exposure than the standard fire alone.

For steel, material properties at high temperatures are well enough defined such that the use of these alternative methods of design are permitted in the structural Eurocodes. Concrete, while having material properties which are dependent upon the heating rate as well as the mechanical conditions (restraint, load and load history) of the concrete in application, is also frequently used in applications where fire safety is based on the predicted response of the structure to a 'real fire'. Although it should be noted that the Eurocodes restrict the use of such techniques for concrete construction to heating rates which are similar to the standard fire [5].

Timber, on the other hand, is not commonly used in applications where performance based design methodologies are used for the fire design. Eurocode 5 provides charring rates which can be used for the design of timber structures in fire based on the parametric fire. However both the mechanical and the thermal properties for calculation are based on the response to the Standard Fire and material properties which are given are effective or empirically derived rather than a complete material model. Calculation of timber response to anything other than the standard fire would therefore rely on the use of models for which the material properties and design parameters are as yet unknown. This significantly limits the potential for timber to be used in performance based design applications.

This report details the results of a series of experiments, and the subsequent analysis of those results, which were conceived in order to evaluate the impact of non-standard fire scenarios on the response of timber elements. The approach taken to the testing focussed on providing a significant amount of data which could be used to develop probabilistic models of the timber elements under different fire exposures. These models are based on the calculation methods which are presented in Eurocode 5 for timber structures exposed to fire and their application in this case is an extension of the methods to non-standard fire exposures.

The report gives an overview of the timber design methods which are given in Eurocode 5 (chapter 1), before describing the approach which was taken towards the testing as well as the results of reference testing of the timber specimens which were used in the tests (chapters 2, 3 and 4).

The results of the tests are split into two sections. The first section (chapter 5) is a report of the response of the elements during the fire tests, and comprises a study of the measured temperatures and the estimation of 1-dimensional charring rates based on these temperatures. Times to failure of the specimens in the tests are also reported in this section. The second section of results (chapter 6) reports on an analysis of the residual sections which remained after the test were performed, and a comparison of the 1-dimensional charring rate estimated from the residual cross section dimensions with that measured based on the temperature records from the test. Notional charring rates are also determined based on the residual cross sections.

Subsequently, the results of the tests are compared with predictions made with the reduced cross-section method (chapter 7). Variations in material strength and charring rate are accounted for, and the thickness of the zero-strength layer is estimated for the different temperature time curves used in the tests.

Finally, a reliability analysis of the timber elements exposed to the different temperature time curves is performed. This is based on the reduced cross section method and accounts for the variations in key parameters measured in the tests and subsequent analyses. Results are reported based on calculations using both the notional charring rates and the 1-dimensional charring rates measured during the tests (chapter 8).

1.2 Design of timber structures in fire

There is exhaustive research on the response of modern and traditional timber construction exposed to Standard Fires, and to real fires, e.g. [4, 6, 8 – 10]. For design applications, the determination of fire resistance is based upon the residual cross section of uncharred timber. This is calculated based upon the charring rate, the time of fire exposure, and accounts for changes of material properties of the residual cross section according to the temperature, and as already stated based on the measured response to a Standard Fire [11]. The char front is typically assumed to follow the 300°C isotherm. However this is not necessarily applicable for all species or variations in the timber material.

Two methods are described in EN 1995-1-2 [11] for determining the load bearing capacity of timber elements in fire, the reduced cross section method and the reduced properties method. Both methods are described in this section. In the Eurocode there is some provision made for evaluating the impact of different heating rates as a result of parametric fire exposure by means of changing the charring rate. However there is no corresponding consideration of changes in the material properties for different heating rates, information which is required for the application of both methods.

1.2.1 Charring rates of timber

In the reduced cross section method, the cross section dimensions are reduced by a thickness corresponding to the charred depth of the timber at a given time. Since the bending strength of a timber section may be given by the elastic section modulus, the strength of the section following removal of the char layer may in principle be determined by considering the dimensions of the residual cross section and the temperature dependent material properties of the uncharred timber. Two charring rates are provided in

EN 1995-1-2, the 1-dimensional charring rate and the notional charring rate, the difference being that the notional charring rate is slightly larger in order to reduce the residual cross section further, so that corner rounding does not need to be taken into account, whereas corner rounding must be taken into account when the 1-dimensional charring rate is used, Figure 1.1.

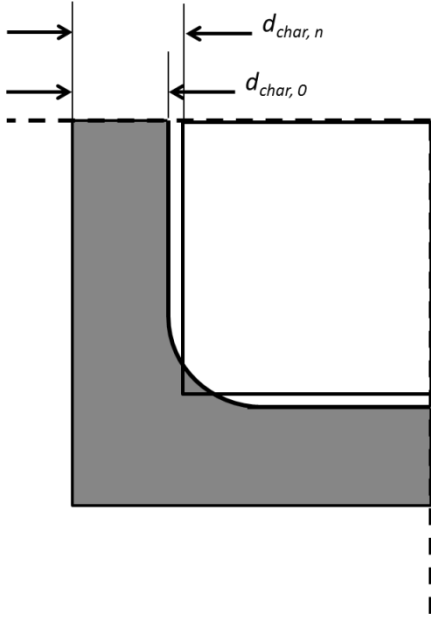


Figure 1.1, charring depth $d_{char,0}$ for one-dimensional charring and notional charring depth $d_{char,n}$ [11]

When using the notional charring rate the shape of the cross section is vastly simplified so that the determination of the strength of the section may be based on a rectangular section. The section modulus of a rectangular section is described in equation 1.1, and the reduced dimensions of the section in terms of the notional charring rate are given in equations 1.2 and 1.3. The section modulus relation to the ultimate moment is given in equation 1.4.

$$W = \frac{I}{y} = \frac{b_{fi}d_{fi}^2}{6} \quad (1.1)$$

$$b_{fi} = b - 2\beta_n t_{fi} \quad (1.2)$$

$$d_{fi} = d - \beta_n t_{fi} \quad (1.3)$$

$$M_u = \sigma_y W \quad (1.4)$$

where W is the elastic section modulus, I is the second moment of area, y is the depth to the centroid of the cross section, b is the original breadth of the section, d is the original depth of the section, b_{fi} is the reduced breadth of the section, d_{fi} is the reduced depth of the section, β_n is the notional charring rate, t_{fi} is the duration of the fire exposure, M_u is the ultimate moment of the section and σ_y is the yield stress in bending. For exposure to the standard fire the notional charring rate given in EN 1995-1-2 [11] for glued laminated timber with a characteristic density of $\geq 290 \text{ kg/m}^3$ is $\beta_n=0.7\text{mm/min}$.

The notional charring rate may be determined from test results by comparing the elastic section modulus of a residual cross section with that of an equivalent rectangular section

and assuming a constant charring depth around the perimeter. The notional charring rate is then given by the constant charring depth divided by the time of fire exposure.

For exposure to parametric fires, EN1995-1-2 [11] proposes a modified char rate, β_{par} , for unprotected soft wood only, equation 1.5.

$$\beta_{par} = 1.5\beta_n \frac{0.2\sqrt{\Gamma}-0.04}{0.16\sqrt{\Gamma}+0.08} \quad (1.5)$$

$$\text{where } \Gamma = \frac{(O/b)^2}{(0.04/1160)^2}$$

O is the opening factor and b is the square root of the thermal inertia of the wall linings. This gives a higher notional charring rate for timber in an enclosure where the conditions lead to a more aggressive increase in temperature with time compared with the standard fire, and a lower notional charring rate where the increase in temperature in time is less aggressive in comparison with the standard fire. Since the parametric fire includes a heating and a cooling phase, this is taken into account when determining the charring rate. There is an increase in char rate followed by a steady state charring rate when a suitably thick char layer has formed during the heating phase of the fire; and a reducing char rate as the temperature in the enclosure cools. According to a corrigendum to EN 1995-1-2 [13] the charred depth is then taken as:

$$d_{char} = \begin{cases} \beta_{par} t & t \leq t_0 \\ \beta_{par} \left(1.5t - \frac{t^2}{4t_0} - \frac{t_0}{4} \right) & t_0 \leq t \leq 3t_0 \\ 2\beta_{par} t_0 & 3t_0 < t \leq 5t_0 \end{cases} \quad (1.6)$$

where $t_0 = 0.009 \frac{q_{t,d}}{O}$, where $q_{t,d}$ is the design fire load density and O is the opening factor. The intended result is an effective charring rate which is constant for a period t_0 , before reducing linearly to 0 for a period corresponding to $2t_0$, figure 2.

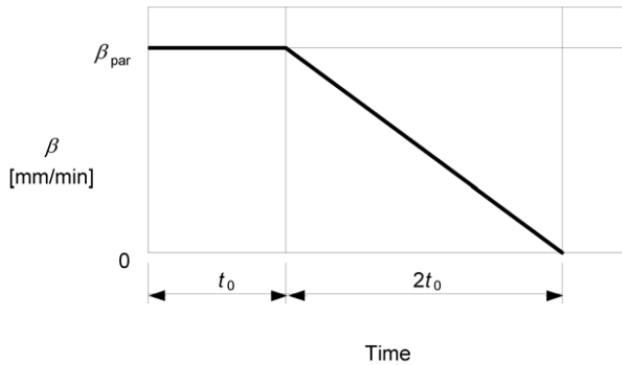


Figure 1.2, relationship between charring rate and time [11]

1.2.2 Reduced cross section method

In addition to the reduced dimensions of the section the reduced cross section method requires the change in material properties ahead of the char front to be accounted for. Timber material properties differ in tension and compression, and as with other materials, stiffness and strength reduce with increased temperature.

To achieve this, the section has a zero-strength layer, z_0 (mm), removed from its dimensions prior to evaluation of the residual capacity, defined by equation 1.7. This

zero-strength layer is intended to account for an area of timber which has lost some of its strength as a result of preheating but has not yet charred.

$$z_0 = k_0 d_0 \quad (1.7)$$

where k_0 is a factor as described in equation 1.8, and d_0 is the final width of the zero-strength layer and is equal to 7mm under standard fire exposure according to EN 1995-1-2 [11].

$$k_0 = \begin{cases} t/20 & t < 20 \text{ minutes} \\ 1 & t \geq 20 \text{ minutes} \end{cases} \quad (1.8)$$

where t is the time in minutes.

The zero strength layer was first described in reports by Bender and Schaffer for members in bending [14] [15]. The concept relies on the assumption that all of the loss in strength in timber may be attributed to a finite and fixed thickness of wood behind the char front of 0.3 inches. This depth was determined based on the conclusion that the depth of heat penetration under standard fire exposure is steady once the char layer has formed and is limited to 40 mm behind the char front. The strength and stiffness losses in this 40 mm layer were then averaged and the full loss of strength in this 40 mm region was attributed to a heated layer of a fixed thickness. The 0.3 inch thickness of the layer has been approximated to 7 mm in EN 1995-1-2 [11]. Bender notes [14] that the method compares favourably with work from the literature which employed a simplified formulation of an analytical solution for timber in fire. An overview of the origins and background to the zero-strength layer is given by Schmid et al [16]., where it is also shown that a zero-strength layer of 7 mm is often non conservative. By reviewing the background to the zero-strength layer and performing calculations they demonstrate that the zero-strength layer is strongly dependent upon the geometry and the loading conditions.

Schmid et al. [17] also carried out a further analysis of 153 fire tests including 117 members in bending. By reanalysing the reported failure times of the members in the tests they estimated the zero-strength layer for each of the members. They concluded that the zero-strength layer for members in bending varies between -6mm (implying some load bearing capacity of the char layer) and 39mm.

Klippel et al. [18] reports on a series of numerical simulations where the zero strength layer in tension and compression as well as in bending is investigated. They find that the depth of the zero-strength layer in tension and compression varies between 6 and 16 mm depending upon the cross-sectional dimensions as well as the loading state. For bending he finds that the zero strength layer varies between 7 and 12 mm depending upon the cross-sectional dimensions as well as the time of fire exposure. In conclusion Klippel finds z_0 to be transient as opposed to constant over the course of fire exposure, since it is a function of heat penetration. They conclude that a constant zero-strength layer may result in an overestimation of the fire resistance time.

There is no description in the Eurocode of any changes which may be made to the reduced cross section method in order to account for the effects of different heating rates. However, since the thickness of material degraded by temperature is dependent upon the heat penetration through a section it seems logical that the heating rate will have an effect upon its depth.

1.2.3 Reduced properties method

Also described in EN 1995-1-2 [11] is the reduced properties method. In this method, no zero-strength layer is assigned to the residual cross section. Rather, the mechanical properties of the cross-section are reduced by a factor $k_{mod,fi}$. This factor is defined as 1 at $t=0$ and by equation 1.9 at time $t \geq 20$ minutes for the strength of members in bending, and by equation 1.10 for the modulus of elasticity of members in bending.

$$k_{mod,fi} = 1 - \frac{1}{200} \frac{p}{A_r} \quad (1.9)$$

$$k_{mod,fi} = 1 - \frac{1}{330} \frac{p}{A_r} \quad (1.10)$$

where p is the perimeter of the residual section and A_r is the cross sectional area of the residual section, in m and m² respectively. Between time $t=0$ and $t \geq 20$ minutes the factor $k_{mod,fi}$ should be determined from linear interpolation.

In the reduced properties method the char depth, and therefore the residual cross section, is determined in the same way as for the reduced cross section method. The reduced properties method is less common than the reduced section method and this report therefore does not further discuss the reduced properties method.

2 Test Specimens

2.1 Material characterisation procedure

Due to the large natural variability of timber material properties all of the timber used in the tests was subject to material characterisation at ambient temperature. A total of 45 glulam beams with the dimensions 140 x 270 x 5400 mm³ were used in the tests and were initially subject to a non-destructive material characterization procedure. Following characterisation the beams were grouped into 5 approximately equal groups in terms of dynamic modulus of elasticity – 4 groups of 8 which were reserved for fire testing and one group of 10 which was reserved for destructive testing at ambient temperatures in order to estimate the strength of the timber batch. 3 beams were retained as spares.

Details of the material characterisation techniques and the groupings are given in this chapter.

2.2 Dynamic modulus of elasticity measurements

All beams were subject to measurement of the modulus of elasticity using a (dynapulse) hammer and (dytran) accelerometer to measure the frequency of vibrations upon impact. In order to carry out the measurement, each beam was suspended above the ground at both ends from an overhead crane. The impact test was carried out at three locations, on the top, middle, and bottom lamella of every beam, and the background frequencies were filtered from the frequency response of each beam. The modulus of elasticity, E , may then be estimated using equation 2.1.

$$E = 4f^2L^2\rho \quad (2.1)$$

Where f is the measured frequency, L is the length and ρ is the density of the beam. The beams were individually numbered in the order of measurement, and stacked, as shown in figure 2.1.



Figure 2.1, beams for testing, shown individually numbered and stacked

The beams were then placed into 5 groups based on the dynamic modulus of elasticity, one group of 10 and 4 of 8, with three additional specimens retained for additional testing if required. A summary of the results of the frequency measurement and the grouping of the beams is shown in Table 2.1, as well as the coefficient of variation (CoV), defined as the ratio of the standard deviation of the normal distribution to its mean. All of the results of the frequency measurement and the modulus of elasticity calculated are shown in Appendix 1.

Table 2.1, summary of grouping of the beams

Group	Beam numbers	Dynamic modulus of elasticity		
		Mean value	Standard deviation within the groups	Coefficient of variation within the groups
		(MPa)	(MPa)	(%)
1	2, 16, 17, 20, 22, 28, 29, 31, 34, 41	13 235	394	3.0
2	1, 6, 8, 9, 11, 30, 42, 43	13 223	401	3.0
3	3, 5, 7, 10, 24, 25, 27, 38	13 229	349	2.6
4	4, 15, 18, 19, 23, 36, 37, 40	13 229	386	2.9
5	12, 13, 26, 32, 33, 35, 39, 44	13 229	356	2.7
spare	14, 21, 45	13 900	207	1.5
Group 1 - 5		13 229		

The distribution of dynamic modulus of elasticity (MoE) between the groups is shown in Figure 2.2. The variation between the groups was very small, with a variation in the coefficient of variation between the groups of 0.032% and a standard deviation between the groups of 4.2 MPa.

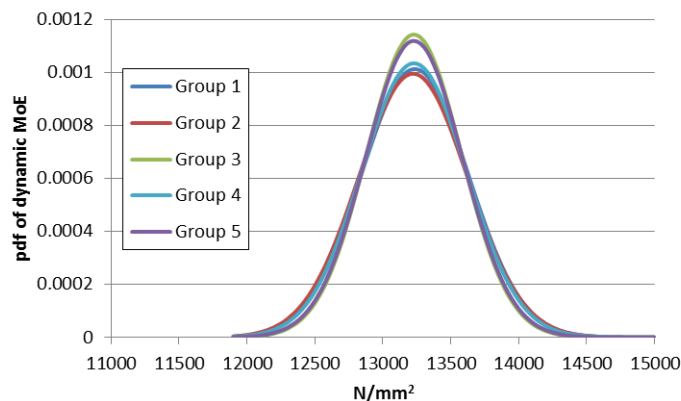


Figure 2.2, distribution of dynamic modulus of elasticity between the groups

2.3 Static modulus of elasticity and bending strength

In order to determine the static modulus of elasticity and the bending strength measured under load, all beams in group 1 were loaded to failure under 4-point bending in accordance with EN 408 as shown in Figure 2.3. The distance between the supports was 4860 mm, and the distance between the points of application of the load was equidistant, at 1620 mm. In all cases, the failure type was in tension of the lower lamella away from the finger joints of the timber, see figure 2.4.



Figure 2.3, measurement of bending strength and modulus of elasticity in 4-point bending



Figure 2.4, failure of the lower lamella

The measured bending strength and modulus of elasticity of each beam are presented in Table 2.2. The mean bending strength within the group was 37.8 MPa with a standard deviation of 6.2 MPa. The mean modulus of elasticity measured under the applied load (static modulus of elasticity) was determined to be 13200 MPa with a standard deviation of 400 MPa. This agrees very well with the mean modulus of elasticity measured using the dynamic testing and the standard deviation of those measurements.

Because it was not possible to measure the bending strength of all of the beams in the groups which were to be subject to fire testing, it was assumed that the distribution of bending strength in group 1 was representative of the bending strength distributions of the other groups.

Table 2.2, measured bending strength and modulus of elasticity.

Beam (nr)	Width (mm)	Height (mm)	Length (mm)	Maximum load (kN)	Bending strength (MPa)	Static modulus of elasticity (MPa)
2	139.2	268.8	5400	91.7	44.3	13,531
20	138.9	269.6	5400	78.8	37.9	11,975
16	139.1	269.0	5400	60.6	29.3	12,230
22	139.2	269.0	5400	90.5	43.7	11,510
17	139.2	269.1	5400	65.9	31.8	13,505
28	138.9	268.8	5400	92.7	44.9	13,442
31	139.1	269.0	5400	65.4	31.6	11,894
29	138.7	268.7	5400	85.5	41.5	12,848
34	138.8	268.2	5400	63.8	31.1	13,041
41	139.6	268.9	5400	86.5	41.6	14,005

2.4 Density and moisture content measurement

Density and moisture content (as a percentage of weight) was measured on parts of the beams used in the fire tests on the day of the test or the day following the test. Density and moisture content were determined by measuring the dimensions and weight of a small sample from the offcut of each beam once it was cut to the required length for the fire test (ca. 50mm x 270mm x 140mm) prior to drying at 105°C for 24 hours and then reweighing after drying. In Table 2.3 the determined density, and moisture content is presented for the beams used in the fire tests, as well as their mean and standard deviation within the groups.

Table 2.3, density and moisture content.

Specimen	Density (kg/m ³)	Moisture content (%)	Specimen	Density (kg/m ³)	Moisture content (%)
Fire test 1			Fire test 2		
Beam 1	440	11.1	Beam 3	454	11.5
Beam 6	451	12.1	Beam 5	451	11.8
Beam 8	420	11.5	Beam 7	462	11.7
Beam 9	445	11.3	Beam 10	479	11.9
Beam 11	472	11.3	Beam 24	449	11.6
Beam 30	470	11.5	Beam 25	439	12.3
Beam 42	483	11.1	Beam 27	469	11.5
Beam 43	441	11	Beam 38	472	11.7
Average	453	11.4	Average	459	11.8
Standard deviation	21	0.4	Standard deviation	13	0.3
Fire test 3			Fire test 4		
Beam 4	475	11.2	Beam 12	441	11.3
Beam 15	441	11.7	Beam 13	491	12
Beam 18	460	11.9	Beam 26	475	11.9
Beam 19	455	12.1	Beam 32	488	11.7
Beam 23	476	12.6	Beam 33	472	11.6
Beam 36	429	11.4	Beam 35	473	11.5
Beam 37	493	12.3	Beam 39	464	11.8
Beam 40	451	12	Beam 44	430	11.4
Average	460	11.9	Average	467	11.7
Standard deviation	21	0.5	Standard deviation	21	0.2

3 Fire Tests

3.1 Test set-up

In total, four fire tests were carried out. In each fire test, one group of eight beams was tested. The fire tests were made in general in accordance with EN 1363-1 and EN 1365-3, but with some deviations.

- The fire exposure used deviated from the Standard Fire test in two of the tests made.
- The standard prescribes a minimum fire exposed length of 4000 mm. In these tests the fire exposed length was shorter in order to maximize the number of beams which could be placed on the furnace. The fire exposed length of the tested beams was 3300 mm. Figures 3.1. and 3.2 show the planned test layout with the positions of the beams on the furnace

The beams were fire exposed on three sides. The top surface of the beams was covered with aerated concrete blocks with dimensions 150 x 200 x 580 mm³ and a density of 535kg/m³ except at the location of the loading points where a wood block was used to transfer the load from an hydraulic actuator to the beam. The aerated concrete blocks were insulated with rock wool on the fire exposed side. Interaction between the blocks on the single beams was reduced by inserting a 5 mm thick light weight insulation material between the blocks. Interaction between the blocks on different beams was reduced by adding a layer of hard and a layer of soft insulation material between the blocks. The beams were simply supported on rollers at each side. The rollers comprised, on one side a steel plate 140 mm x 140 mm and a 25 mm external radius steel pipe section of length 140 mm. On one end the pipe was welded to the plate and on the other the two were secured under friction only between the beam and the furnace perimeter frame.

The steel plate was used to spread the load over the underside of the beam. There was no measureable indent in the promatec board which was beneath the pipe section following any of the tests.

The rollers as well as the supporting steel beam which comprised the perimeter frame of the furnace were insulated with ceramic fibre blankets during the fire exposure. Figure 3.3 shows one of the beams from test 1 placed on the furnace, including the roller support (note the incorrect orientation of the roller support which was later corrected), aerated concrete blocks and the insulation material between the beams. The ends of the furnace were covered by massive concrete blocks, one of which can also be seen in Figure 3.3. Figure 3.3 shows all of the test specimens from test 1 placed on the furnace with the loading system in position prior to the test.

In all tests, prior to cutting of the beams to fit the furnace, the location of any finger joints was determined and the beams were cut and positioned so that no finger joints were located in the bottom two lamella between the two loading points.

During the tests, in order to prevent any transfer of rotation, as a result of torsion, between the beams, the ends of the beams were cross-braced against one another, see Figure 3.5. It was considered that this arrangement would not have any impact upon the behaviour of the individual beams as a result of flexure while allowing the timber elements to brace against one another to prevent rotation about the longitudinal axis.

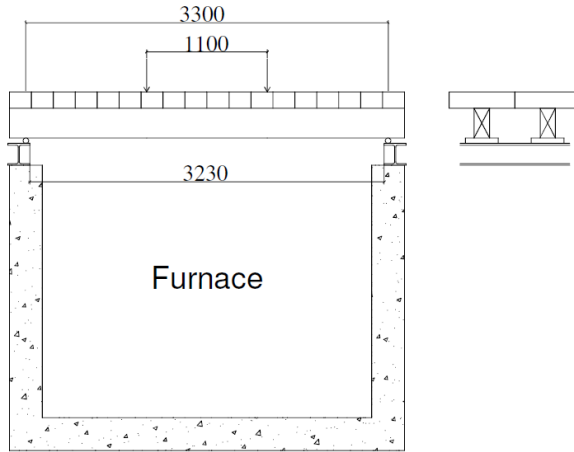


Figure 3.1, section through the furnace indicating support location and the loading positions

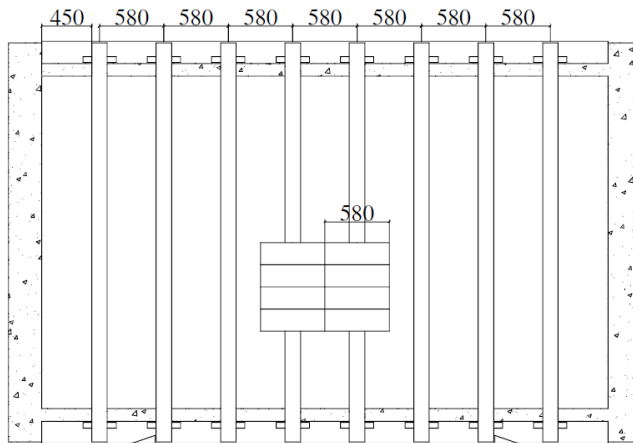


Figure 3.2, plan view of the test layout



Figure 3.3, one of the beams just after being placed in position on the furnace for fire test 1 (note the incorrect orientation of the roller support which was later corrected)



Figure 3.4, experimental set-up seen from above.



Figure 3.5, cross-bracing of the ends of the timber beams

3.2 Measurement of furnace temperature and pressure

The furnace temperature was measured by plate thermometers, arranged according to Figure 3.6 and Figure 3.7. A total of 20 plate thermometers were used in each test, evenly distributed around the test specimens. A photograph of the location of the plate thermometers is shown in Figure 3.8. Some of the plate thermometers were located between the beams facing the adjacent beam in order to assess any shadow effect resulting from having so many specimens in the furnace at one time whereas others were located below the beams facing the nearest of the short sides of the furnace and some were located below the level of the beams facing the floor of the furnace. The furnace temperature was initially controlled using the output from the plate thermometers which were facing the walls and the floor. During the fire tests some of the plate thermometers failed when the individual beams broke. As this continued over the course of the tests the plate thermometers which were facing the adjacent beams were used to control the temperature in the furnace. As can be seen from the results of test 1 however, there was little to no difference between the temperature of the plate thermometers which were below the level of the beams and those which were facing the adjacent beams.



Figure 3.8, view from inside the furnace showing the test specimens, plate thermometers and insulation of steel beam and roller supports.

3.3 Temperature measurements in the test specimens

Thermocouples were mounted within the cross section of the beams in order to determine the temperature rise during the fire exposure. These measurements can give an indication of the charring rate during the fire test. In each beam in the first three tests, 10 thermocouples were mounted, see figures 3.9 to 3.12.

Thermocouples were numbered TC1 - TC5 at the west, or 'low', end of the beam. Thermocouple number 1 was located at a depth of 260 mm from the upper surface of the beams, or 10 mm from the heated surface, and all other thermocouples were located at 10 mm intervals from the heated surface so that TC5 was located at a depth of 220 mm or 50 mm from the heated surface. At the east, or 'high', end of the beam three thermocouples, numbered TC6, TC7 and TC8, were located at depths coinciding with TC1, TC3 and TC5 at the low end of the beam. In addition, TC9 and TC10 were positioned 90 mm from the bottom surface and 50 and 30 mm respectively from the vertical surface of the beams.

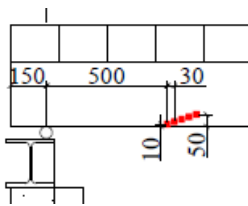


Figure 3.9, section of the west end of a beam showing the thermocouple location

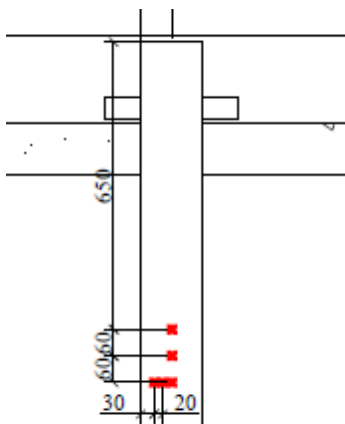


Figure 3.10, plan of the west end of a beam showing the thermocouple location

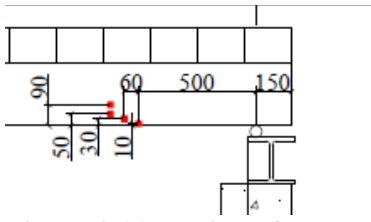


Figure 3.11, section of the east end of a beam showing the thermocouple location

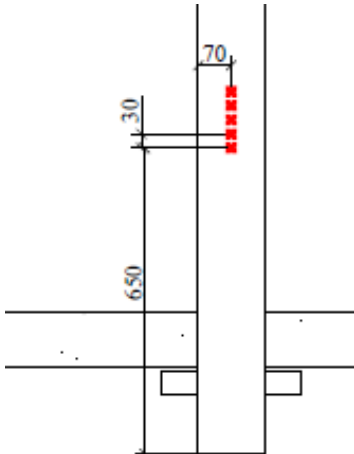


Figure 3.12, plan of the east end of a beam showing the thermocouple location

In fire test 4, two additional thermocouples (TC11 and TC12) were positioned 60 and 70 mm from the bottom surface of the beams, in line with TC6 – TC8.

The thermocouples were mounted in holes drilled from the top surface of the beam. The holes had a diameter of 3 mm. The thermocouples used were of type K with a diameter of 0.5 mm. The tip of the thermocouples was joined with a quick-tip of diameter 2.5mm. After the thermocouple had been inserted in the drilled hole, the hole was sealed with putty. Measurements were made from the thermocouples with a frequency of 0.2 Hz after the test had started.

Ideally, the thermocouple wires should be installed such that they run parallel with the isotherms of the beams. However as a result of the test configuration this would have necessitated cutting the beams to install the thermocouples meaning that the beams could not have been loaded during the fire tests. It was therefore decided to install the thermocouples in the way described - at the bottom of holes drilled vertically from the top of the beams. During set up of the test specimens the angle and depth of the holes was checked on an ad-hoc basis. Negligible deviation in the depth was found in all of the cases and deviations in the angle of no more than 3° from vertical were found although the majority of test specimens had an angular deviation of less than 2° . Figures 3.13 and 3.14 show the arrangement of the thermocouples in one of the beams from test 1 prior to filling of the holes with putty.

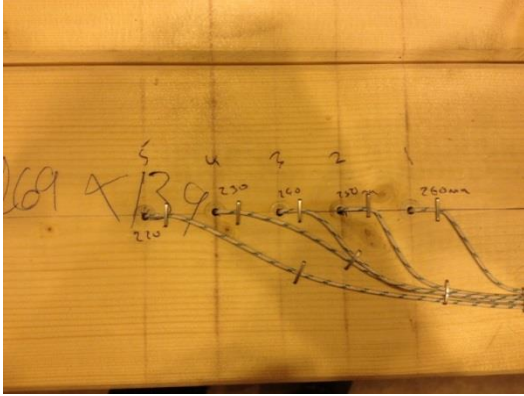


Figure 3.13, thermocouples 1-5

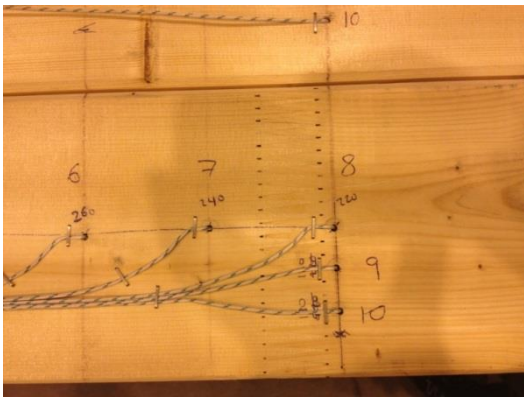


Figure 3.14, thermocouples 6-10

3.4 Load and deflection measurements

Each beam was loaded at two points using hydraulic actuators. The two actuators were coupled in parallel in order to achieve the same oil pressure, and thus the same load. The load was measured with a load cell on one of the actuators applying load to every beam, see Figure 3.15, and recorded from the time that the load was applied until the end of the test. The beams were 'paired' so that the same load was applied to both beams in a pair.



Figure 3.15, load cell mounted on the actuator

The deflection of each beam was measured with a resistive deformation transducer as shown in Figure 3.16. The transducer was mounted on a beam placed along the longitudinal direction of the furnace. The beam was supported by the concrete blocks resting on the steel frame going around the furnace, and thus not connected to the test specimens. It was decided to measure the deflection adjacent to one of the loading points,

as will be described in section 3.5. Deflection measurement was taken from a plate welded to the head of a 200 mm long screw with a smooth shaft for 150 mm below the head which was driven through the concrete block directly into the timber beam.

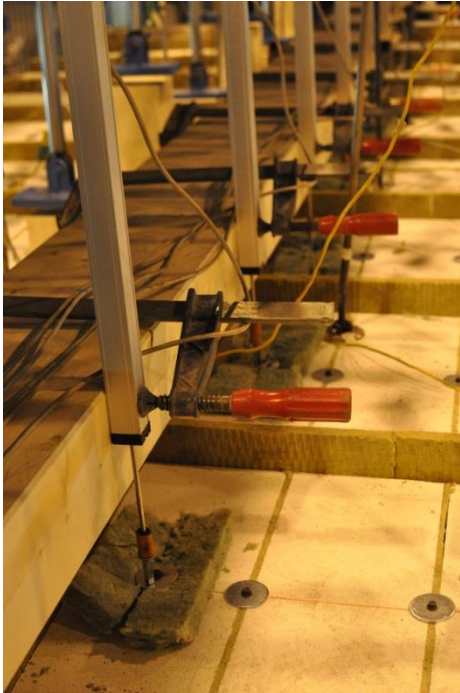


Figure 3.16, transducers used for deflection measurements.

3.5 Test procedure

The test procedure was designed in such a way that the following criteria could be satisfied:

1. The beams should be allowed to fail independently of one another without losing integrity of the furnace
2. There should be no interaction between the test specimens during the test
3. Immediately following completion of the test it should be possible to remove the specimens from the furnace with a minimum of delay to extinguish any residual burning

The test setup was designed in such a way that criteria 1 and 2 could be fulfilled. Any potential shear interaction between the beams was reduced by the use of mineral wool boards between the light weight cement blocks which were placed on top of the furnace, and the concrete blocks were deeper than the anticipated displacement at failure. Nevertheless upon failure of the beams some loss of integrity did occur on top of the furnace. When this happened the relevant actuators were retracted and mineral wool board was used to cover the openings in the furnace.

The third criteria was achieved by placing all of the test specimens directly onto a steel frame which was installed at the top of the furnace. Immediately following failure of the final beam in each test any remaining actuators were retracted and the loading frame was pushed to one side. Concurrently, all thermocouple wires were cut from the data loggers and all other measurement devices were disconnected. Once the loading frame was fully

removed from the test setup a 20 tonne crane was used to lift the entire test assembly from the furnace and move it over to rest on 4 support frames so that the timber could be extinguished from underneath. This whole procedure took approximately 6 minutes in every case. In some of the tests, during removal of the test setup the remains of one of the beams fell into the furnace.

It was decided to measure displacement adjacent to one of the loading points, and not between them. This meant that the actuators did not need to be retracted as far to come over the top of the beam supporting the deformation transducers and could be installed lower. All actuators were the same, with a maximum extension of 500 mm. One actuator and one loading point on each beam had the load cell which was 200 mm long fitted, this meant that the actuator without the load cell had to be positioned 200 mm lower so that the actuators had the same extension and could be raised over the displacement measurement system.

4 Fire curves

4.1 Overview

The objective of running 4 tests was to conduct one test of the timber elements exposed to a standard fire curve and three where the timber elements were exposed to parametric fire curves. However the loading system failed during the first standard fire test and so this was repeated. We therefore obtained two sets of charring results from the standard fire exposure, one loaded and one unloaded, and two parametric fire tests.

The parametric fires chosen were intended to represent a long-cool fire and a short-hot fire. Therefore the timber elements would be exposed to a slow heating rate for a long period in one of the fires and to a fast heating rate for a short period in the other. As far as was possible during the tests where a parametric fire was used, the cooling regime of the parametric fire was followed, until the last of the beams failed.

4.2 Fire curves

As stated the first two of the fire tests were carried out under standard fire exposure. This represents a parametric fire curve with an opening factor of 0.04 and a thermal inertia of the wall linings of $1.35 \times 10^6 \text{ J}^2/\text{m}^4\text{sK}^2$.

The other two fire tests were conducted using parametric fire curves as defined in EN 1991-1-2 [5] intended to represent reasonable extremes above and below the standard fire curve. The parameters required to define the parametric fire in all three instances are summarised in Table 4.1. The resulting fire curves are shown in Figure 4.1.

Table 4.1, parameters used in the definition of the fire curves in the tests.

Test	Opening factor, $O \text{ (m}^{1/2}\text{)}$	$\sqrt{\rho c \lambda} \text{ (J/m}^2\text{s}^{1/2}\text{K)}$	fire growth rate	$q_f \text{ (} q_{td} \text{) (MJ/m}^2\text{)}$
Fire test 1 and 2 (standard fire)	0.04	1160		
Fire test 3	0.12	1160	medium	250 (92)
Fire test 4	0.02	1160	medium	250 (92)

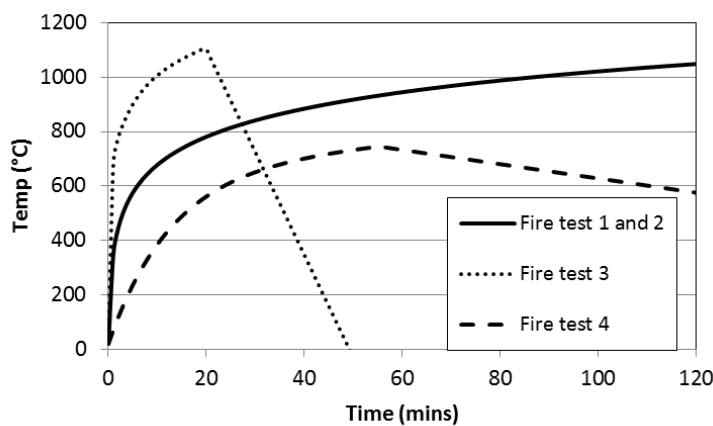


Figure 4.1, fire curves used in the fire tests

Details about the actual predicted loads to failure are given in section 5.6.

5 Results from fire tests

5.1 Fingerjoint positioning

As stated previously, prior to carrying out each of the fire tests, the positions of the finger joints in each of the specimens was recorded. The specimens were oriented and cut such that, where possible, no finger joints would be located in the second from bottom lamella between the two loading points. This is because it was expected that the lower lamella would char significantly during the test and that the strength of the second from bottom lamella would prove critical for the load bearing function. This same procedure was followed for all tests. Finger joint positions for all 4 tests are recorded in Appendix 2.

5.2 Fire test 1 – Standard fire

5.2.1 Furnace conditions

The conditions in the furnace are reported in figures 5.1 and 5.2. Figure 5.1 shows the temperature measured by all of the plate thermometers during the test along with the standard fire curve from EN 1363-1. Plate thermometer numbers 12, 16 and 19 failed during the test and were not used to control the furnace. Recalling that some of the plate thermometers were designated as slave plate thermometers during the test and were positioned such that they faced adjacent beams as opposed to the furnace walls, a comparison between the master and slave plate thermometer average temperature measurements is given in figure 5.2. It can be seen that there is no impact or shadow effect from the proximity of the adjacent beams on the plate thermometer measurements.

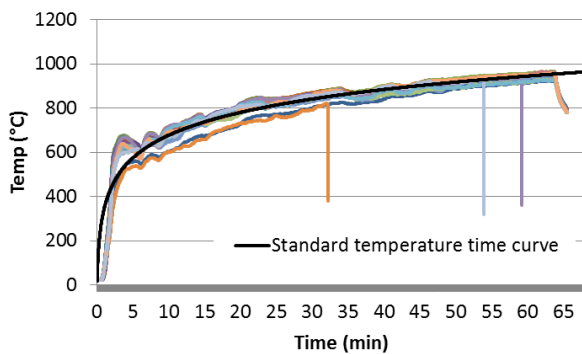


Figure 5.1, measured furnace temperature with all individual plate thermometers

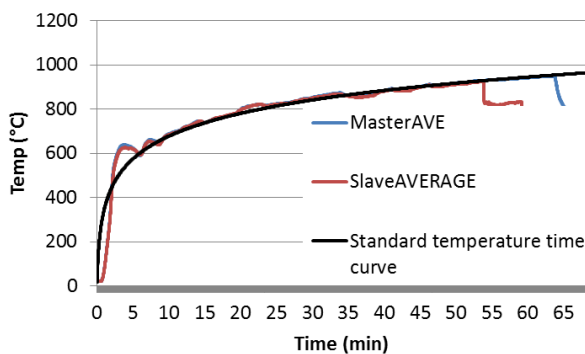


Figure 5.2, mean temperature of master and slave plate thermometers

5.2.2 Specimen temperatures

As described, temperature measurements were made at various depths and positions within the beams. For each of the locations of temperature measurement within this test, the average measured temperature profiles are shown in Figures 5.3, 5.4 and 5.5. These correspond with the temperature penetration measured from the bottom of the beam using five thermocouples at the east end of the beam; from the bottom of the beam using 3 thermocouples at the west end of the beam; and from the side of the beam using two thermocouples respectively.

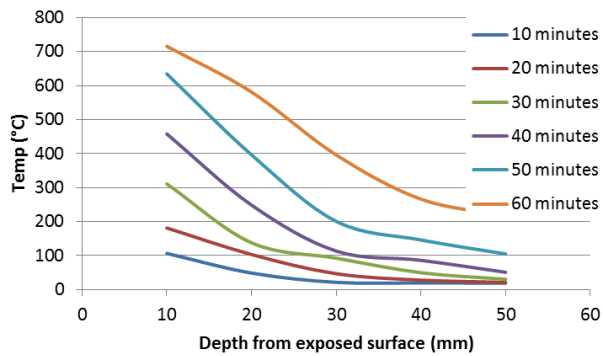


Figure 5.3, average temperature profiles from all beams in the first fire test measured at the east end of the beams

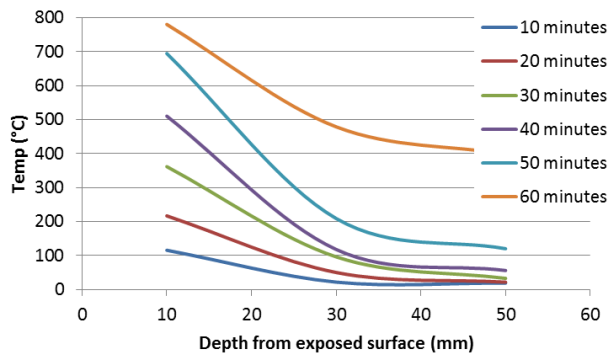


Figure 5.4, average temperature profiles from all beams in the first fire test measured at the west end of the beams

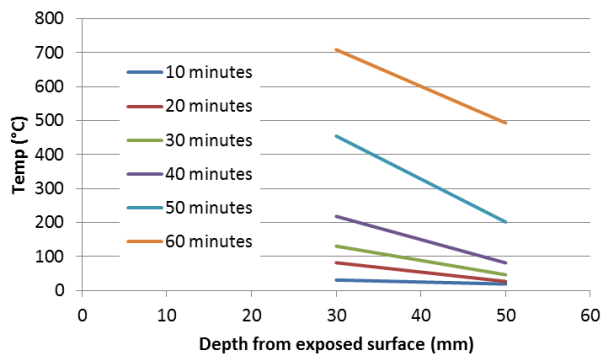


Figure 5.5, average temperature profiles from all beams in the first fire test measured from the sides of the beams

The coefficient of variation of these measurements are shown in Figures 5.6, 5.7 and 5.8. Each of these figures shows the variation corresponding to the same set of measurements as are shown in Figure 5.3, 5.4 and 5.5. It can be seen that the typical variance is very high, typically between 20 and 40%. However there are some very large differences in the variance which are most likely the result of fissuring in the specimens during heating. Table 5.1 shows the individual temperature profiles from each of the measuring points in each of the beams during the tests. The temperature profiles in the east end of beam 9 are affected by the failure of one of the thermocouples during the test (at 20mm depth), and this has been removed from the calculation of the average and coefficient of variation of all of the temperature profiles.

The temperature profiles show generally a good consistency in the trend observed. As indicated thermocouples in beam 9 did fail during the test and this is reflected in the measurements. Nevertheless they are reported here for completeness. The occurrence of fissures in some profiles, exposing individual thermocouples is also apparent, and is evidenced by the peaks observed at later times at greater depths in some of the profiles.

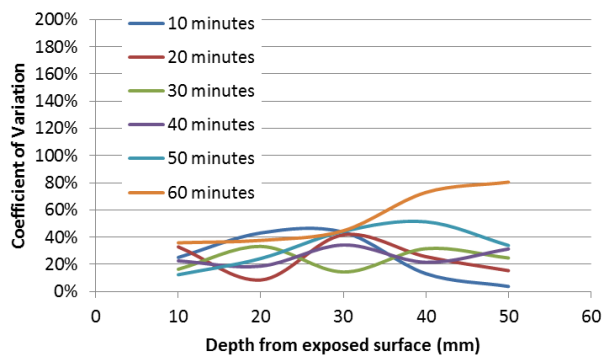


Figure 5.6, coefficient of variation of temperature profiles from all beams in the first fire test measured at the east end of the beams

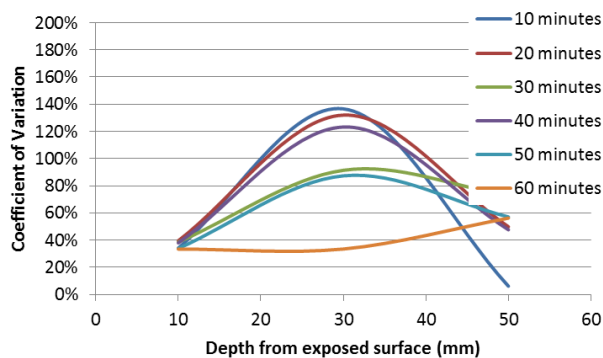


Figure 5.7, coefficient of variation of temperature profiles from all beams in the first fire test measured at the west end of the beams

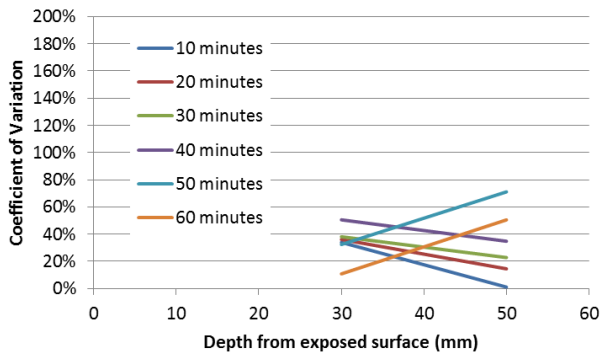
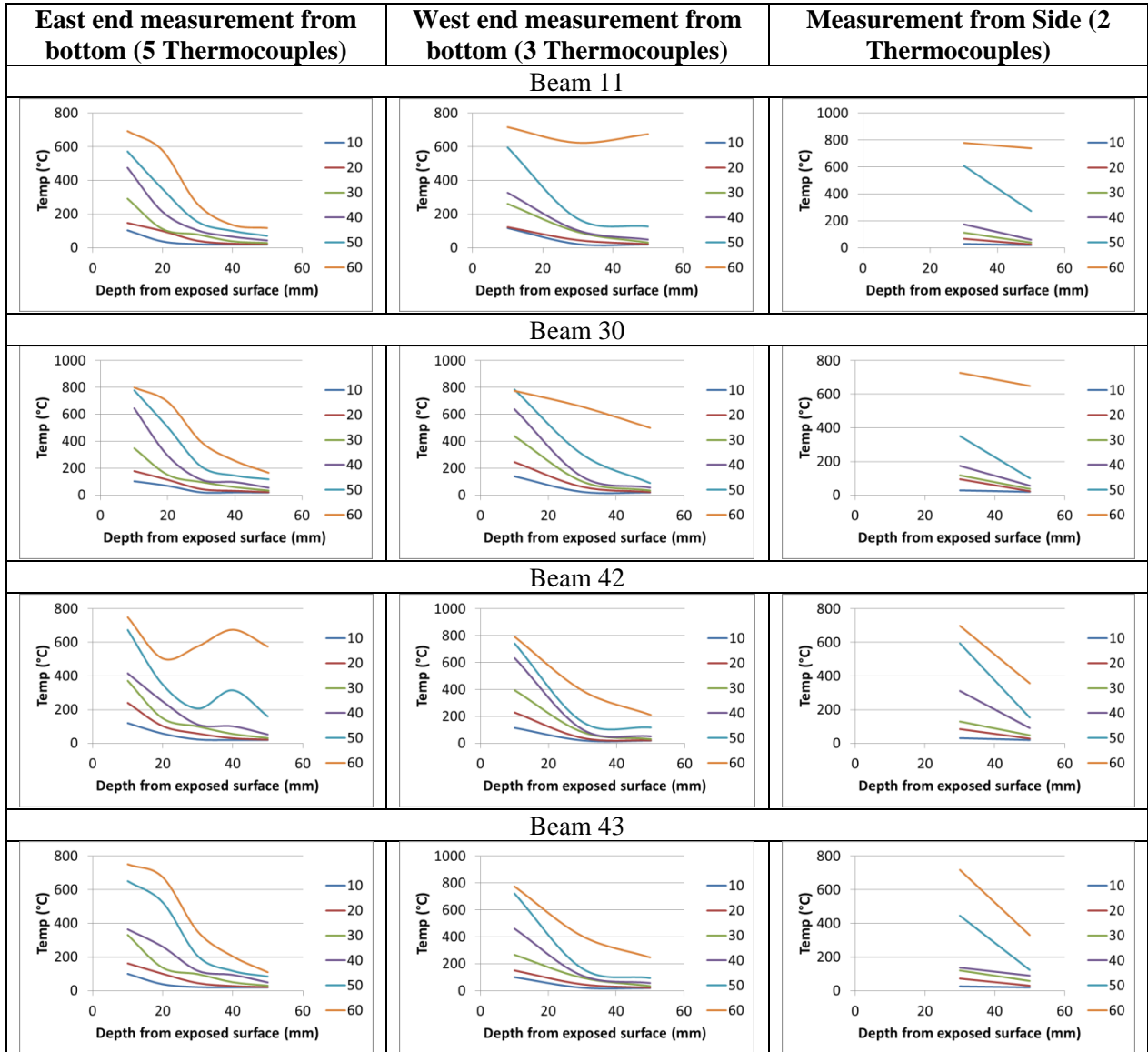


Figure 5.8, coefficient of variation of temperature profiles from all beams in the first fire test measured from the sides of the beams

Table 5.1, measured temperature profiles in all beams during the first fire test; the legend indicates the time in minutes at which each isotherm is presented

East end measurement from bottom (5 Thermocouples)	West end measurement from bottom (3 Thermocouples)	Measurement from Side (2 Thermocouples)
Beam 1		
Beam 6		
Beam 8		
Beam 9		



5.2.3 Charring rate

The charring rate may be estimated based on the time taken for the isotherm corresponding to the charring temperature to reach the thermocouples which are embedded in the timber specimen. Assuming that charring occurs at a given temperature, the charring rate is then given by the following expression:

$$\beta = \frac{d_{tc}}{t_{Tchar}} \quad (5.1)$$

where β is the charring rate in mm/min, d_{tc} is the depth of the thermocouple measured from the nearest surface, and t_{Tchar} is the time in minutes taken for the thermocouple to reach the charring temperature from the start of the test. It should be noted that this expression gives an average charring rate over the distance in question as opposed to the 'real' or instantaneous charring rate. The instantaneous charring rate at the different thermocouple positions may be estimated by replacing d_{tc} with the difference in depth between the thermocouple in question and the thermocouple next closest to the surface ; and t_{Tchar} with the difference in time to reach the charring temperature between the two thermocouples.

The instantaneous values of charring rate estimated at the different thermocouple positions from fire test 1 are shown in Figure 5.9. In preparation of Figure 5.9, and subsequent estimations of the charring rate based on the measured temperatures, a charring temperature of 270°C has been assumed. This was based on a visual inspection of the charred depth of the sections around the thermocouple locations and the temperatures observed at the thermocouples around the end of the fire tests. The region between brackets indicates that linear extrapolation was used to estimate the charring rate at this time since the test had already stopped. In this case, it is assumed that the gradient of the isotherm is constant and would remain so under continued fire exposure.

It is clear that the charring rate is in fact changing over time under the fire exposure. At the end of the fire test, the average charring rate is approximately 0.6 mm/min, as opposed to 0.4 mm/min measured at the start of the test. This is as opposed to the constant figure of 0.7 mm/min which is quoted in EN 1995-1-2.

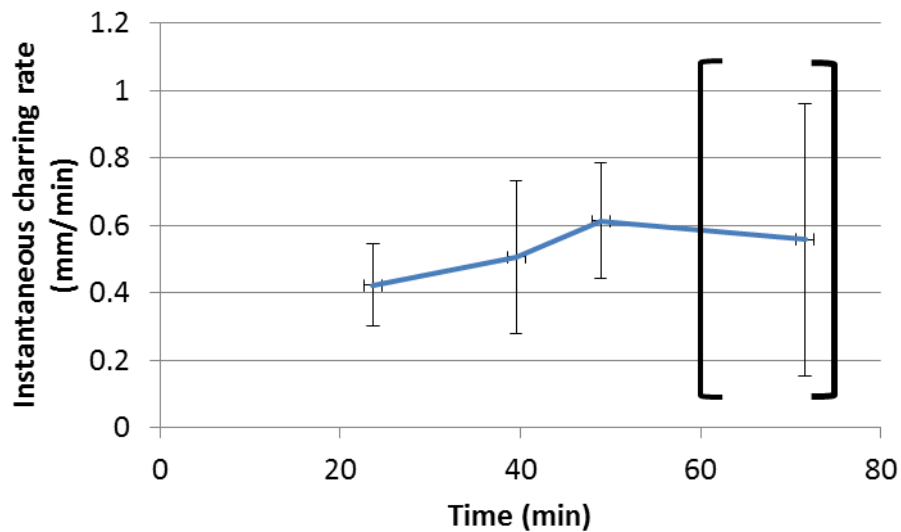


Figure 5.9, charring rate estimated from thermocouple measurements in fire test 1 – error bars indicate the coefficient of variation (brackets denote region of linear extrapolation of charring rate based on the isotherm gradient at the end of the test)

5.3 Fire test 2 – Standard fire

5.3.1 Furnace conditions

Plate thermometer measurements from the furnace are shown in Figure 5.10 in the same format as the first fire test. In this test a number of plate thermometers failed over the course of the test (at different times) and these are not included in the figure. However they were used to control the furnace until the time of failure. As plate thermometers failed, the slave plate thermometers were used to control the furnace temperature as well as the master plate thermometers.

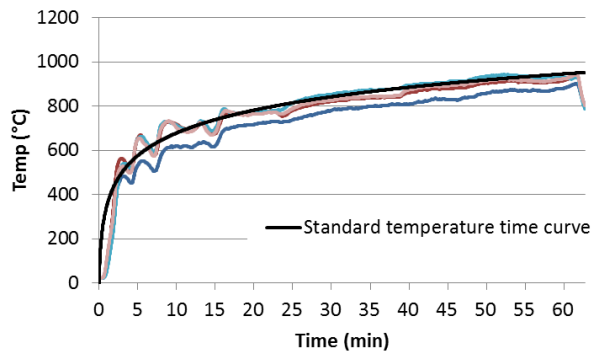


Figure 5.10, measured furnace temperature with individual plate thermometers in fire test 2

5.3.2 Specimen temperatures

Through depth temperatures are shown in Figures 5.11, 5.12 and 5.13, averaged for all of the beams in the fire test at the different locations where temperature measurements were made. The coefficient of variation is also shown in Figures 5.14, 5.15 and 5.16. These are typically lower in this test than in the previous test, ranging from around about 10 to 30%. In calculating the average temperatures for the isotherms and the coefficient of variation of the isotherms, any failed thermocouples were removed from the calculation. In total however, there were only two failed thermocouples in the timber elements.

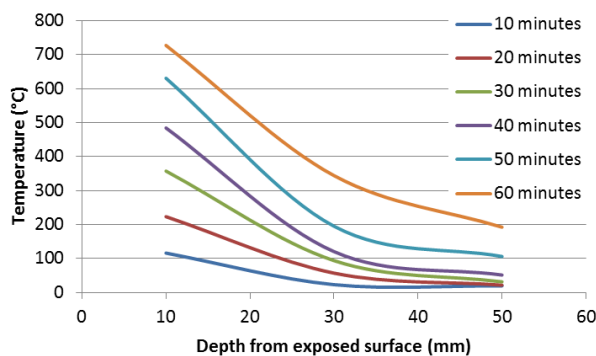


Figure 5.11, average temperature profiles from all beams in the second fire test measured at the east end of the beams

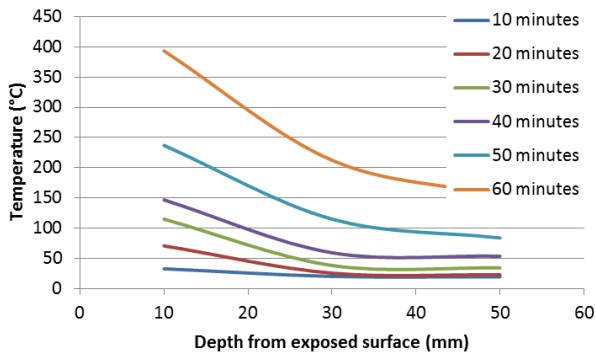


Figure 5.12, average temperature profiles from all beams in the second fire test measured at the west end of the beams

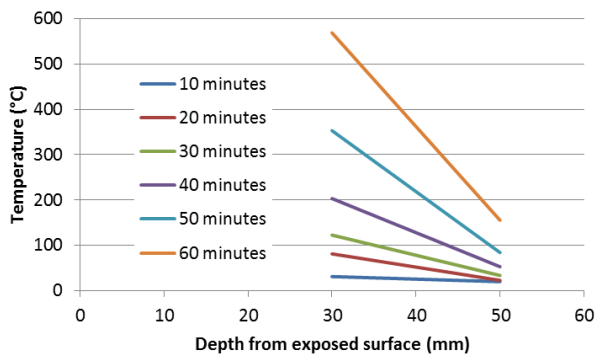


Figure 5.13, average temperature profiles from all beams in the second fire test measured from the sides of the beams

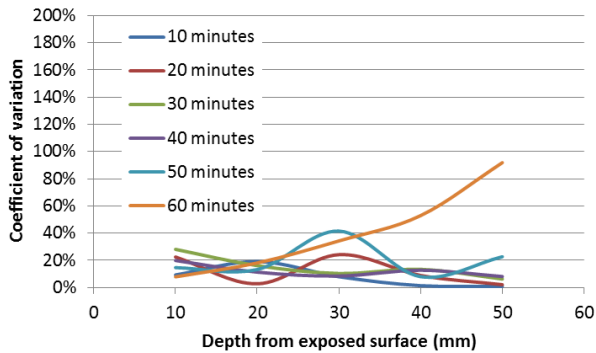


Figure 5.14, coefficient of variation of temperature profiles from all beams in the second fire test measured at the east end of the beams

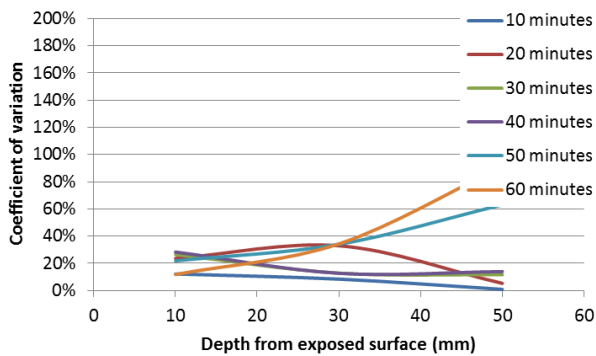


Figure 5.15, coefficient of variation of temperature profiles from all beams in the second fire test measured at the west end of the beams

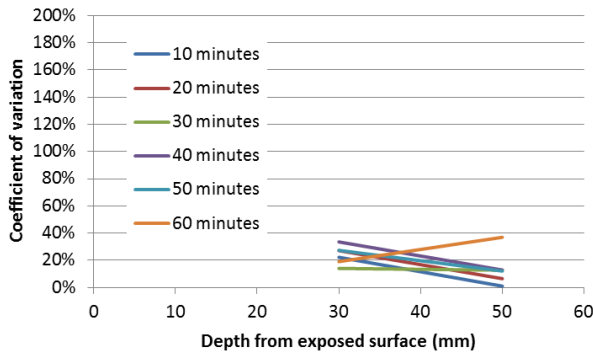
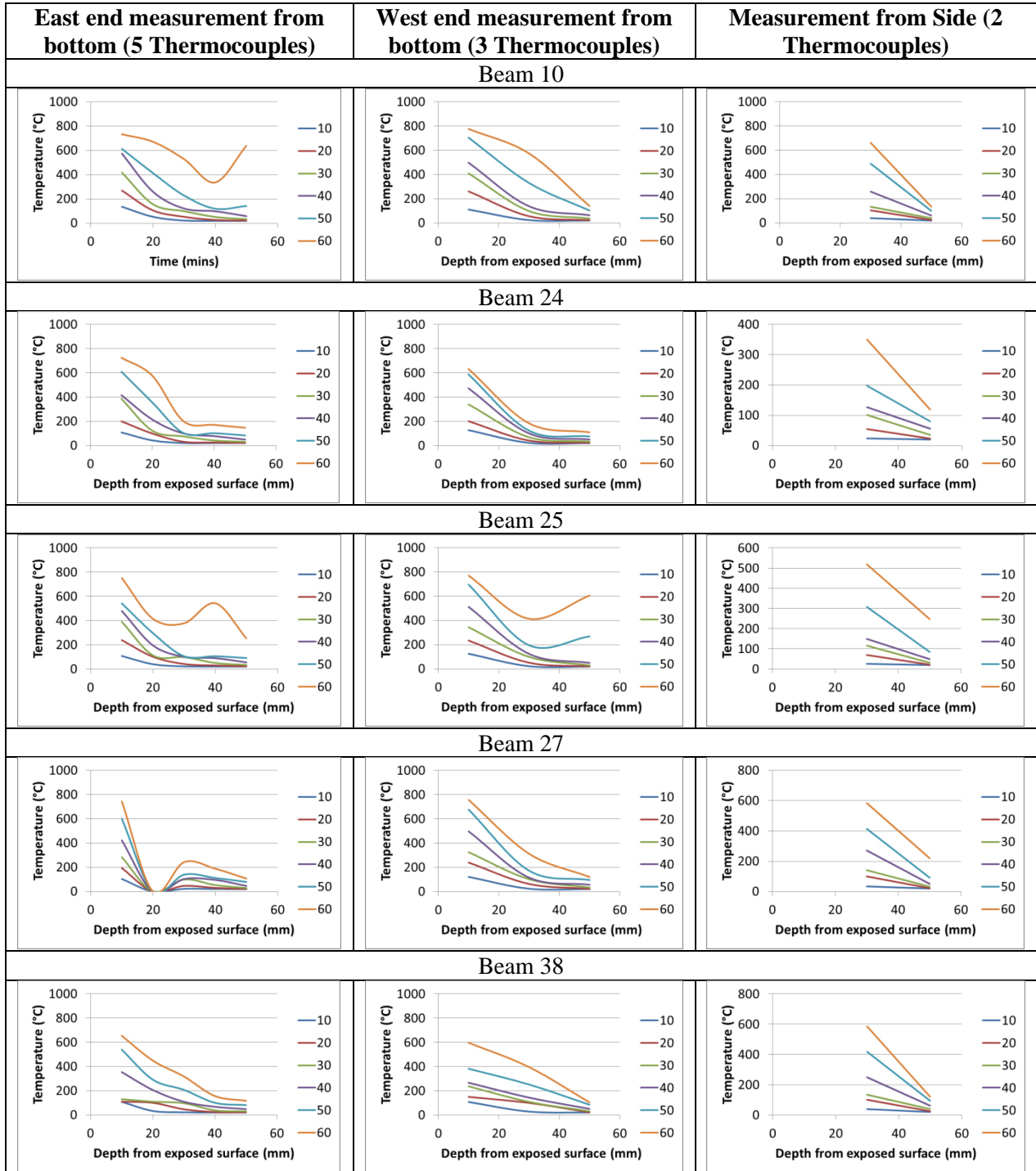


Figure 5.16, coefficient of variation of temperature profiles from all beams in the second fire test measured from the sides of the beams

The individual temperature distributions at each of the measuring points are shown in Table 5.2. The failed thermocouples can be seen in the isotherms from beam 7, in the measurements from the side of the beam at the west end, and in beam 27 in the measurements from the bottom at the east end. As before, fissuring and cracking can be seen to occur at the later stages of the test, exposing some of the deeper thermocouples to higher temperatures than the shallower thermocouples.

Table 5.2, measured temperature profiles in all beams during the second fire test; the legend indicates the time in minutes at which each isotherm is presented

East end measurement from bottom (5 Thermocouples)	West end measurement from bottom (3 Thermocouples)	Measurement from Side (2 Thermocouples)
Beam 3		
Beam 5		
Beam 7		



5.3.3 Charring rate

Figure 5.17 shows the instantaneous charring rate estimated based on the thermocouple temperatures in fire test 2. In this test the measured charring rates are generally slightly

lower than in fire test 1.

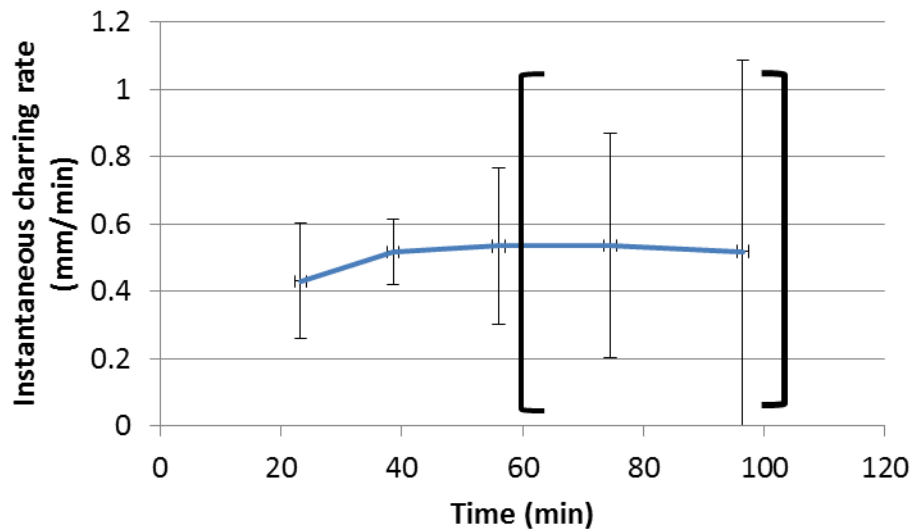


Figure 5.17, charring rate estimated from thermocouple measurements in fire test 2 – error bars indicate the coefficient of variation (brackets denote region of linear extrapolation of charring rate based on the isotherm gradient at the end of the test)

5.4 Fire test 3 – Short hot fire

5.4.1 Furnace conditions

The plate thermometer measurements from the 3rd fire test are shown in Figure 5.18 along with the fire curve which was used in this test. The failure of one of the plate thermometers can be seen at the end of the heating phase. Following a cooling phase (such as that associated with the parametric fire) is not something which is typically done in fire resistance testing however the plate thermometer temperatures follow it fairly well for about 10 minutes after the heating phase and until the end of the test.

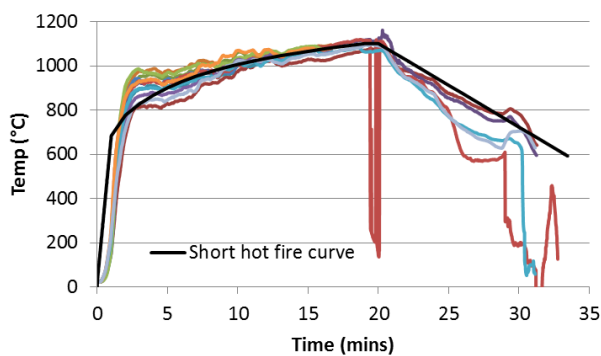


Figure 5.18, measured furnace temperature with individual plate thermometers in fire test 3

5.4.2 Specimen temperatures

Average temperature distributions for the measuring points in the beams in the third test are shown in Figures 5.19, 5.20 and 5.21. As before, any thermocouples which broke during the fire tests are removed from the averaging calculation. It should be noted also that the cooling phase is clear in the temperature distributions, where a maximum temperature close to the heated surface occurs after about 20 minutes, see Figures 5.19 and 5.20. It can be seen in these figures that the position of maximum temperature continues to move through the specimens, away from the heated surface, as would be expected after this time.

The coefficient of variation in the isotherms is shown in Figures 5.22, 5.23 and 5.24. As with the second standard fire test, these are typically between 10 and 30% for the isotherms measured from the bottom of the beams, although the variation does increase over the course of the test and with distance from the heated surface. For the measurements from the side of the beams, there is a considerably higher coefficient of variation, especially later in the test (over 100%).

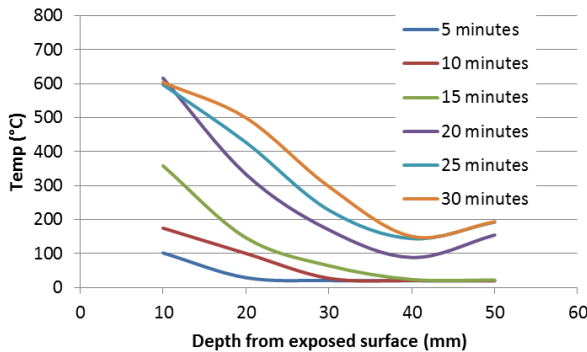


Figure 5.19, average temperature profiles from all beams in the third fire test measured at the east end of the beams

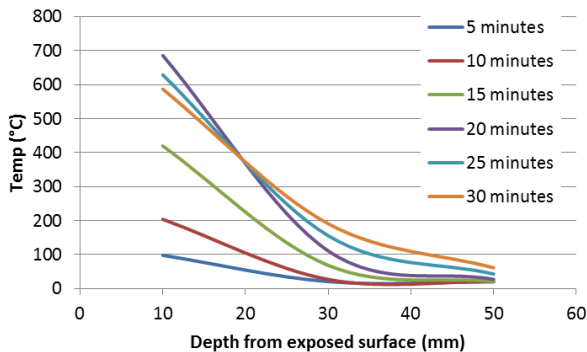


Figure 5.20, average temperature profiles from all beams in the third fire test measured at the west end of the beams

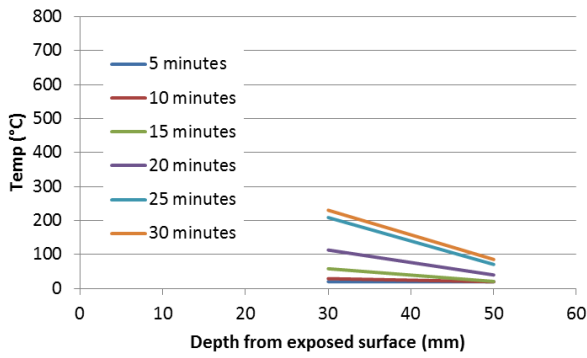


Figure 5.21, average temperature profiles from all beams in the third fire test measured from the sides of the beams

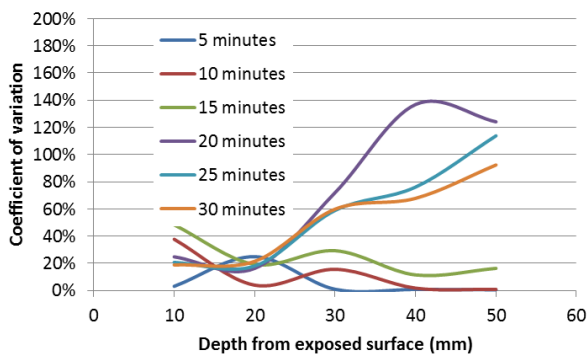


Figure 5.22, coefficient of variation of temperature profiles from all beams in the third fire test measured at the east end of the beams

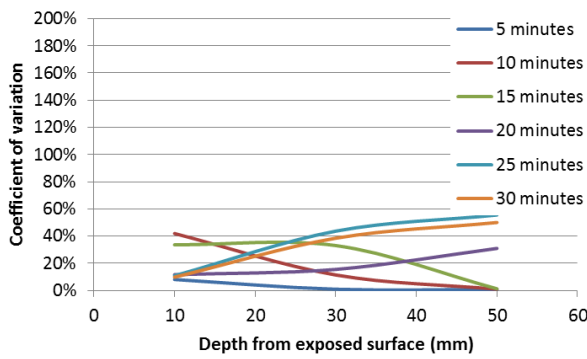


Figure 5.23, coefficient of variation of temperature profiles from all beams in the third fire test measured at the west end of the beams

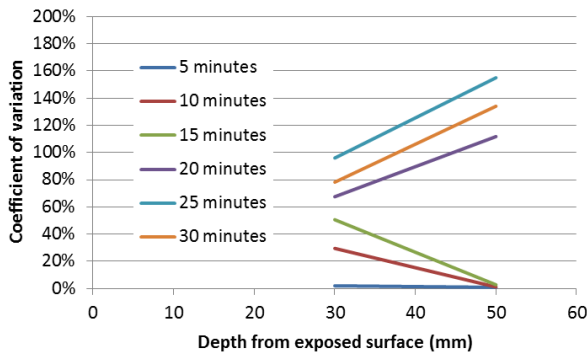
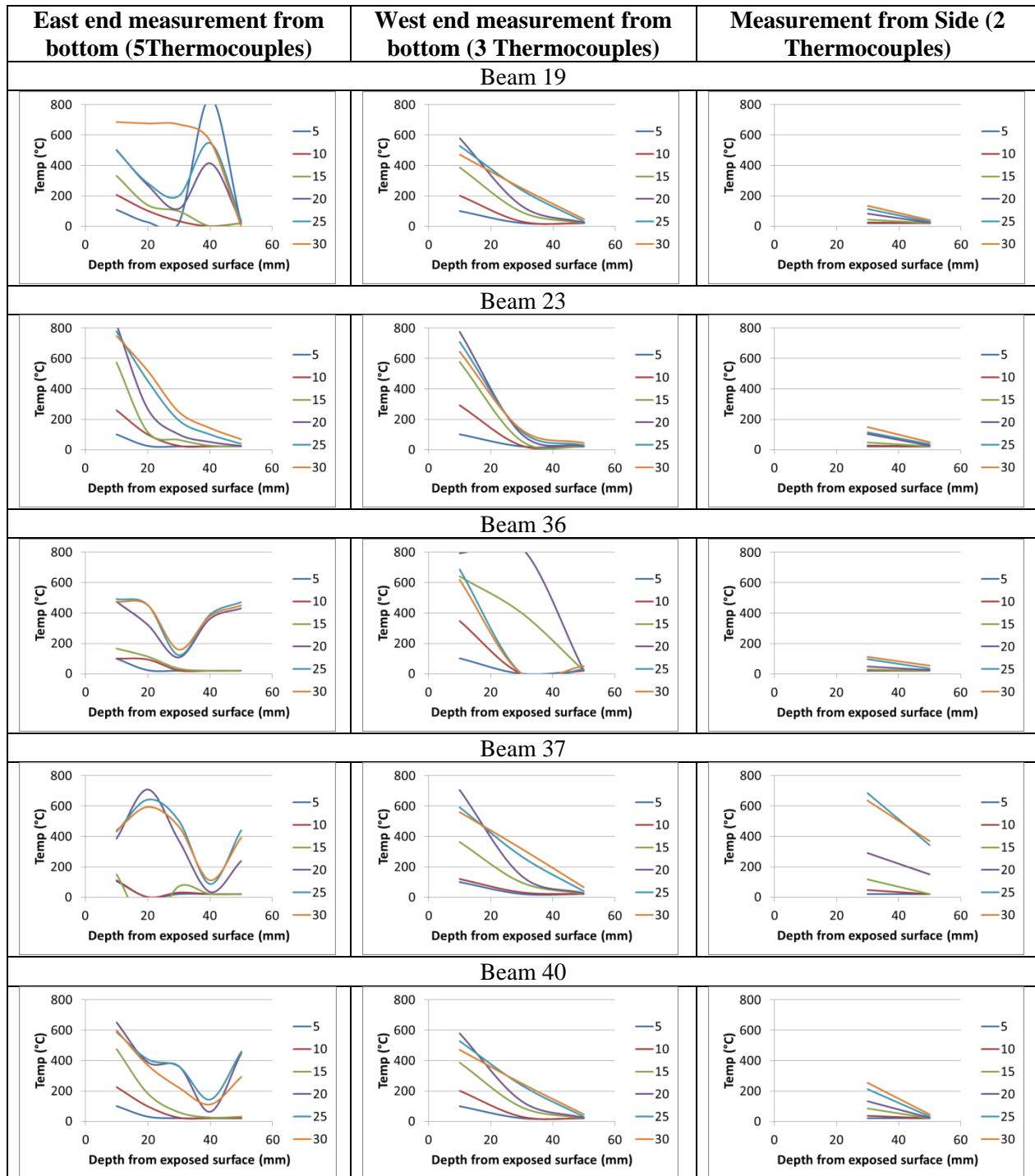


Figure 5.24, coefficient of variation of temperature profiles from all beams in the third fire test measured from the sides of the beams

For comparison, the individual temperature measurements plotted against depth and at different times during the fire test are shown in Table 5.3. There is again good consistency between the measurements in the individual beams, although the presence of cracking or fissuring is again evident (e.g. east end of beam 36) as is the failure of a number of thermocouples (e.g. east end of beam 4, bottom measurement at the west end of beam 36).

Table 5.3, measured temperature profiles in all beams during the third fire test; the legend indicates the time in minutes at which each isotherm is presented

East end measurement from bottom (5 Thermocouples)	West end measurement from bottom (3 Thermocouples)	Measurement from Side (2 Thermocouples)
Beam 4		
Beam 15		
Beam 18		



5.4.3 Charring rate

The estimated instantaneous charring rate during fire test 3 is shown in figure 5.25. The impact of the end of heating on the charring rate is clear between 20 and 30 minutes. Again the brackets denote the portion of the graph which is based on linear extrapolation of the isotherm following the end of the test. Since it is not likely that the gradient of the isotherm increases during the cooling phase this linear extrapolation is a conservative assumption.

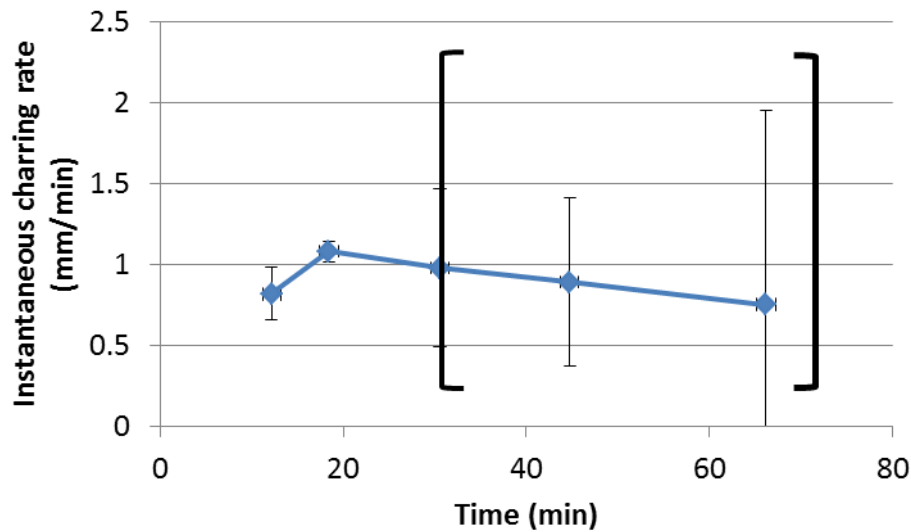


Figure 5.25, charring rate estimated from thermocouple measurements in fire test 3 – error bars indicate the coefficient of variation (brackets denote region of linear extrapolation of charring rate based on the isotherm gradient at the end of the test)

5.5 Fire test 4 – Long cool fire

5.5.1 Furnace conditions

Plate thermometer temperatures in the 4th fire test are shown in Figure 5.26 along with the target fire curve for the furnace. As in all of the other tests, some of the plate thermometers failed during the test, although in all cases this was towards the end of the heating phase or during the cooling phase. Only 3 plate thermometers failed during this test. Overall it was possible to follow the target fire curve very well during the cooling phase, although the slightly slower ramp up in temperature was a challenge.

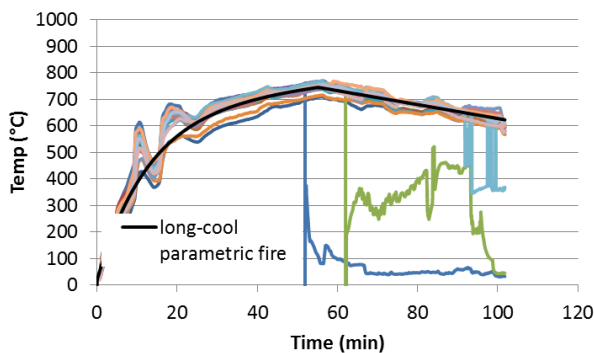


Figure 5.26, measured furnace temperature with individual plate thermometers in fire test 4

5.5.2 Specimen temperatures

Specimen through depth temperatures at different times are plotted in figures 5.27, 5.28 and 5.29. In this test, the opportunity was taken to include thermocouples at depths of 60 and 70 mm from the heated surface at the west ends of the beams in addition to the other temperature measurements. These are shown in Figure 5.28, although the x-axes of all of the figures in this section have been increased to allow for a better comparison. Because of the less dramatic cooling phase for the fire in this test, the temperature continues to

increase close to the heated surface of the specimens, as opposed to the 3rd fire test where it was seen to drop during the cooling phase which was part of the test.

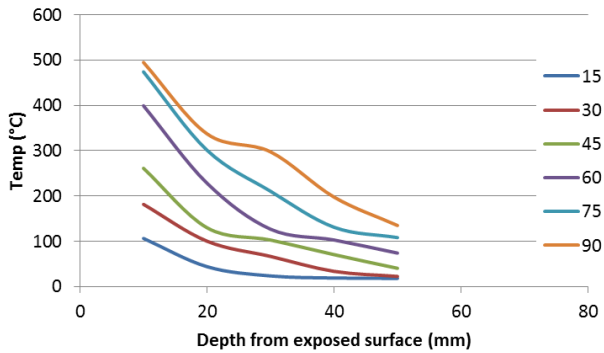


Figure 5.27, average temperature profiles from all beams in the fourth fire test measured at the east end of the beams

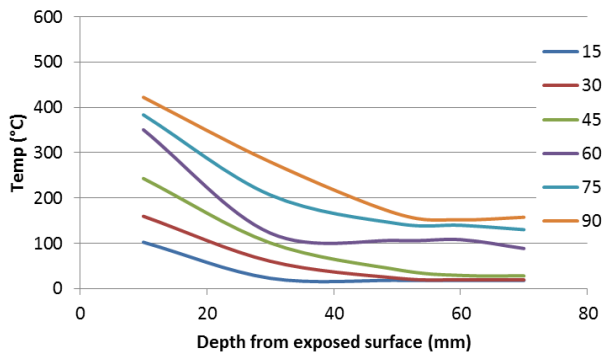


Figure 5.28, average temperature profiles from all beams in the fourth fire test measured at the west end of the beams

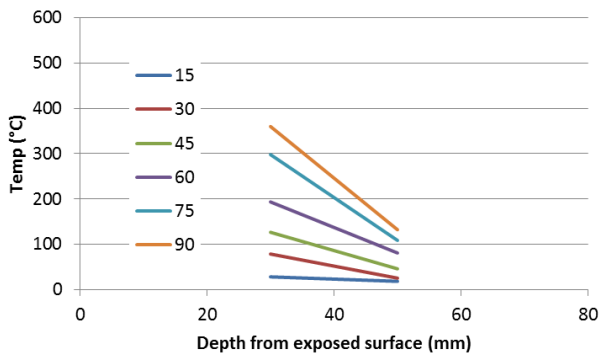


Figure 5.29, average temperature profiles from all beams in the fourth fire test measured from the sides of the beams

The coefficient of variation of the through depth temperature measurements is shown in Figures 5.30, 5.31 and 5.32. These are consistent with the 2nd and 3rd fire tests, where the coefficient of variation was typically between 10% and 30%, although in the later stages of the fire this is seen to increase at the west end of the beam, although it does decrease again during the cooling phase (Figure 5.31).

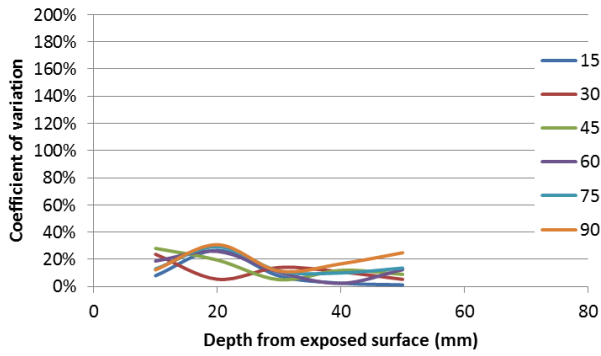


Figure 5.30, coefficient of variation of temperature profiles from all beams in the fourth fire test measured at the east end of the beams

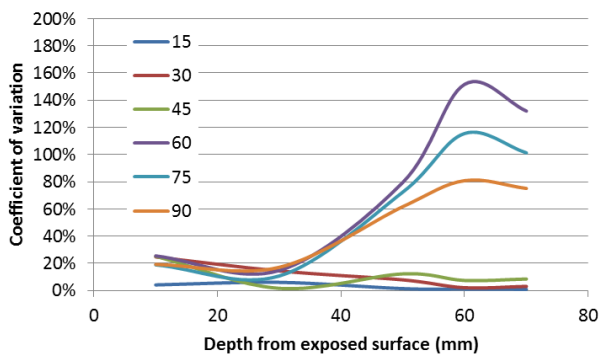


Figure 5.31, coefficient of variation of temperature profiles from all beams in the fourth fire test measured at the west end of the beams

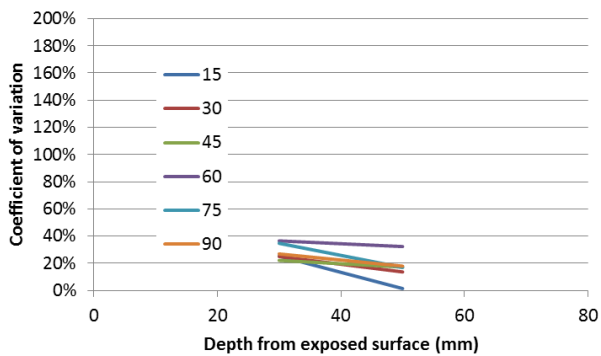
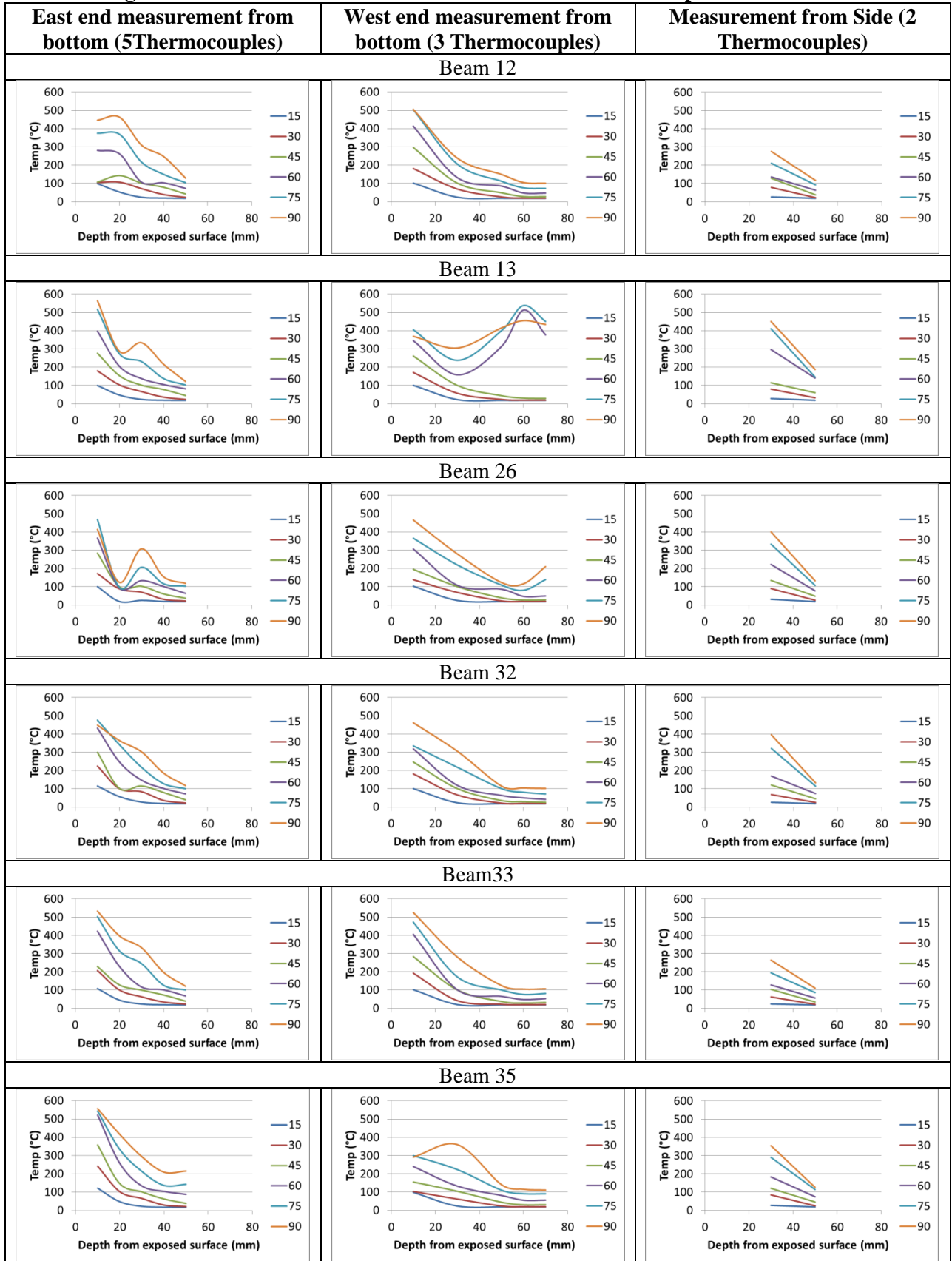
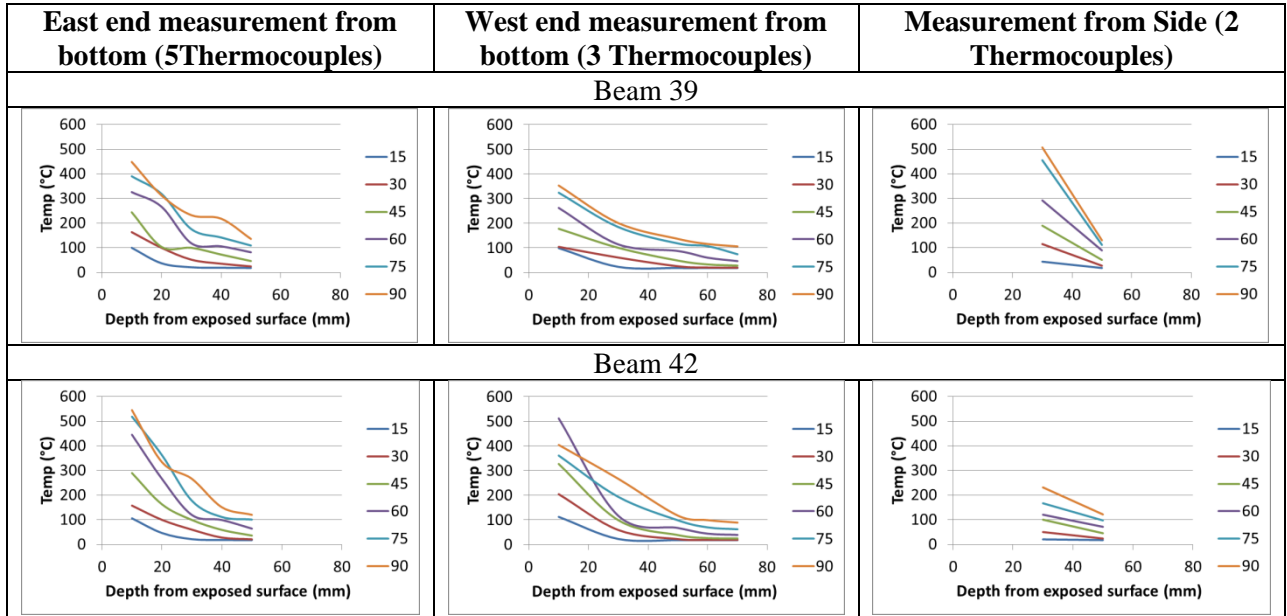


Figure 5.32, coefficient of variation of temperature profiles from all beams in the fourth fire test measured from the sides of the beams

The individual temperature distributions in all of the beams and at all locations in the fourth fire test is shown in table 5.4. In this fire test, none of the thermocouples in the beams actually failed. Fissuring or cracking is again evident in some of the specimens (e.g. the measurement from the bottom of the west end of beam 13).

Table 5.4, measured temperature profiles in all beams during the fourth fire test; the legend indicates the time in minutes at which each isotherm is presented





5.5.3 Charring rate

The charring rate from the fourth fire test estimated based on the time to reach an assumed charring temperature (270°C) is shown in Figure 5.33. The char rate increases over the course of fire exposure, as in the other three fire tests. before reducing during the cooling phase.

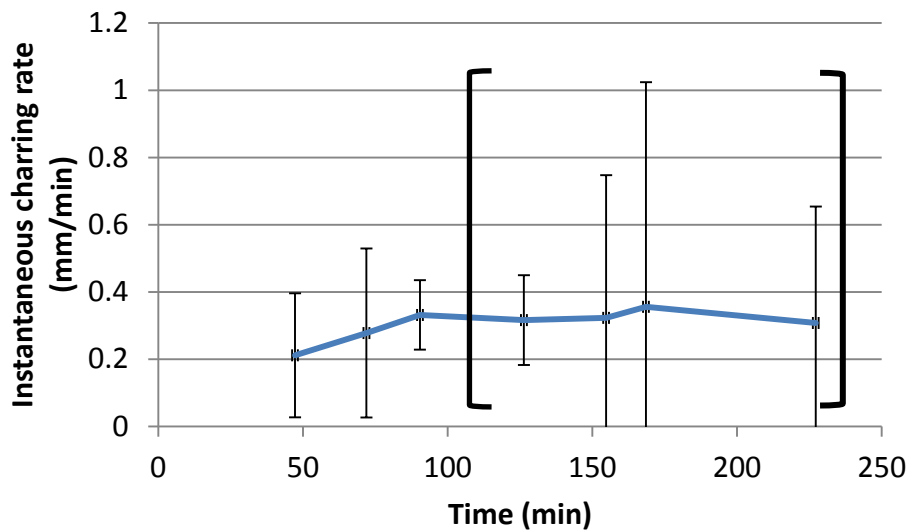


Figure 5.33, charring rate estimated from thermocouple measurements in fire test 4 – error bars indicate the coefficient of variation (brackets denote region of linear extrapolation of charring rate based on the isotherm gradient at the end of the test)

5.6 Summary of average charring rates

The estimated 1-dimensional charring rates averaged over the thermocouple depths from all of the fire tests are summarised in figure 5.34 and 5.35 below. The red bars indicate charring rate measured from the bottom of the beams and the green bars indicate charring rate measured from the side of the beams. All of these reported charring rates are based on the average times to reach a charring temperature of the thermocouples at different

depths within all of the beams in this test. That is to say that for each of the average values reported these are based on at least 8, and at most 16 thermocouples, depending upon reliability of the measurements.

Figure 5.34 shows the 1-dimensional charring rate estimated based on temperatures at fixed depths from the bottom of the beams; Figure 5.35 shows the same result but based on temperatures measured at fixed distances from the exposed sides. In both figures it is clear that there is some difference between the first and the second fire tests despite the fact that the specimens in these tests were all exposed to the same temperature-time curve. More work is clearly needed to understand if this was a result of the fact that the second test was loaded or if it was due to the natural variations in the wood. Nevertheless they are similar, and the trend of increasing charring rate is consistent across all four tests, with decreasing charring rate during the cooling phase of the parametric fire curves. This is true whether the char rate is estimated based on temperatures measured at fixed depths from the bottom surface of the beams or from the sides.

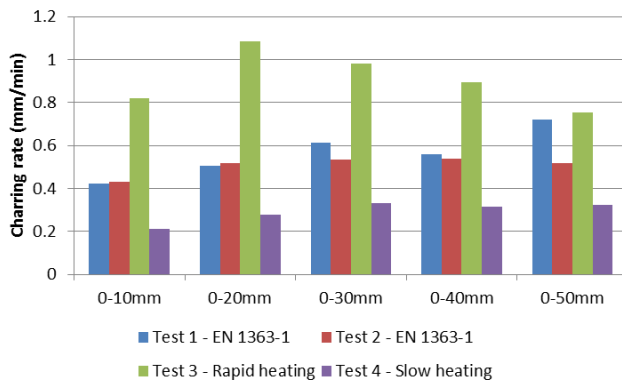


Figure 5.34, summary of charring rates from the bottom of the test specimens estimated from thermocouple measurements in all fire tests

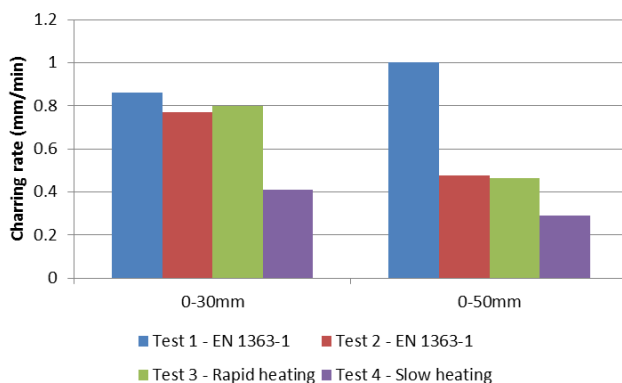


Figure 5.35, summary of charring rates from the sides of the test specimens estimated from thermocouple measurements in all fire tests

A comparison of the charring rate estimated based on measurements from the bottom of the beam with the charring rate based on measurements from the sides of the beam shows that the charring rate from the side was in fact higher in some cases than the charring rate measured from the bottom. This suggests that corner rounding at the bottom of the beam was not so progressed that it significantly impacted upon the charring rate. It is unlikely that this is due to orientation of the char front relative to the grain since both charring from the side and the bottom is parallel to the grain. It is also unlikely that the thermal exposure on the sides were higher since the plate thermometers which were facing the

adjacent beams and the walls showed no tendency to record higher temperatures during the test. The different charring rates are therefore difficult to explain by means of thermal exposure. However, natural variations in the wood density may explain the differences, since it is common to use denser timber for the upper and lower lamella in glulam beams and the density may have contributed to the lower charring rate since the measurements from the sides of the beams were taken from around about mid depth.

In all of these average charring rate figures, it should be noted that in most cases, after 30 mm of char had formed the test stopped. Therefore the reported results for char at 40 and 50 mm are based on very few cases where charring occurred, likely due to the formation of fissures or cracks in the wood, increasing the charred depth locally.

5.7 Mechanical failure of specimens during the fire tests

For all of the fire tests, the failure load as a function of time was estimated based upon the reduced cross section method. Based on the loading arrangement, figure 5.36, the maximum moment in the beam may be determined from equation 1.4. As described in section 2.1.3, the mean of the bending strength was determined to be 37.8 MPa and this was used in all of the predictions of the load required until failure.

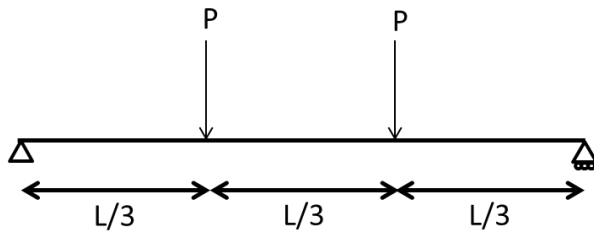


Figure 5.36, loading arrangement indicating support and load distribution.

5.7.1 Failure of specimens in fire test 1

As already discussed, there was a failure of the loading system during fire test 1. Therefore no results of the loaded response are reported for the first fire test.

5.7.2 Failure of specimens in fire test 2, 3 and 4

The predicted and measured time to failure in fire test 2 is shown in Figure 5.37. The same thing is shown for the 3rd and 4th fire tests in Figure 5.38 and 5.39. In this case, calculation of the load until failure assumes a zero strength layer of 7 mm in all cases since no alternative suitable for parametric fire curves is given in the method in the Eurocode.

There is a clear difference in the predicted and the measured load until failure. In both the standard fire test, fire test 2, and the long-cool fire test, fire test 4, the predicted load until failure was higher than the measured load until failure. In the short-hot fire test, the predicted and measured load until failure showed good agreement. A summary of the predicted and actual failure loads and times in all of the fire tests is shown in table 5.5.

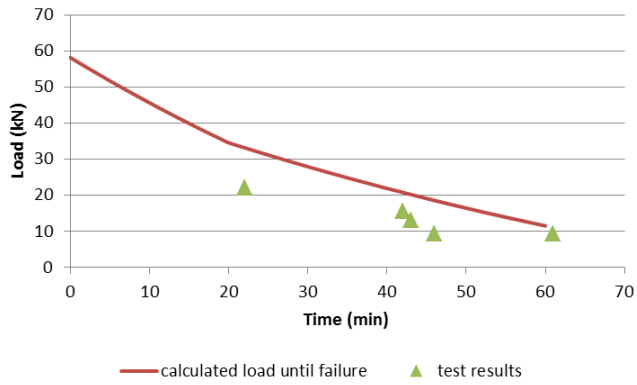


Figure 5.37, predicted and measured failure times in fire test 2

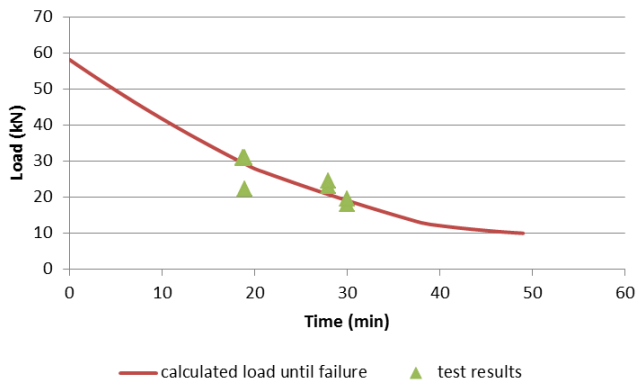


Figure 5.38, predicted and measured failure times in fire test 3

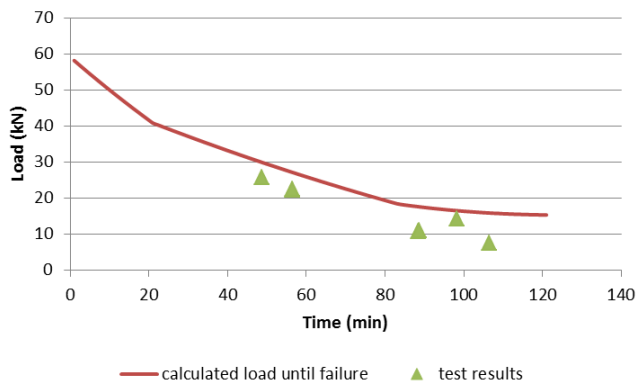


Figure 5.39, predicted and measured failure times in fire test 4

Table 5.5, predicted and actual failure loads of the beams during the fire tests

Pair	Failure time (min)	Predicted failure load (kN)	Actual failure load (kN)	Failed beam number	Predicted load factor (based on mean strength of group 1)	Actual load factor (based on mean strength of group 1)
Standard fire (group 3)						
A	43	20.2	12.9	5	0.36	0.23
			-	-	-	-
B	22	33.1	22.2	7	0.59	0.40
			-	-	-	-
C	42	20.7	15.5	24	0.37	0.28
			-	-	-	-
D	46	18.5	9.3	27	0.33	0.17
	61	11	9.3	38	0.20	0.17
Short hot fire (group 4)						
A	30	19.1	18	4	0.34	0.32
	30	19.1	19.5	15	0.34	0.35
B	20	27.9	22.3	18	0.50	0.40
	20	27.9	31	19	0.50	0.56
C	19	29.2	31	23	0.52	0.56
	19	29.2	30.8	36	0.52	0.55
D	28	20.7	23	37	0.37	0.41
	28	20.7	24.4	40	0.37	0.44
Long Cool fire (group 5)						
A	89	17.4	10.8	12	0.31	0.19
	89	17.4	11	13	0.31	0.20
B	49	29.5	25.7	26	0.53	0.46
	-	-	-	-	-	-
C	56	26.9	22.2	35	0.48	0.40
	56	26.9	22.5	33	0.48	0.40
D	98	16.5	14.1	44	0.30	0.25
	107	15.8	7.5	39	0.28	0.13

6 Sectional analysis

6.1 Methodology

Following completion of the fire tests the residual cross sections were analysed to determine a variety of parameters: the dimensions of the residual cross-sections, the 1-dimensional charring rate, the residual second moment of area and the notional charring rate. Because of uncertainties as to when the charring process actually stopped, the charring rates were calculated based on a duration of burning corresponding to the duration that the furnace was actually 'on', i.e. that the burners were active; as well as the time at which the specimens were actually removed from the furnace. This was typically 6 minutes after the time at which the burners were switched off.

The geometry of the test specimen was 3.3m, with loading points at $1/3^{\text{rd}}$ of the length from the end. From each of these $1/3^{\text{rd}}$ s, a ca. 20 centimetre long piece was cut from the middle of the $1/3^{\text{rd}}$, Figure 6.1. This piece was then squared off at both ends using a circular saw before being cleaned as required. This left, for each beam, depending upon the location of any breakages, 3 x 20 centimetre long sections taken from the middle of each third. Both ends of these sections were then photographed with a scale resting on the top of the section.

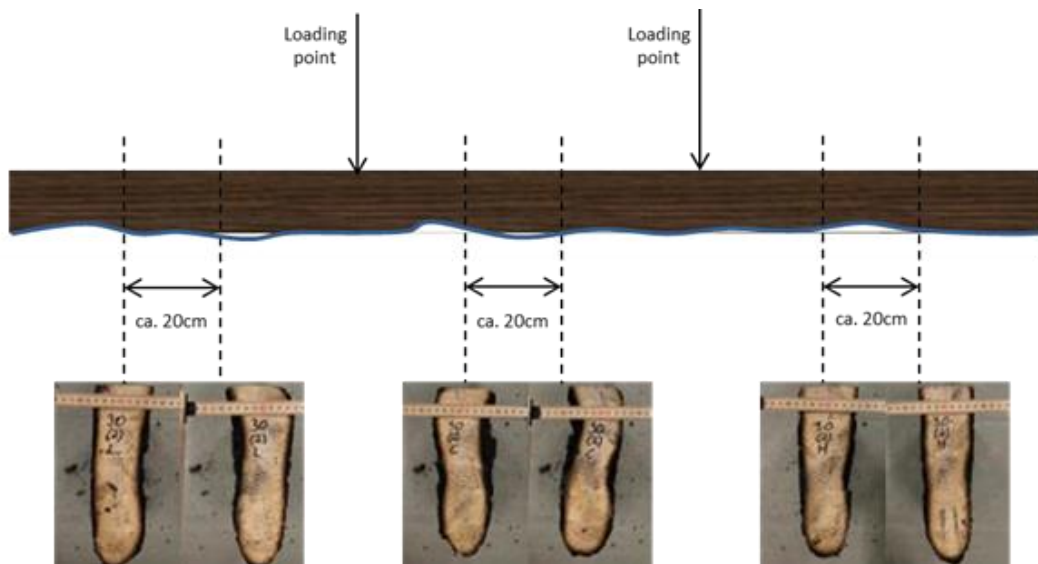


Figure 6.1, locations where sections were cut from the residual timber

Each of these photographs was imported into AutoCAD and scaled based on the reference scale which was placed on top of the section. These photographs were adjusted in order to highlight the transition from charred region to virgin or partially heated region. The image was then used to determine the area, the centroid of the section and the second moment of area of the residual section. The residual depth was also determined as well as the residual width of each individual lamella, measured at the mid-height of every lamella.

In total, therefore, 154 sections were studied, typically comprising 5 residual lamella each (i.e. 1 lamella from each beam had been consumed during the fire tests). The resulting sectional analysis is summarised in appendix 3. Clearly the lower lamella was subject to corner rounding as a result of 2-sided heating and therefore the width of the lower lamella was excluded from any further assessment. It is nevertheless included in the appendices for completeness

Based on the residual second moment of area and the y -ordinate of the centroid of each section, the notional charring rate was estimated by solving the system of equations which define the elastic section modulus, Equation 6.1, based on the residual width, Equation 6.2, and depth, Equation 6.3, of an equivalent rectangular cross section.

$$W = \frac{I}{y} = \frac{b_{fi}d_{fi}^2}{6} \quad (6.1)$$

$$b_{fi} = b - 2\beta_n t_{fi} \quad (6.2)$$

$$d_{fi} = d - \beta_n t_{fi} \quad (6.3)$$

where W is the elastic section modulus, I is the second moment of area, y is the depth to the centroid of the cross section, b is the original breadth of the section, d is the original depth of the section, b_{fi} is the reduced breadth of the section, d_{fi} is the reduced depth of the section, β_n is the notional charring rate and t_{fi} is the duration of the fire test.

6.2 Statistical analysis

Both the Weibull and the Normal distributions were tested on the data for goodness of fit. The R-squared result of a Quartile-Quartile (Q-Q) plot for the normal distribution was compared with the R-squared value of the plot of the log of the data points against $\ln\left(-\ln\left(1 - \hat{F}(x)\right)\right)$, where $\hat{F}(x)$ is the empirical cumulative distribution function, to determine the best distribution of the two to fit to the data. Plotting the data in this way also allowed any statistical outliers to be identified. All apparent outliers were removed from the data sets prior to fitting of the distributions however they are retained in the total data set for comparison in this section.

A summary of the distributions and the R-squared values is shown in table 6.1. Generally both distributions have a good fit to the data. However the Normal distribution better approximates the data in the majority of cases, not only within the individual tests but also across the tests. We have therefore chosen the normal distribution as the distribution for all of the variables arising from the tests. In table 6.1, t_{fi} denotes the time during which the burners were active in the furnace and t_{fi+6} denotes the total time during which the specimens were on the furnace including the time taken to remove the specimens from the furnace. Both the 1-dimensional charring rate, β_0 , and the notional charring rate, β_n , are reported for these times.

The Q-Q plots of all of the variables are all included in appendix 4.

The coefficient of variance (CoV), defined as the ratio of the standard deviation of the normal distribution to its mean, is shown in table 6.2 for all of the variables. There is a clear difference in the CoV between tests 1 and 2 which were both exposed to the standard fire. There are a number of ways of interpreting the differences in CoV, however if fire severity is defined as, e.g. a function of either the total duration or the heating rate, then the CoV tends to increase with increasing fire severity. There are however clearly exceptions to this trend.

Table 6.1, distribution parameters and R-squared values for the results of the sectional analysis

	Residual width (mm)	1-d charring rate, β_o , over t_{fi} (mm/min)	1-d charring rate, β_o , over t_{fi+6} (mm/min)	Residual depth (mm)	Second moment of area (mm ⁴)	Notional charring rate, β_{nr} , over t_{fi} (mm/min)	Notional charring rate β_{nr} , over t_{fi+6} (mm/min)
Test 1							
Normal parameters							
average	55.3	0.7	0.6	213.7	4.00E+07	0.8	0.7
stdev	5.40	0.03	0.03	3.81	3.44E+06	0.03	0.03
RSQ	0.83	0.93	0.93	0.97	0.99	0.99	0.99
Weibull parameters							
alpha	9.9	29.7	29.7	79.2	1.44E+01	37.6	37.6
beta	57.80	0.72	0.66	215.17	4.15E+07	0.82	0.74
RSQ	0.98	0.89	0.89	0.91	0.94	0.92	0.92
Test 2							
Normal parameters							
average	62.7	0.6	0.6	219.2	5.04E+07	0.7	0.7
stdev	6.58	0.04	0.04	4.70	7.31E+06	0.06	0.06
RSQ	0.96	0.92	0.92	0.92	0.90	0.87	0.87
Weibull parameters							
alpha	11.6	18.2	18.2	64.8	8.14E+00	14.5	14.5
beta	65.52	0.66	0.60	221.11	5.35E+07	0.74	0.67
RSQ	0.98	0.93	0.92	0.95	0.93	0.75	0.75
Test 3							
Normal parameters							
average	83.8	0.9	0.8	231.2	8.04E+07	1.0	0.9
stdev	5.25	0.06	0.05	3.97	5.85E+06	0.12	0.05
RSQ	0.97	0.98	0.98	0.97	0.93	0.83	0.93
Weibull parameters							
alpha	20.3	18.9	18.9	82.6	1.72E+01	10.2	23.3
beta	86.00	0.95	0.79	232.76	8.28E+07	1.07	0.91
RSQ	0.96	0.97	0.97	0.98	0.82	0.92	0.98
Test 4							
Normal parameters							
average	68.8	0.3	0.3	221.5	5.78E+07	0.36	0.35
stdev	9.85	0.03	0.03	4.52	6.98E+06	0.02	0.02
RSQ	0.97	0.97	0.97	0.99	0.96	0.92	0.92
Weibull parameters							
alpha	8.3	14.3	8.1	68.5	9.93E+00	20.2	20.2
beta	72.9	0.3	0.3	223.3	6.07E+07	0.37	0.35
RSQ	0.99	0.98	0.97	0.96	0.88	0.96	0.96

Table 6.2, coefficient of variation of the variables assuming normal distribution

	Residual width (mm)	1-d charring rate, β_0 , over t_{fi} (mm/min)	1-d charring rate, β_0 , over t_{fi+6} (mm/min)	Residual depth (mm)	Second moment of area (mm ⁴)	Notional charring rate, β_n , over t_{fi} (mm/min)	Notional charring rate β_n , over t_{fi+6} (mm/min)
Test 1	9.77%	4.49%	4.49%	1.79%	8.58%	3.55%	3.55%
Test 2	10.49%	6.92%	6.92%	2.15%	14.50%	8.51%	8.51%
Test 3	6.26%	6.67%	6.67%	1.72%	7.27%	11.77%	5.50%
Test 4	14.32%	8.63%	8.63%	2.04%	12.07%	5.56%	5.71%

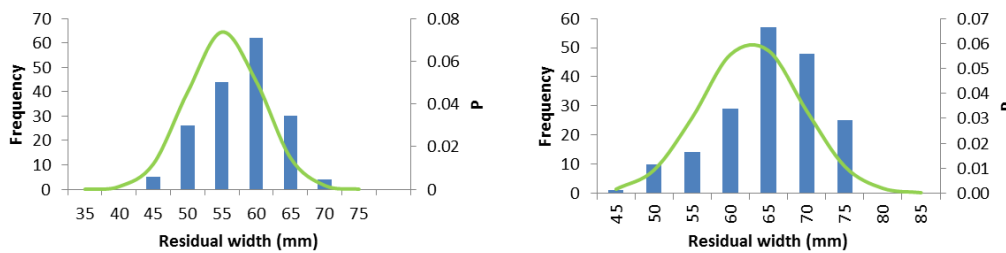
6.3 Standard fire tests

Since there were two fire tests conducted with the standard fire curve, there are two sets of data available for this test. A comparison between the results of these two tests in Table 6.1 and table 6.2 however suggests differences in all of the distributions between the tests. This suggests that the two sets of results cannot simply be merged and indicates poor repeatability between the tests, as well as differences in the mean values from the two tests there are significant differences in the variance - with the standard deviation of the results from test two being systematically higher than those from test 1.

In the following sections, the distributions described in table 6.1 for the standard fire are reproduced along with histograms of the raw data.

6.3.1 1-dimensional charring rate

The residual width of the individual lamella, determined according to the procedure described in section 6.1 is shown in Figure 6.2 for both test 1 and test 2, the standard fire tests. Based on the measured lamella thicknesses and the duration of the fire test – in this case 60 minutes, the 1-dimensional charring rate is shown in figures 6.2 and 6.3, again for both tests 1 and 2. Figure 6.3 shows the 1-dimensional charring rate assuming that the charring stops after the furnace is switched off, i.e. the duration of burning is 60 minutes. Figure 6.4 shows the same charring rate assuming that the charring stops once the specimens are lifted off the furnace and the first water is applied, i.e. the duration of burning is 66 minutes. Figure 6.5 shows the distribution of residual depth from all of the sections which were studied.

**Figure 6.2, distribution of residual width, left test 1; right test 2**

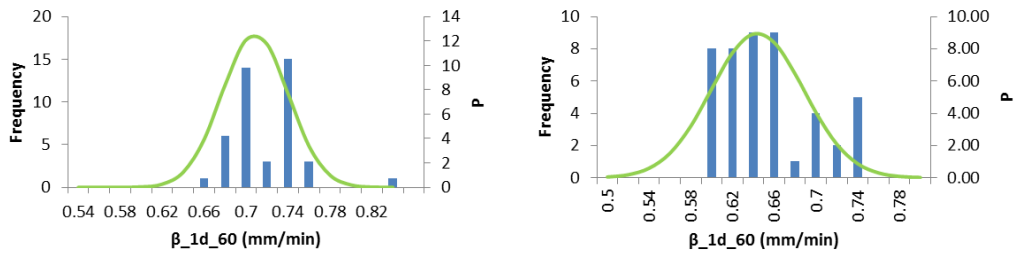


Figure 6.3, distribution of 1-dimensional charring rate assuming a burning duration of 60 minutes, left test 1; right test 2

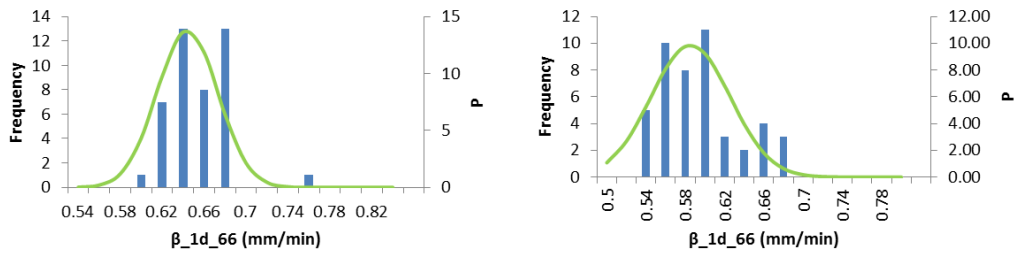


Figure 6.4, distribution of 1-dimensional charring rate assuming a burning duration of 66 minutes, left test 1; right test 2

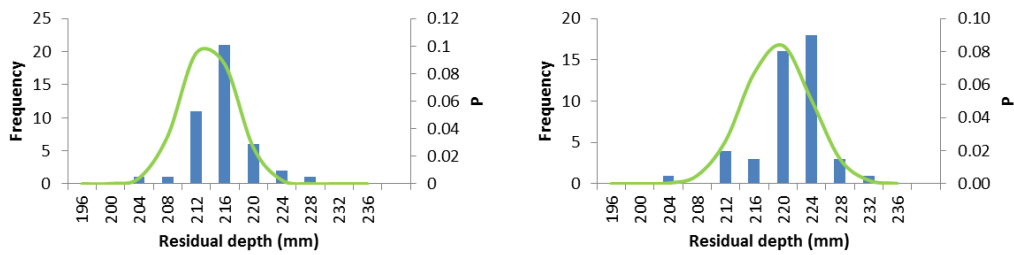


Figure 6.5, distribution of residual depth of the section, left test 1; right test 2

6.3.2 Second moment of area

The distribution of second moment of area from both tests 1 and 2 is shown in Figure 6.6.

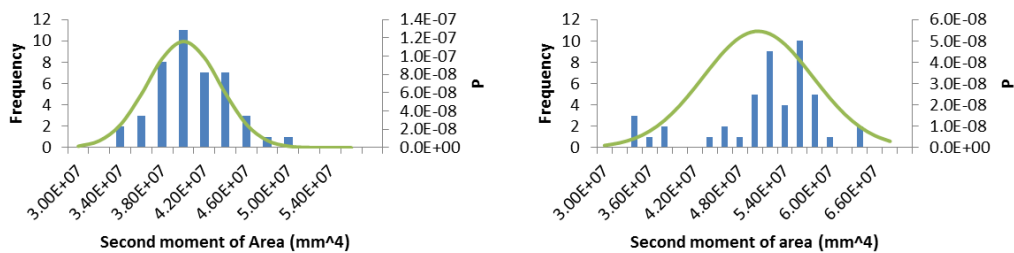


Figure 6.6, distribution of second moment of area, left test 1; right test 2

6.3.3 Notional charring rate

The notional charring rate, based on the properties of the residual section, are shown in Figure 6.7 and 6.8 for tests 1 and 2. Again, two charring rates are reported under both the assumption that the charring stops when the furnace burners are turned off and that the charring stops upon first application of water, after 60 and 66 minutes respectively.

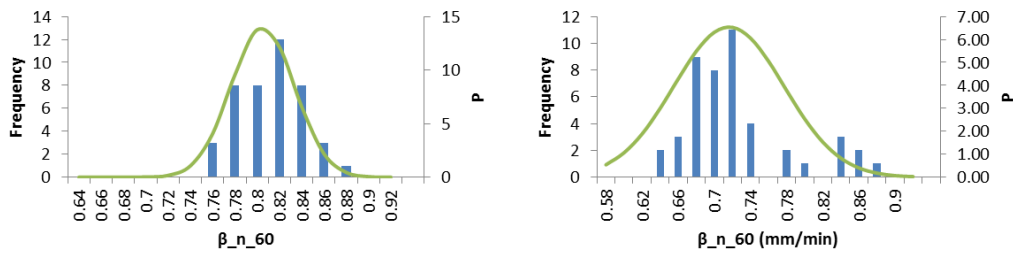


Figure 6.7, distribution of notional charring rate assuming a burning duration of 60 minutes, left test 1; right test 2

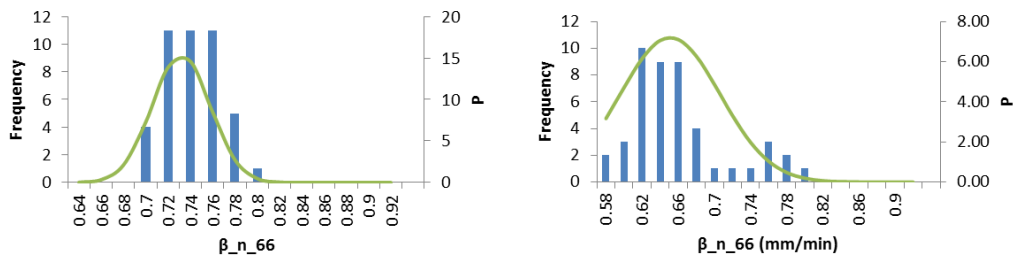


Figure 6.8, distribution of notional charring rate assuming a burning duration of 66 minutes, left test 1; right test 2

6.4 Short hot fire

This section contains reproductions of the histograms and resulting distributions for the variables studied in the sectional analysis from the short-hot fire test.

6.4.1 1-dimensional charring rate

The distribution of residual width of the individual lamella are shown in Figure 6.9, Figures 6.10 and 6.11 show the resulting estimates of the 1-dimensional char rates. Again, 6.10 is based on the assumption that the charring stops at the moment the furnace burners are switched off, i.e. after 30 minutes. Figure 6.11 is based on the assumption that charring stops upon first application of water, after a further 6 minutes. Figure 6.12 shows the distribution of the residual depth of the sections.

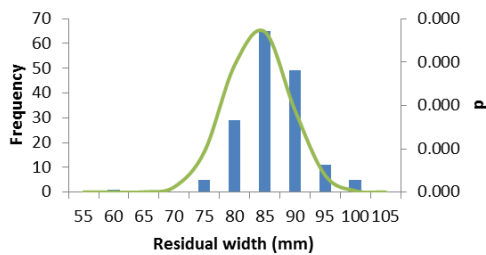


Figure 6.9, distribution of residual width

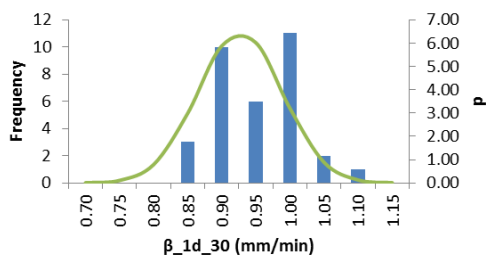


Figure 6.10, distribution of 1-dimensional charring rate assuming a burning duration of 30 minutes

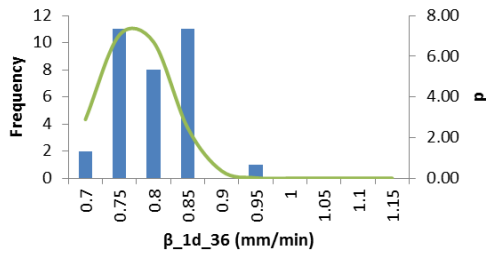


Figure 6.11, distribution of 1-dimensional charring rate assuming a burning duration of 36 minutes

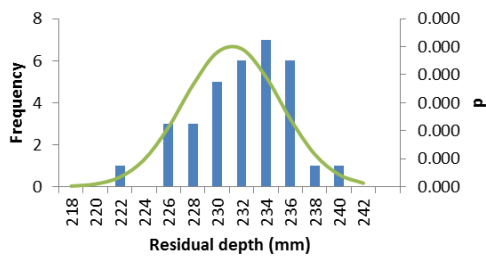


Figure 6.12, distribution of residual depth of the section

6.4.2 Second moment of area

The distribution of second moment of area at the end of the test is shown in Figure 6.13.

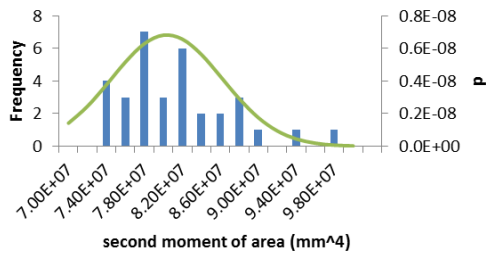


Figure 6.13, distribution of second moment of area

6.4.3 Notional charring rate

The distributions of notional charring rate in the short-hot fire, based on the sectional analysis are shown in figures 6.14 and 6.15. Again these are based on two different durations of charring, 30 minutes and 36 minutes respectively.

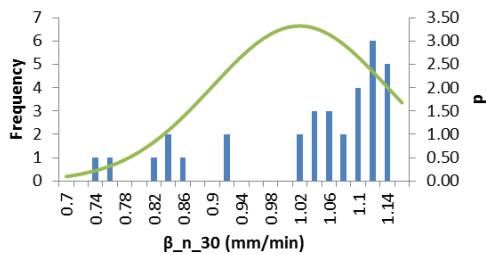


Figure 6.14, distribution of notional charring rate assuming a burning duration of 30 minutes

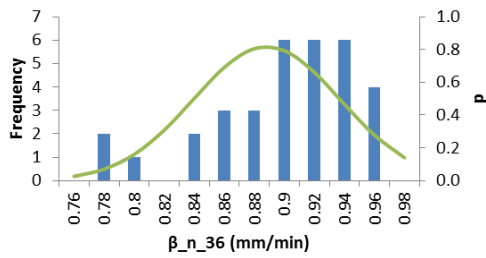


Figure 6.15, distribution of notional charring rate assuming a burning duration of 36 minutes

6.5 Long cool fire

This section contains reproductions of the histograms and resulting distributions for the variables studied in the sectional analysis from the long-cool fire test.

6.5.1 1-dimensional charring rate

The distribution of residual width of the individual lamella are shown in Figure 6.16, Figures 6.17 and 6.18 show the resulting estimates of the 1-dimensional char rates. As with the other 3 tests, 6.16 is based on the assumption that the charring stops after 107 minutes at the moment the furnace burners are switched off. Figure 6.18 is based on the assumption that charring stops 6 minutes later once water is applied. Figure 6.19 shows the distribution of the residual depth of the sections.

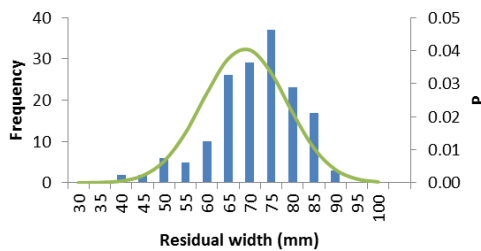


Figure 6.16, distribution of residual width

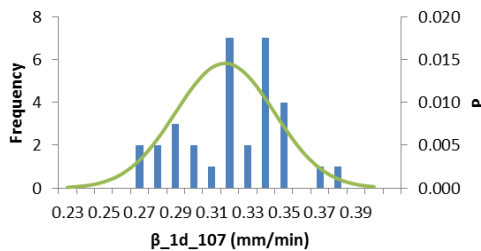


Figure 6.17, distribution of 1-dimensional charring rate assuming a burning duration of 107 minutes

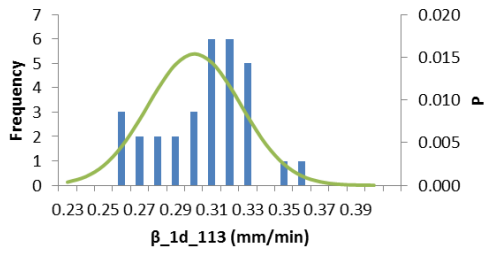


Figure 6.18, distribution of 1-dimensional charring rate assuming a burning duration of 113 minutes

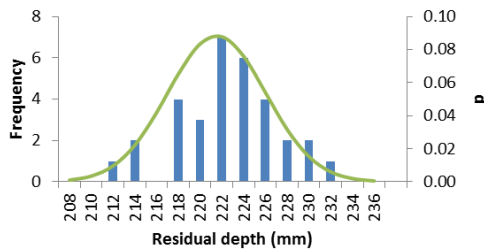


Figure 6.19, distribution of residual depth of the section

6.5.2 Second moment of area

The distribution of second moment of area of the sections is shown in Figure 6.20.

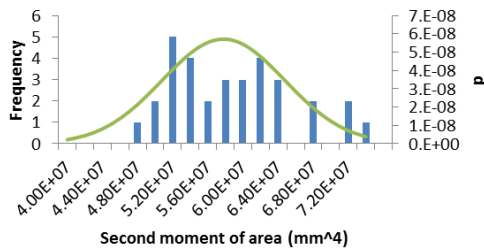


Figure 6.20, distribution of second moment of area

6.5.3 Notional charring rate

Figure 6.21 and 6.22 show the notional charring rate of the sections, estimated based on the residual cross sections and assuming charring stops after the burners are switched off, at t=107 minutes, and after first application of water, at t=113 minutes, respectively.

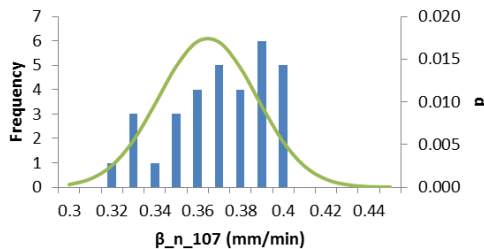


Figure 6.21, distribution of notional charring rate assuming a burning duration of 107 minutes

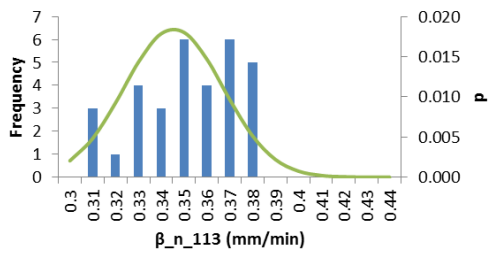


Figure 6.22, distribution of notional charring rate assuming a burning duration of 113 minutes

6.6 Comparison of 1-d char rates with char rates based on temperature measurements

In this section the 1-d char rates which were measured from the residual cross section are plotted along with the 1-d char rates estimated based on the temperature measurements reported in section 5. As in section 6, the estimated charring rates based on temperature measurement have been extrapolated to the deepest thermocouple in all of the tests. In none of the tests did the char front reach the depths implied here – the time to reach the depths suggested has simply been extrapolated from the rate of progression of the char front at the end of the test.

The results for fire test 1 are plotted in Figure 6.23. The error bars indicate the coefficient of variation. Figures 6.24 to 6.26 show the results for fire tests 2 to 4. Both charring rates from the sectional analysis are plotted, assuming that charring stops when the furnace burners are switched off, and also that it continues until the first application of water 6 minutes later.

It can be seen that in all cases the methods are reasonably consistent when predicting the charring rate. The uncertainty implied by the temperature measurements is considerably higher than the uncertainty implied by the reduced cross section analysis. Variations in measured temperatures may be a result of local properties of the material itself as well as errors in the positioning of the thermocouples.

Nevertheless, the 1-dimensional charring rates for the standard fire agree conservatively with the charring rate given in EN 1995-1-2 of 0.65mm/min for softwood and glulam timber with a density of over 290 kg/m³.

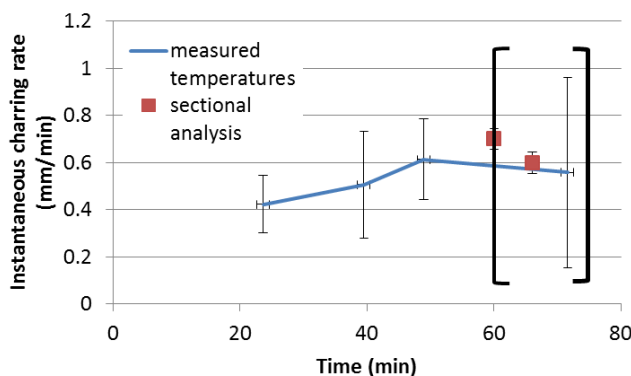


Figure 6.23, 1-dimensional charring rate in fire test 1, based on measured temperatures and the residual section (brackets denote the region where linear extrapolation is used to estimate charring rate based on temperature measurements since the fire test had already stopped)

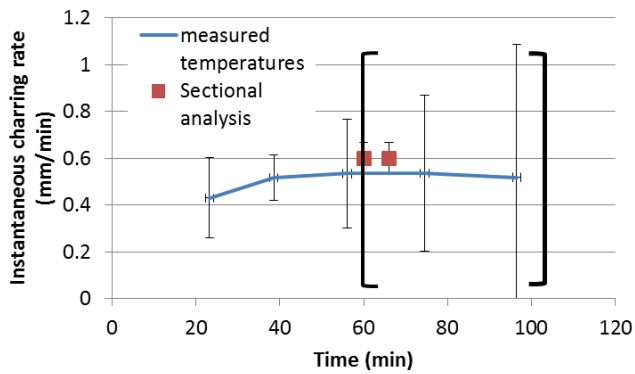


Figure 6.24, 1-dimensional charring rate in fire test 2, based on measured temperatures and the residual section (brackets denote the region where linear extrapolation is used to estimate charring rate based on temperature measurements since the fire test had already stopped)

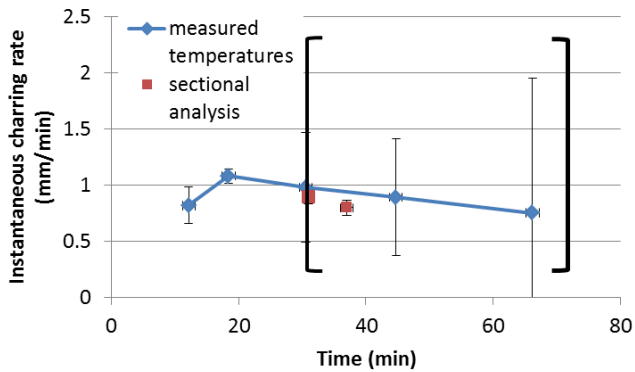


Figure 6.25, 1-dimensional charring rate in fire test 3, based on measured temperatures and the residual section (brackets denote the region where linear extrapolation is used to estimate charring rate based on temperature measurements since the fire test had already stopped)

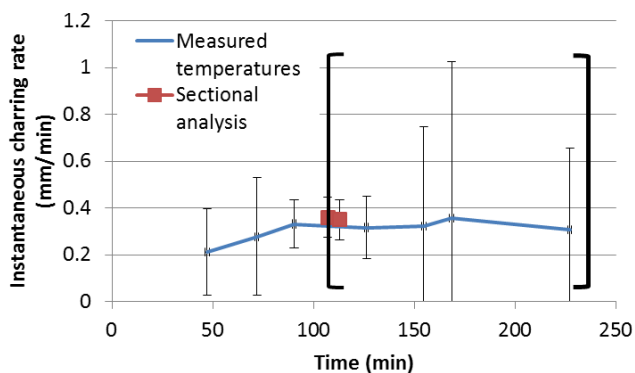


Figure 6.26, 1-dimensional charring rate in fire test 4, based on measured temperatures and the residual section (brackets denote the region where linear extrapolation is used to estimate charring rate based on temperature measurements since the fire test had already stopped)

6.7 Discussion

Much of the data which is presented in this section is based on an analysis of the charred cross section after the fire tests. As such, there is an inevitable degree of subjectivity to the results. However because of the large number of sections evaluated after the tests it may be reasonably expected that the resulting distributions are representative of the real response. A comparison between the 1-dimensional charring rate based on the sectional analysis and the measured temperatures also support the methodology used.

In evaluating the data, we tried both the Weibull and the normal distribution. Both distributions were evaluated on a Q-Q plot for goodness of fit with the data. In the case of the Weibull distribution, the resulting distribution was linearised prior to checking the goodness of fit. Both distributions fit well with an R-squared value of over 0.9, however the normal distribution tended to have a better fit in the majority of cases once outliers had been removed. As such the normal distribution is concluded to better represent the statistical variations in the results of the tests.

The coefficient of variation varies between the results of the two standard fire tests, and is typically higher for the second fire test than the first. Nevertheless, the coefficient of variation appears to increase for almost all of the variables evaluated with increasing duration of fire exposure.

7 Application of measured and estimated charring rates to loading calculations

7.1 Notional charring rates

The measured notional charring rates are applied to the prediction of the load until failure shown earlier. In this case, the notional charring rate used for prediction is the mean value. Results from fire tests 2, 3 and 4 are shown in Figures 7.1, 7.2 and 7.3 respectively. In these calculation we assume a zero strength layer of 7mm for all fires, as before. For both the standard fire and the long-cool fire the prediction is still higher than the measured failure loads during the tests, even accounting for the distribution of the charring rate. The distribution is indicated on the figures as the error bars which indicate the boundaries of the predicted load until failure using the 5th or the 95th percentile of the charring rate. In these examples there is no adjustment made in accordance with equation 1.6 to the charring rate, which is assumed constant for the entire fire. In fact, the fit is only marginally better than the fits in figures 5.37, 5.38 and 5.39. It can be seen that the uncertainty associated with the notional charring rate does not account for the discrepancy.

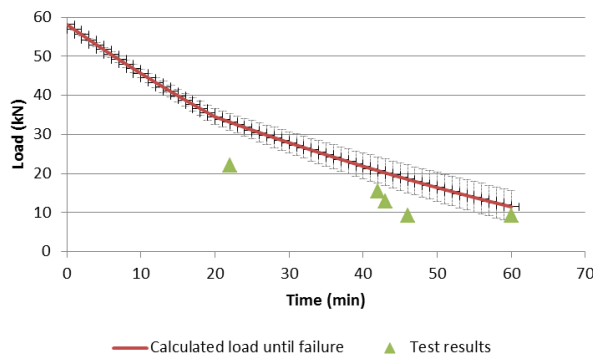


Figure 7.1, predicted failure load of beams based on measured notional charring rate applied to fire test 2 (the error bars represent the load calculated using the 5th and the 95th percentile of the notional charring rate)

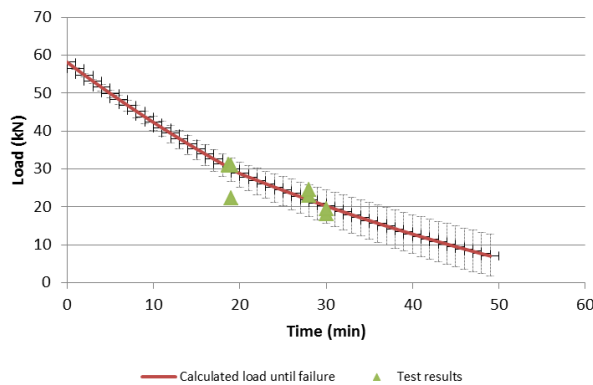


Figure 7.2, predicted failure load of beams based on measured notional charring rate applied to fire test 3 (the error bars represent the load calculated using the 5th and the 95th percentile of the notional charring rate)

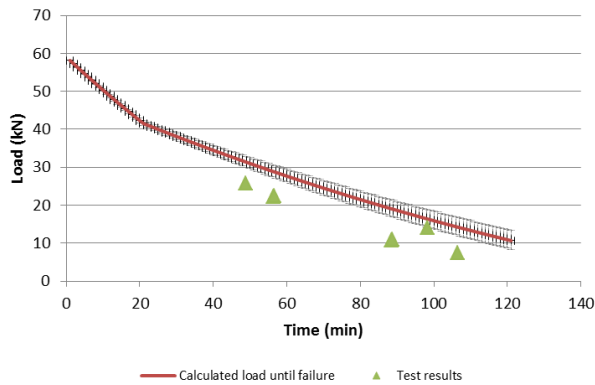


Figure 7.3, predicted failure load of beams based on measured notional charring rate applied to fire test 4 (the error bars represent the load calculated using the 5th and the 95th percentile of the notional charring rate)

The uncertainty associated with the yield strength of the sections is shown added to the uncertainty associated with the charring rate in Figures 7.4, 7.5 and 7.6. It can be seen that the combined uncertainty in charring rate and timber strength does not account for the differences between the measured load until failure and the predicted load until failure.

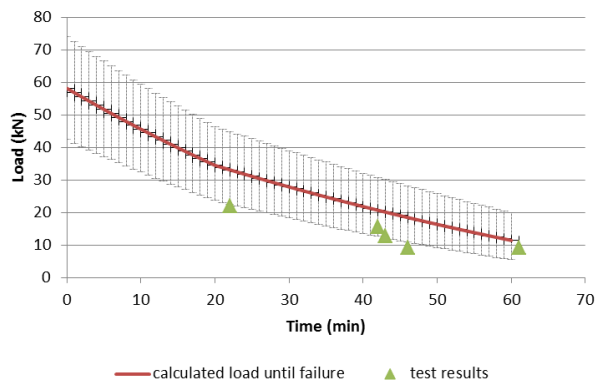


Figure 7.4, predicted failure load of beams based on measured notional charring rate applied to fire test 2 (the error bars represent the load calculated using the 5th and the 95th percentile of the notional charring rate and the yield strength in bending)

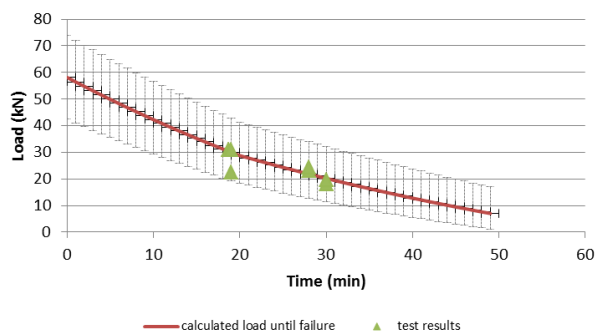


Figure 7.5, predicted failure load of beams based on measured notional charring rate applied to fire test 3 (the error bars represent the load calculated using the 5th and the 95th percentile of the notional charring rate and the yield strength in bending)

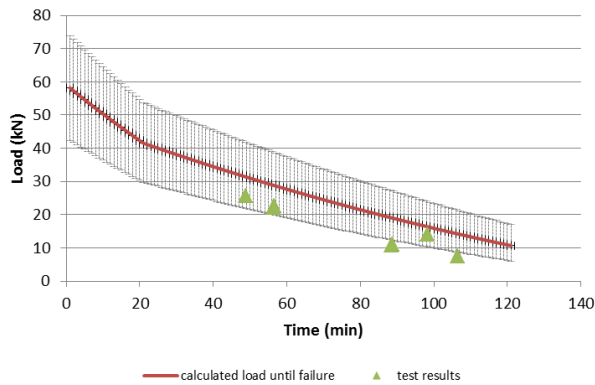


Figure 7.6, predicted failure load of beams based on measured notional charring rate applied to fire test 4 (the error bars represent the load calculated using the 5th and the 95th percentile of the notional charring rate and the yield strength in bending)

In order to improve the fit the zero-strength layer is therefore adjusted. Since this is intended to account for the loss of strength in timber which is heated although not yet charred, it is logical that for a long-cool fire there will be preheating of the timber to a greater depth and therefore a deeper zero-strength layer. Conversely, for a short-hot fire there will be a shallower zero-strength layer as a result of the steeper thermal gradient. This assumption is supported by the temperature data reported in chapter 5.

In order to determine the mean zero strength layer in each of the fire tests, the procedure described in reference [17] is followed. Firstly, an exponential relationship with time is fitted to the ratios of the failure loads with the ambient failure loads. Corrected failure loads are then calculated to correct for variations in the strength of the timber. The zero strength layer is then recalculated based on the corrected loads to failure assuming the constant charring rate determined in the sectional analysis. The exponential relationship provides the best fit to the experimental results, bearing in mind that at time $t=0$ the load ratio must be 1 (the reduced cross section method results in a bilinear relationship between time and load to failure of the beams). The resulting parameters are shown in table 7.1, including the adjusted zero strength layer depth, d_0 , and the notional charring rate which was used for these calculations. The uncorrected zero-strength layer values shown in Figure 7 a, b and c vary considerably and suggest that the calculation of zero-strength layer is quite sensitive.

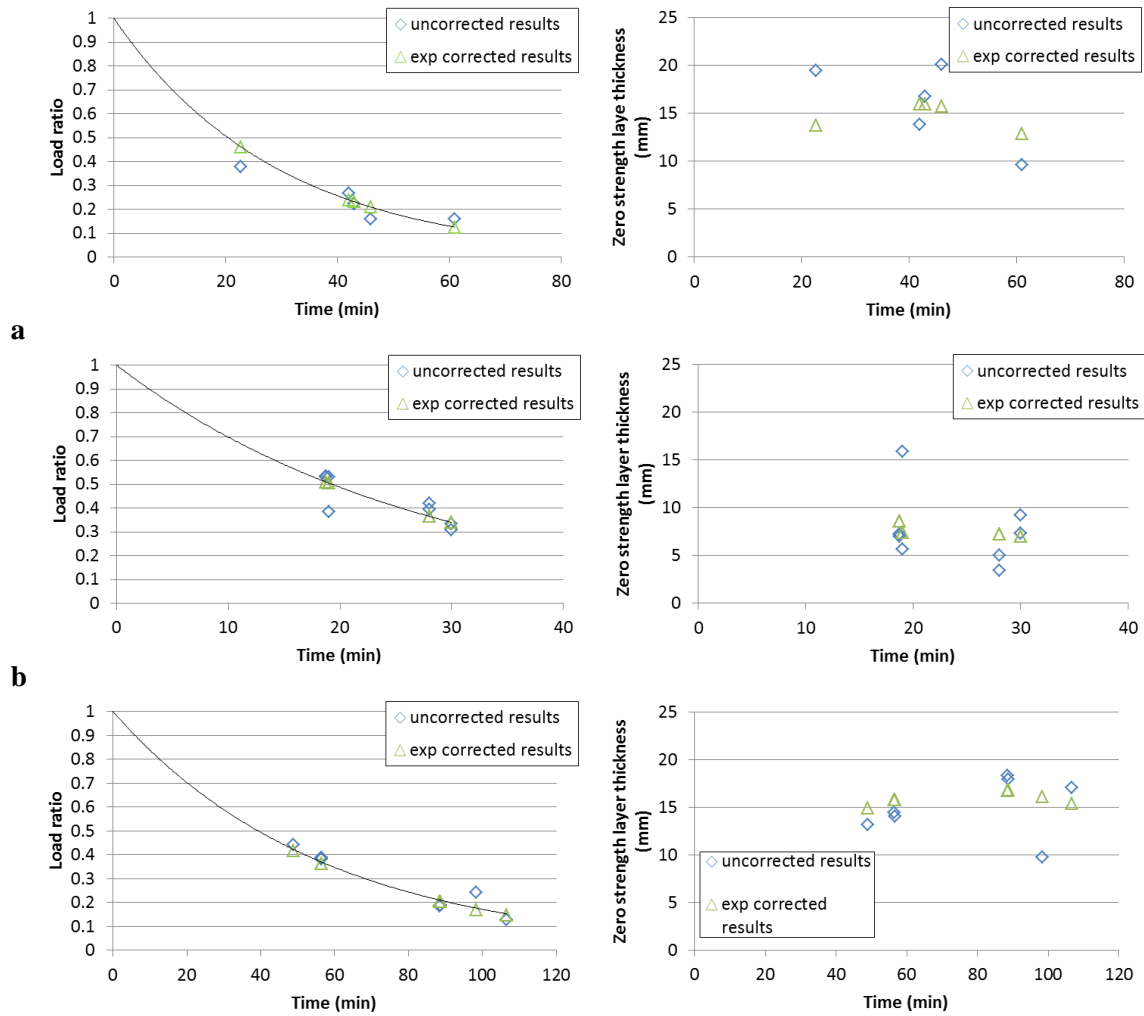


Figure 7.7, loads to failure corrected to fit an exponential function and the resulting zero-strength layer; a) fire test 2, b) fire test 3; and c) fire test 4

Table 7.1, parameters for calculation of load until failure based on measured results for each test

Test number	β_n average (mm/min)	β_n standard deviation (mm/min)	d_0 average (mm)	d_0 standard deviation (mm)
2	0.72	0.06	14.8	1.45
3	1.02	0.12	7.6	0.67
4	0.36	0.02	16.0	0.68

Results of the application of these corrected zero strength layers to the predicted load until failure are plotted in figures 7.8, 7.9 and 7.10. A far better correlation can be seen and the variations between the test results and the predicted loads until failure are now fully enclosed between the 9th and 95th percentiles of the predicted loads to failure.

Of note in these figures is the increasing width of the error bars with heating rate of the fire. The long-cool parametric fire has the lowest uncertainty associated with the load prediction whereas the short-hot parametric fire, with the more aggressive heating rate, has a larger variance associated with the results.

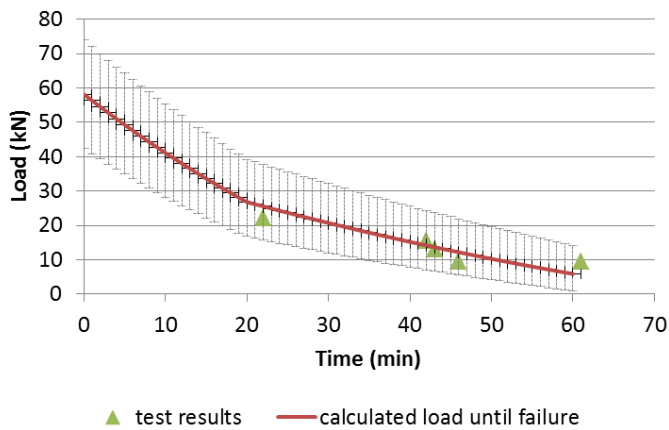


Figure 7.8, load until failure in fire test 2 based on mean notional charring rate corrected by adjusting the zero-strength layer (the error bars represent the load calculated using the 5th and the 95th percentile of the notional charring rate, the zero strength layer and the strength of the sections)

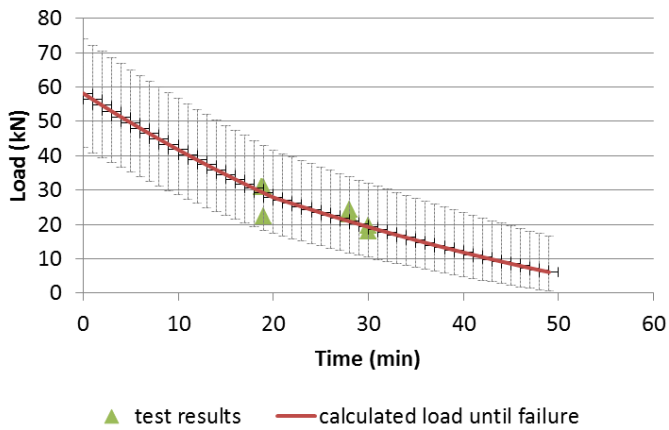


Figure 7.9, load until failure in fire test 3 based on mean notional charring rate corrected by adjusting the zero-strength layer (the error bars represent the load calculated using the 5th and the 95th percentile of the notional charring rate, the zero strength layer and the strength of the sections)

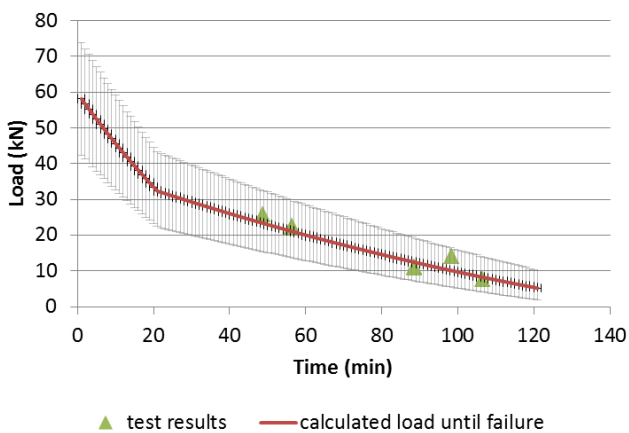


Figure 7.10, load until failure in fire test 4 based on mean notional charring rate corrected by adjusting the zero-strength layer (the error bars represent the load calculated using the 5th and the 95th percentile of the notional charring rate, the zero strength layer and the strength of the sections)

7.2 1-dimensional charring rates

In order to estimate the residual capacity of the timber beams using the measured 1-dimensional charring rates, the residual cross section was evaluated considering the corner rounding. The radius of corner rounds was assumed to be equal to the charred depth. Figures 7.13, 7.14 and 7.15 show the predicted failure loads of the beams plotted against the experimental results from fire tests 2, 3 and 4 respectively. The predictions are based on the measured one-dimensional charring rates from the cross-sectional analysis. As with the plots of the predicted strength using the notional charring rate presented in the previous section, the error bars in these figures represent the load required to failure using a combination of the 5th and the 95th percentile of the charring rate and the strength in bending respectively for the positive error bars; and vice versa for the negative error bars. The zero strength layer which was used in these calculations is 7mm.

It can be seen in all of the figures that the results of the experiment fit well with the predicted results. However, Figures 7.11 and 7.13 show that the mean prediction is generally a non-conservative prediction in comparison with the experimental results for fire tests 2 and 4 (the standard fire and the long-cool fire). Conversely, the mean prediction in fire test 3 corresponds well with the experimental results. These all agree generally with the trend observed with the load until failure calculated using the notional charring rate using a zero strength layer of 7mm.

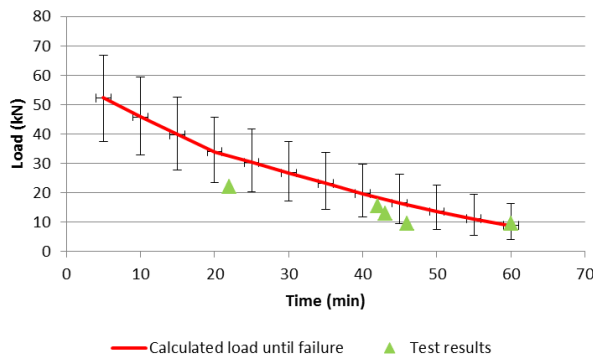


Figure 7.11, load until failure for fire test 2 calculated based on mean 1-dimensional char rate determined from the residual cross section (the error bars represent the load calculated using the 5th and the 95th percentile of the notional charring rate and the yield strength in bending)

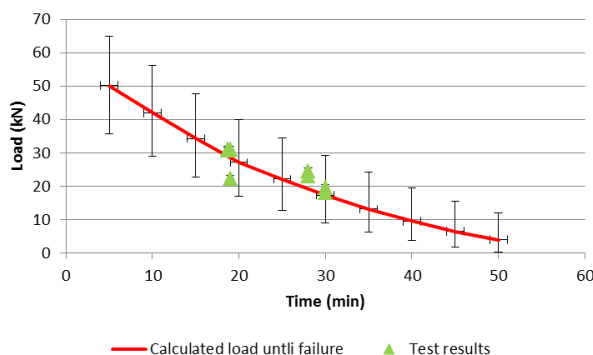


Figure 7.12, load until failure for fire test 3 calculated based on mean 1-dimensional char rate determined from the residual cross section (the error bars represent the load calculated using the 5th and the 95th percentile of the notional charring rate and the yield strength in bending)

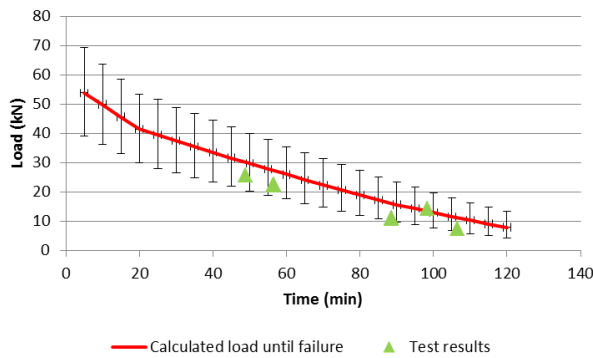


Figure 7.13, load until failure for fire test 4 calculated based on mean 1-dimensional char rate determined from the residual cross section (the error bars represent the load calculated using the 5th and the 95th percentile of the notional charring rate and the yield strength in bending)

Figures 7.14, 7.15 and 7.16 show the same calculations repeated for fire tests 2, 3 and 4 respectively but this time accounting for the calculated zero strength layer thickness from Table 7.1. Once more, the inclusion of the corrected zero strength layer results in the calculated load until failure being far closer to the test results in all cases, with the average predictions no longer being unconservative.

Comparison of Figures 7.8, 7.9 and 7.10 with Figures 7.14, 7.15 and 7.16 respectively in fact shows that the use of the 1-dimensional charring rate may be slightly more conservative than the use of the notional charring rate when using the same zero strength layer thickness.

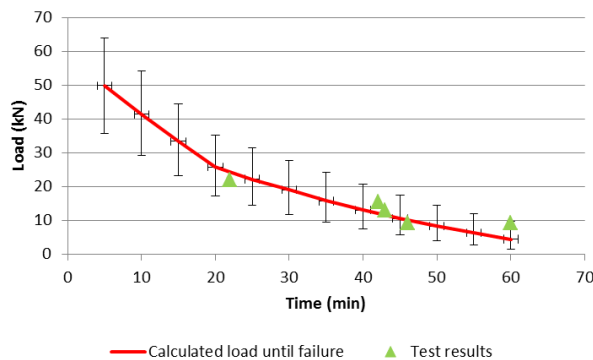


Figure 7.14, load until failure for fire test 2 calculated based on mean 1-dimensional char rate determined from the residual cross section including the calculated zero strength layer thickness from table 7.1 (the error bars represent the load calculated using the 5th and the 95th percentile of the notional charring rate and the yield strength in bending)

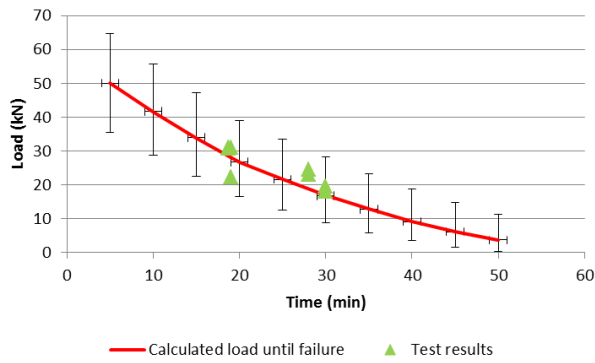


Figure 7.15, load until failure for fire test 3 calculated based on mean 1-dimensional char rate determined from the residual cross section including the calculated zero strength layer thickness from table 7.1 (the error bars represent the load calculated using the 5th and the 95th percentile of the notional charring rate and the yield strength in bending)

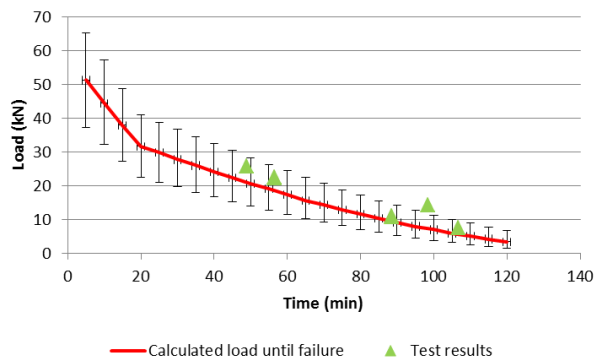


Figure 7.16, load until failure for fire test 4 calculated based on mean 1-dimensional char rate determined from the residual cross section including the calculated zero strength layer thickness from table 7.1 (the error bars represent the load calculated using the 5th and the 95th percentile of the notional charring rate and the yield strength in bending)

8 Reliability calculations

8.1 Overview of reliability

To summarise the concept of reliability, the standard stress-strength model is shown in Figure 8.1. The load on the system is represented by normally distributed random variable Q , and the resistance of the system is represented by normally distributed random variable R . The probability of failure of the system is the probability that the resistance will be less than the load, i.e.

$$P_f = P(R < Q) \quad (8.1)$$

For some characteristic value, Q^* , of Q , this is:

$$P_f = P(R < Q) = \int_{Q^*}^{\infty} R dLoad \quad (8.2)$$

or, where Q is also unknown:

$$P_f = P(R < Q) = \int_{-\infty}^{\infty} \int_Q^{\infty} R Q d^2 Load \quad (8.3)$$

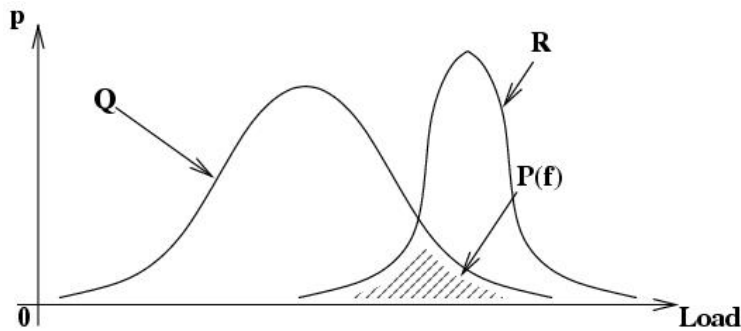


Figure 8.1, standard stress-strength model

The reliability of a system, S_R , is the probability that the strength is greater than the stress on the system, i.e. $S_R = P(Q < R)$ [20].

$$S_R = P(Q < R) = \int_{-\infty}^R Q dLoad \quad (8.4)$$

$$S_R = P(Q < R) = \int_{-\infty}^{\infty} \int_{-\infty}^R Q R d^2 Load \quad (8.5)$$

8.2 Margin of safety and reliability index

The margin of safety is the margin between the load and the resistance of the system. For characteristic values of these, Figure 8.2, this is:

$$M = R^* - Q^* \quad (8.6)$$

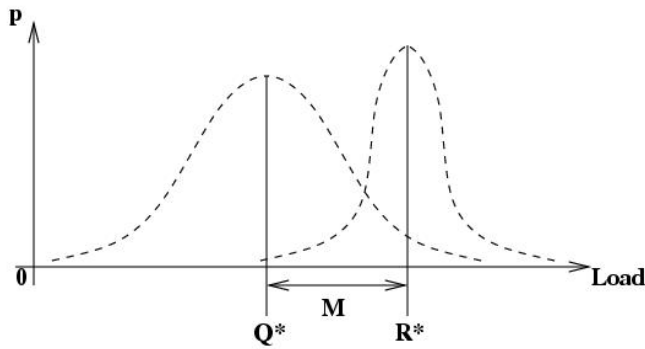


Figure 8.2, margin of safety is the margin between the resistance and the load

For normally distributed values of Q and R , the margin of safety is also normally distributed and has mean and variance:

$$\mu_M = \mu_R - \mu_Q \quad (8.7)$$

$$\text{Var}(M) = \sigma_M^2 = \sigma_R^2 + \sigma_Q^2 \quad (8.8)$$

The Hassofer Lind reliability index, β , is then defined as the number of standard deviations of the margin of safety between its mean and 0, Figure 8.3:

$$\beta = \frac{\mu_M}{\sigma_M} \quad (8.9)$$

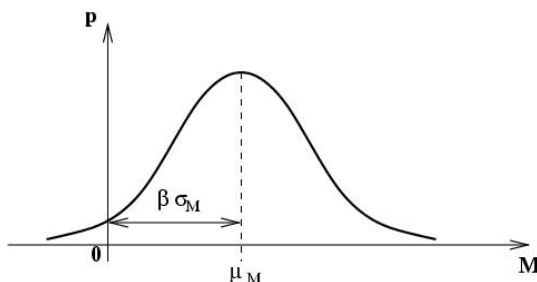


Figure 8.3, β is the number of standard deviations between the mean of the margin of safety and 0

8.3 Reliability of timber structures in fire

Research on the estimation of probabilistic response of structures includes the use of analytical or first order reliability models [19] [20] as described in the Eurocode basis of structural design [21]; as well as Monte Carlo techniques [22]. Random sampling can be both computationally expensive and time consuming since the number of calculations required increases with the number of variables in the system. In the case of estimating reliability using the reduced cross section method applied to timber structures exposed to fire however random sampling is a reasonable approach since the calculation methods are computationally inexpensive.

In order to illustrate the effect of fire scenario in timber reliability, a simple analysis was carried out using random sampling to vary the specimens. Results are presented in Figure 8.4 using the notional charring rate. In the analysis, 1000 individual samples were taken at each of the time points shown. Parameters varied in the analysis were the depth of the zero strength layer, the notional charring rate and the strength of the timber specimen. The distributions of these variables were taken from the appropriate sections of this

report, and in each sample at each time step all of the variables were resampled. In all cases the design bending moment was assumed to be deterministic and was taken to be 46% of the mean load ratio at ambient.

Both of the tests exposed to a standard fire start off with a reliability index of about 2.5. It can be seen in figure 8.4 that the reliability index of the timber in these tests have very similar variation with time. In both cases, the reliability index reduces to 0 at between 23 and 27 minutes into the fire tests. Test 2 which had a higher mean notional charring rate and a lower coefficient of variation in the notional charring rate has a faster rate of decline in reliability than test 1. Comparing the reliability when the timber is exposed to the long-cool and the short-hot fire with the reliability when the timber is exposed to the standard fires, it can be seen that the reliability of the timber exposed to the short-hot fire reduces to zero marginally quicker than the timber exposed to the standard fires, however because of the smaller zero-strength layer it has a higher initial reliability and actually endures for as long as the standard fire in this case and the reliability index reduces to zero after approximately 26 minutes. However, the long-cool fire endures a significantly longer duration of burning before the reliability index tends to zero, 50 minutes – nearly double the time as compared to the cases where timber is exposed to the standard fire.

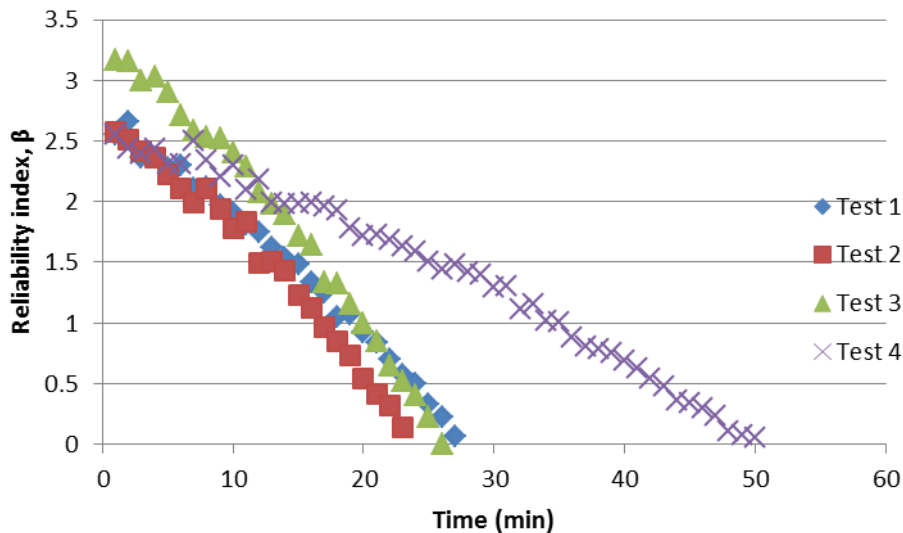


Figure 8.4, reliability index of timber beams exposed to the different fires using notional charring rates to determine the capacity

For comparison, the same calculation was repeated, using the 1-dimensional charring rates and accounting for corner rounding by assuming that the corners have the same radius as the depth of the char layer. The results of this calculation are shown in figure 8.5. Using this slightly more refined method yields little difference in the calculated reliability index of the beams exposed to the different temperature time curves. Test 1 has a reliability of 0 after 23 minutes, test 2 after 27 minutes, test 3 after 26 minutes and test 4 has a reliability of 0 after 50 minutes.

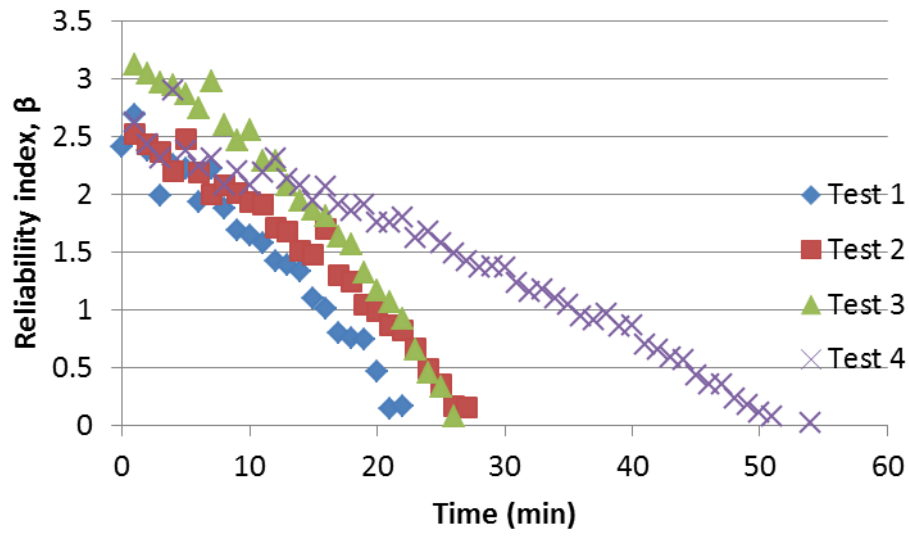


Figure 8.5, reliability index of timber beams exposed to the different fires using 1-dimensional charring rates to determine the capacity

9 Discussion and conclusions

This report has detailed a series of tests carried out on a large number of timber elements on a horizontal fire resistance furnace. The resulting output from the tests performed comprised not only a large amount of statistical information as to the global response of the elements themselves exposed to fire, but also the charring rate measured with both thermocouples and using a sectional analysis performed over multiple samples cut from the timber beams following the tests.

During the testing, some plate thermometers were placed between the beams facing the adjacent beam, whereas some were placed facing the nearest parallel wall. No significant difference was seen between the two sets of measurements. It is therefore concluded that influence from adjacent specimens burning is minimal on the results of the tests for the configuration described.

The different methods which are used to estimate the charring rate yield similar results, but with vastly different degrees of uncertainty. For example, the charring rates estimated using the temperature measurements taken from within the beams do give an indication of the charring rate over time, but the impact of localised features such as fissuring in the char layer, as well as possibly small errors in thermocouple placement contribute to a significant variation in the charring rates estimated using this method. Conversely, 1-dimensional charring rates estimated based on the sectional analysis which followed the tests had comparatively low variance and the means agreed well. Clearly though, the sectional analysis could only reveal time averaged information about the charring rate until the end of the fire tests.

It is shown that timber elements exposed to fire have generally a large variation in their response, even when the reference testing suggests that the timber has relatively similar properties. This is possibly due to variations in the density of the individual lamella, although no study was carried out of this, and this should be verified.

The resistance of the specimens which were used in the tests reported here was calculated based on the reduced cross section method described in Eurocode 5. This method was extended in this report to include timber elements exposed to parametric fires, often used in design for steel and concrete buildings, although not currently used for the design of timber buildings for fire. Although Eurocode 5 does describe variations to the charring rate of timber exposed to natural fires, the key feature of the reduced cross-section method, the zero-strength layer, has never been characterised for parametric fires. Through comparison between the test results and predicted results of the timber elements resistance to bending, the zero strength layer depth for timber elements exposed to parametric fires is deduced. This layer is found to decrease with increasing heating rate, or 'aggression' of fire scenario, while the variance in the thickness of the layer increases with the same. Further, it is found that the zero strength layer thickness of 7 mm, prescribed by Eurocode 5 for elements in bending exposed to the standard fire is unconservative for the case studied here, and a more appropriate thickness of zero strength layer would be 15mm.

In the application of the method in studying the test results, we have shown that variations in the resistance of fire tested timber elements may be fully accounted for by the natural variation in strength of the specimens, as well as the variations in charring rate which are observed and the variations in the zero-strength layer, whereas the latter is critical in order to fully explain the differences between the tested and the predicted response of the timber elements.

The modified zero-strength layer depths however agree with conclusions raised in the literature, i.e. that a zero-strength layer of 7mm for timber elements exposed to the standard fire may be unconservative. In fact, the modified zero-strength layer is seen to decrease depending upon the heating rate. This is intuitively reasonable since a faster heating rate will result in less through depth heating of a section, especially in the early stages of a fire.

It can be seen from the presented results that the variation in strength of timber elements exposed to cooler parametric fires is considerably lower than when elements are exposed to short hot parametric fires. This is further reinforced by reliability studies presented in this report of timber elements exposed to the different fires. In these studies, using both the notional charring rate and the one dimensional charring rate measured from the residual cross sections following the tests, the reliability index of timber exposed to the less aggressive fires is seen to reduce to 0 over a period of time of nearly double that when exposed to the standard fire or the more aggressive parametric fire. The opposite may not be said of the short hot fire exposure presented, which is seen to have a reliability index reducing to 0 only marginally faster than when timber is exposed to the standard fire. This certainly has positive implications not only for the confidence with which timber may be designed for under parametric fire conditions but also for the reliability of timber used as part of open plan structures where ventilation conditions and localised / travelling fire exposure may result in a less severe heating of the timber element. All this is of course dependent upon the characterisation of the zero-strength layer under parametric or other fire conditions. This report details only two such sets of results, and the extension of this to include other fires seems to be the most obvious target for further research.

11 References

- [1] K. Odeen, “Standard Fire Endurance Tests - Discussion, Criticism, and Alternatives,” in *ASTM STP 464*, 1970, pp. 30 – 56.
- [2] T. Z. Harmathy and T. T. Lie, “Fire Test Standard in the Light of Fire Research,” in *ASTM STP 464*, 1970, pp. 85 – 97.
- [3] N. Cameron, “The Behaviour and Design of Composite Floor Systems in Fire,” The University of Edinburgh, 2003.
- [4] D. Hopkin, T. Lennon, J. El-Rimawi, and V. Silberschmidt, “Failure Mechanisms of Structural Insulated Panel (SIP) Systems Under Natural Fire Conditions,” in *6th International Conference Structures in Fire (SiF '10)*, 2010.
- [5] “EN 1991-1-2:2002 Eurocode 1 : Actions on structures — Part 1-2: Actions on structures exposed to fire.” CEN, European Committee for Standardization, Brussels, 2002.
- [6] J. König, “Effective thermal actions and thermal properties of timber members in natural fires,” *Fire Mater.*, vol. 30, no. 1, pp. 51–63, Jan. 2006.
- [7] J. König, J. Noren, F. B. Olesen, and F. T. Hansen, “Timber Frame Assemblies Exposed to Standard and Parametric Fires Part 1 - Fire Tests,” Stockholm, 1997.
- [8] L. Lu, O. B. Isgor, and G. Hadjisophocleous, “A computer model for light-frame wood floor assemblies under fire attack,” in *11th World Conference on Timber Engineering*, 2010.
- [9] T. Lennon, D. Hopkin, J. El-Rimawi, and V. Silberschmidt, “Large scale natural fire tests on protected engineered timber floor systems,” *Fire Saf. J.*, vol. 45, no. 3, pp. 168–182, Apr. 2010.
- [10] K. L. Friquin, “Material properties and external factors influencing the charring rate of solid wood and glue-laminated timber,” *Fire Mater.*, vol. 35, no. November 2010, pp. 303–327, 2011.
- [11] “EN 1995-1-2 Eurocode 5 : Design of timber structures – Part 1-2 : General – Structural fire design.” CEN, European Committee for Standardization, Brussels, 2004.
- [12] B. Adl-zarrabi, L. Bostrom, and U. Wickstrom, “Using the TPS method for determining the thermal properties of concrete and wood at elevated temperature,” *Fire Mater.*, no. August 2005, pp. 359–369, 2006.
- [13] “EN 1995-1-2:2004/AC:2010 Eurocode 5 : Design of timber structures – Part 1-2 : General – Structural fire design,” no. 122457. CEN, European Committee for Standardization, Brussels, 2004.
- [14] E. L. Schaffer, C. M. Marx, D. A. Bender, and F. E. Woeste, “FPL 467 Strength Validation and Fire Endurance of Glued-Laminated Timber Beams.”

- [15] D. A. Bender, F. E. Woeste, E. L. Schaffer, and C. M. Marx, "FPL 460 Reliability Formulation for the Strength and Fire Endurance of Beams," 1985.
- [16] J. Schmid, J. König, and A. Just, "The Reduced Cross-Section Method for the Design of Timber Structures Exposed to Fire—Background, Limitations and New Developments," *Struct. Eng. Int.*, vol. 22, no. 4, pp. 514–522, 2012.
- [17] J. Schmid, M. Klippel, A. Just, and A. Frange, "Review and analysis of fire resistance tests of timber members in bending, tension and compression with respect to the Reduced Cross-Section Method," *Fire Saf. J.*, Jan. 2014.
- [18] M. Klippel, J. Schmid, and A. Frangi, "The Reduced Cross-Section Method for timber members subjected to compression, tension and bending in fire," in *International council for research and innovation in building construction, working commission W18 - timber structures*, 2012, no. August.
- [19] A. Usmani, D. Lange, A. Webb, C. S. Manohar, and V. S. Sundar, "Reliability of Structural Members Subjected to Fire," in *Fifth International ASRANet conference (ASRANet 2010)*, 2010.
- [20] C. Albrecht and D. Hosser, "A risk informed framework for performance based structural fire protection according to the eurocode fire parts," in *12th International Fire Science and Engineering Conference (Interflam 2010)*, 2010.
- [21] *EN 1990:2002 Eurocode — Basis of structural design*. 2002.
- [22] D. Lange, A. Usmani, and J. Torero, "A Risk Based Framework for Performance Based Fire Safety Design of Steel and Composite Structures," in *Fifth International Conference on Advances in Steel Structures (Icass '07)*, 2007, no. December.
- [23] H. Frantzich, "Risk analysis and fire safety engineering," *Fire Saf. J.*, vol. 31, pp. 313–329, 1998.
- [24] M. Nilsson and M. Ödén, "Metod för dimensionering av bärförmåga vid brand med riskanalys," Lund University of Technology, 2007.
- [25] C. Fahleson, B. Johansson, and O. Lagerqvist, "Probabilistic design of steel structures in fire," 2009.

12 Appendix 1 - Material reference testing

This section details the dynamic modulus of elasticity testing which was carried out for each of the beams prior to grouping. Each beam was suspended above the floor and was struck on the upper lamella, close to the centre, and at the bottom lamella and the frequencies were measured. The method is detailed in §2.1. By filtering out the background frequencies it is possible to estimate the modulus of elasticity of the beams.

The residual frequency and dynamic modulus of elasticity for each beam at the top, middle and bottom of the section is detailed in Table A1.1.

Table A1.1, dynamic modulus of elasticity measurement of each of the beams

Beam Nr	width (mm)	height (mm)	length (mm)	weight (kg) (nominal)	density (kg/m ³) (nominal)	frequency (kHz)	length (mm)	Dynamic MoE (N/mm ²)	point of measurement
1	140	270	5400	95.94	470.0	490	5400	13163	top
1	140	270	5400	95.94	470.0	490	5400	13163	mitten
1	140	270	5400	95.94	470.0	490	5400	13163	bottom
2	140	270	5400	95.94	470.0	500.4	5400	13728	top
2	140	270	5400	95.94	470.0	500.6	5400	13739	middle
2	140	270	5400	95.94	470.0	500.6	5400	13739	bottom
3	140	270	5400	95.94	470.0	484.4	5400	12864	top
3	140	270	5400	95.94	470.0	484.4	5400	12864	middle
3	140	270	5400	95.94	470.0	484.4	5400	12864	bottom
4	140	270	5400	95.94	470.0	496.3	5400	13504	top
4	140	270	5400	95.94	470.0	496.3	5400	13504	middle
4	140	270	5400	95.94	470.0	496.3	5400	13504	bottom
5	140	270	5400	95.94	470.0	491.9	5400	13265	top
5	140	270	5400	95.94	470.0	491.9	5400	13265	middle
5	140	270	5400	95.94	470.0	491.9	5400	13265	bottom
6	140	270	5400	95.94	470.0	495.6	5400	13466	top
6	140	270	5400	95.94	470.0	495.6	5400	13466	middle
6	140	270	5400	95.94	470.0	495.6	5400	13466	bottom
7	140	270	5400	95.94	470.0	490	5400	13163	top
7	140	270	5400	95.94	470.0	490	5400	13163	middle
7	140	270	5400	95.94	470.0	490	5400	13163	bottom
8	140	270	5400	95.94	470.0	489.4	5400	13131	top
8	140	270	5400	95.94	470.0	489.4	5400	13131	middle
8	140	270	5400	95.94	470.0	489.4	5400	13131	bottom
9	140	270	5400	95.94	470.0	478.1	5400	12531	top
9	140	270	5400	95.94	470.0	478.8	5400	12568	middle
9	140	270	5400	95.94	470.0	479.4	5400	12600	bottom
10	140	270	5400	95.94	470.0	498.8	5400	13640	top
10	140	270	5400	95.94	470.0	498.8	5400	13640	middle
10	140	270	5400	95.94	470.0	498.8	5400	13640	bottom
11	140	270	5400	95.94	470.0	502.5	5400	13843	top

Beam Nr	width (mm)	height (mm)	length (mm)	weight (kg) (nominal)	density (kg/m3) (nominal)	frequency (kHz)	length (mm)	Dynamic MoE (N/mm2)	point of measurement
11	140	270	5400	95.94	470.0	502.5	5400	13843	middle
11	140	270	5400	95.94	470.0	502.5	5400	13843	bottom
12	140	270	5400	95.94	470.0	490.6	5400	13195	top
12	140	270	5400	95.94	470.0	490.6	5400	13195	middle
12	140	270	5400	95.94	470.0	490	5400	13163	bottom
13	140	270	5400	95.94	470.0	501.9	5400	13810	top
13	140	270	5400	95.94	470.0	501.9	5400	13810	middle
13	140	270	5400	95.94	470.0	501.9	5400	13810	bottom
14	140	270	5400	95.94	470.0	504.4	5400	13948	top
14	140	270	5400	95.94	470.0	504.4	5400	13948	middle
14	140	270	5400	95.94	470.0	504.4	5400	13948	bottom
15	140	270	5400	95.94	470.0	487.5	5400	13029	top
15	140	270	5400	95.94	470.0	487.5	5400	13029	middle
15	140	270	5400	95.94	470.0	487.5	5400	13029	bottom
16	140	270	5400	95.94	470.0	486.3	5400	12965	top
16	140	270	5400	95.94	470.0	486.3	5400	12965	middle
16	140	270	5400	95.94	470.0	486.3	5400	12965	bottom
17	140	270	5400	95.94	470.0	488.8	5400	13099	top
17	140	270	5400	95.94	470.0	488.8	5400	13099	middle
17	140	270	5400	95.94	470.0	488.8	5400	13099	bottom
18	140	270	5400	95.94	470.0	498.1	5400	13602	top
18	140	270	5400	95.94	470.0	498.1	5400	13602	middle
18	140	270	5400	95.94	470.0	498.1	5400	13602	bottom
19	140	270	5400	95.94	470.0	484.4	5400	12864	top
19	140	270	5400	95.94	470.0	484.4	5400	12864	middle
19	140	270	5400	95.94	470.0	484.4	5400	12864	bottom
20	140	270	5400	95.94	470.0	476.3	5400	12437	top
20	140	270	5400	95.94	470.0	476.3	5400	12437	middle
20	140	270	5400	95.94	470.0	476.9	5400	12469	bottom
21	140	270	5400	95.94	470.0	503.1	5400	13876	top
21	140	270	5400	95.94	470.0	503.1	5400	13876	middle
21	140	270	5400	95.94	470.0	503.1	5400	13876	bottom
22	140	270	5400	95.94	470.0	494.4	5400	13400	top
22	140	270	5400	95.94	470.0	494.4	5400	13400	middle
22	140	270	5400	95.94	470.0	495	5400	13433	bottom
23	140	270	5400	95.94	470.0	501.3	5400	13777	top
23	140	270	5400	95.94	470.0	500.6	5400	13739	middle
23	140	270	5400	95.94	470.0	501.3	5400	13777	bottom
24	140	270	5400	95.94	470.0	485.6	5400	12928	top
24	140	270	5400	95.94	470.0	485.6	5400	12928	middle
24	140	270	5400	95.94	470.0	485.6	5400	12928	bottom
25	140	270	5400	95.94	470.0	500.6	5400	13739	top
25	140	270	5400	95.94	470.0	500.6	5400	13739	middle

Beam Nr	width (mm)	height (mm)	length (mm)	weight (kg) (nominal)	density (kg/m ³) (nominal)	frequency (kHz)	length (mm)	Dynamic MoE (N/mm ²)	point of measurement
25	140	270	5400	95.94	470.0	500.6	5400	13739	bottom
26	140	270	5400	95.94	470.0	485	5400	12896	top
26	140	270	5400	95.94	470.0	485	5400	12896	middle
26	140	270	5400	95.94	470.0	495.6	5400	13466	bottom
27	140	270	5400	95.94	470.0	481.9	5400	12731	top
27	140	270	5400	95.94	470.0	481.9	5400	12731	middle
27	140	270	5400	95.94	470.0	481.9	5400	12731	bottom
28	140	270	5400	95.94	470.0	491.3	5400	13233	top
28	140	270	5400	95.94	470.0	491.3	5400	13233	middle
28	140	270	5400	95.94	470.0	491.3	5400	13233	bottom
29	140	270	5400	95.94	470.0	489.4	5400	13131	top
29	140	270	5400	95.94	470.0	489.4	5400	13131	middle
29	140	270	5400	95.94	470.0	489.4	5400	13131	bottom
30	140	270	5400	95.94	470.0	491.3	5400	13233	top
30	140	270	5400	95.94	470.0	491.3	5400	13233	middle
30	140	270	5400	95.94	470.0	491.9	5400	13265	bottom
31	140	270	5400	95.94	470.0	488.8	5400	13099	top
31	140	270	5400	95.94	470.0	488.8	5400	13099	middle
31	140	270	5400	95.94	470.0	488.1	5400	13061	bottom
32	140	270	5400	95.94	470.0	484.4	5400	12864	top
32	140	270	5400	95.94	470.0	484.4	5400	12864	middle
32	140	270	5400	95.94	470.0	484.4	5400	12864	bottom
33	140	270	5400	95.94	470.0	483.8	5400	12832	top
33	140	270	5400	95.94	470.0	483.8	5400	12832	middle
33	140	270	5400	95.94	470.0	483.8	5400	12832	bottom
34	140	270	5400	95.94	470.0	495	5400	13433	top
34	140	270	5400	95.94	470.0	495	5400	13433	middle
34	140	270	5400	95.94	470.0	495	5400	13433	bottom
35	140	270	5400	95.94	470.0	486.9	5400	12997	top
35	140	270	5400	95.94	470.0	486.9	5400	12997	middle
35	140	270	5400	95.94	470.0	486.9	5400	12997	bottom
36	140	270	5400	95.94	470.0	494.4	5400	13400	top
36	140	270	5400	95.94	470.0	494.4	5400	13400	middle
36	140	270	5400	95.94	470.0	494.4	5400	13400	bottom
37	140	270	5400	95.94	470.0	482.5	5400	12763	top
37	140	270	5400	95.94	470.0	483.1	5400	12795	middle
37	140	270	5400	95.94	470.0	483.1	5400	12795	bottom
38	140	270	5400	95.94	470.0	496.3	5400	13504	top
38	140	270	5400	95.94	470.0	496.3	5400	13504	middle
38	140	270	5400	95.94	470.0	496.3	5400	13504	bottom
39	140	270	5400	95.94	470.0	495.6	5400	13466	top
39	140	270	5400	95.94	470.0	496.3	5400	13504	middle
39	140	270	5400	95.94	470.0	496.3	5400	13504	bottom

Beam Nr	width (mm)	height (mm)	length (mm)	weight (kg) (nominal)	density (kg/m3) (nominal)	frequency (kHz)	length (mm)	Dynamic MoE (N/mm2)	point of measurement
40	140	270	5400	95.94	470.0	485	5400	12896	top
40	140	270	5400	95.94	470.0	484.4	5400	12864	middle
40	140	270	5400	95.94	470.0	485	5400	12896	bottom
41	140	270	5400	95.94	470.0	501.9	5400	13810	top
41	140	270	5400	95.94	470.0	501.9	5400	13810	middle
41	140	270	5400	95.94	470.0	501.9	5400	13810	bottom
42	140	270	5400	95.94	470.0	496.9	5400	13536	top
42	140	270	5400	95.94	470.0	496.9	5400	13536	middle
42	140	270	5400	95.94	470.0	496.9	5400	13536	bottom
43	140	270	5400	95.94	470.0	484.4	5400	12864	top
43	140	270	5400	95.94	470.0	484.4	5400	12864	middle
43	140	270	5400	95.94	470.0	483.8	5400	12832	bottom
44	140	270	5400	95.94	470.0	497.5	5400	13569	top
44	140	270	5400	95.94	470.0	497.5	5400	13569	middle
44	140	270	5400	95.94	470.0	497.5	5400	13569	bottom
45	140	270	5400	95.94	470.0	503.1	5400	13876	top
45	140	270	5400	95.94	470.0	503.1	5400	13876	middle
45	140	270	5400	95.94	470.0	503.1	5400	13876	bottom

13 Appendix 2 – Finger joint positioning

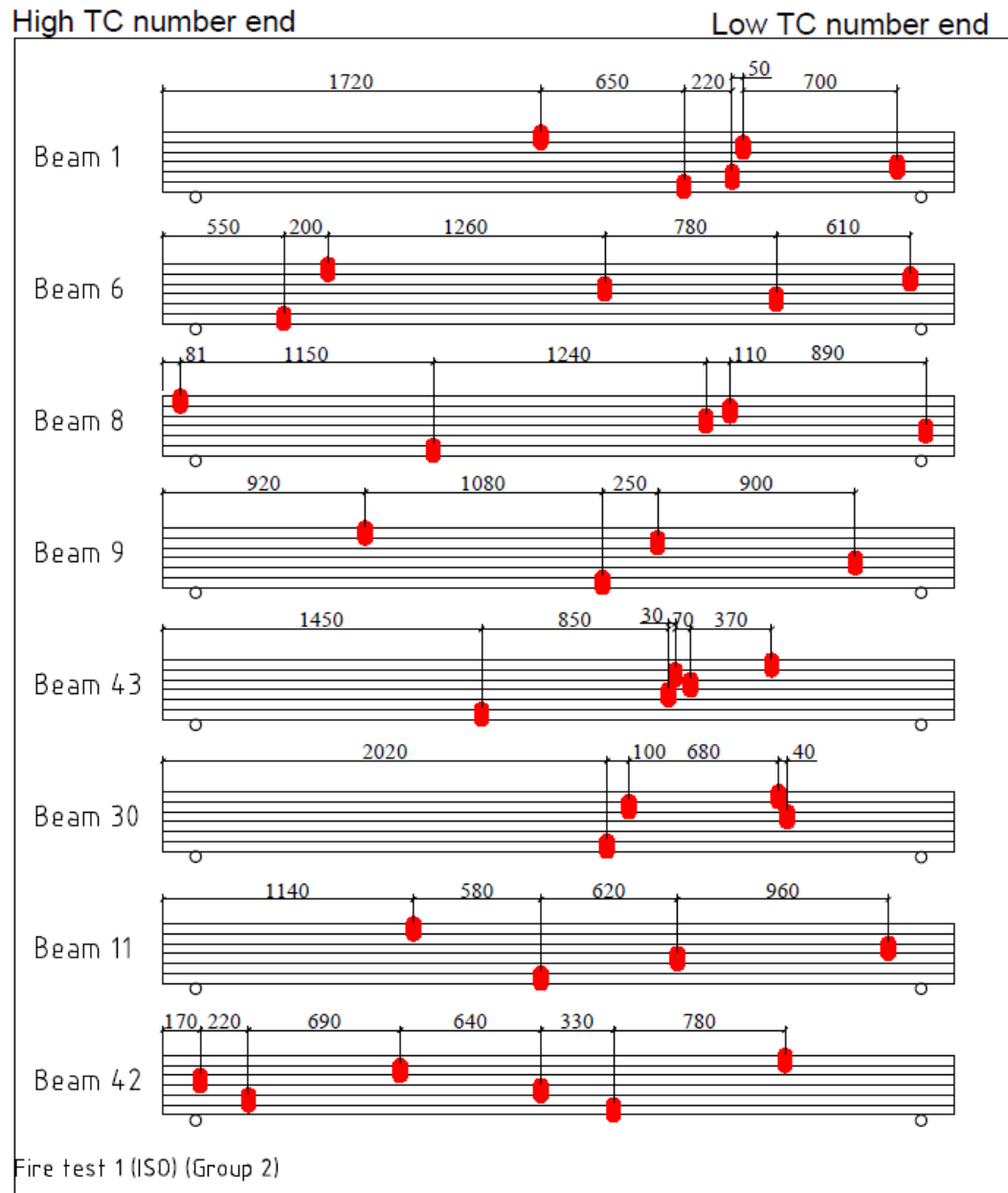


Figure 13.1, finger joint layout in fire test 1. All distances are marked in mm from the East ends of the beams, as described in the test setup

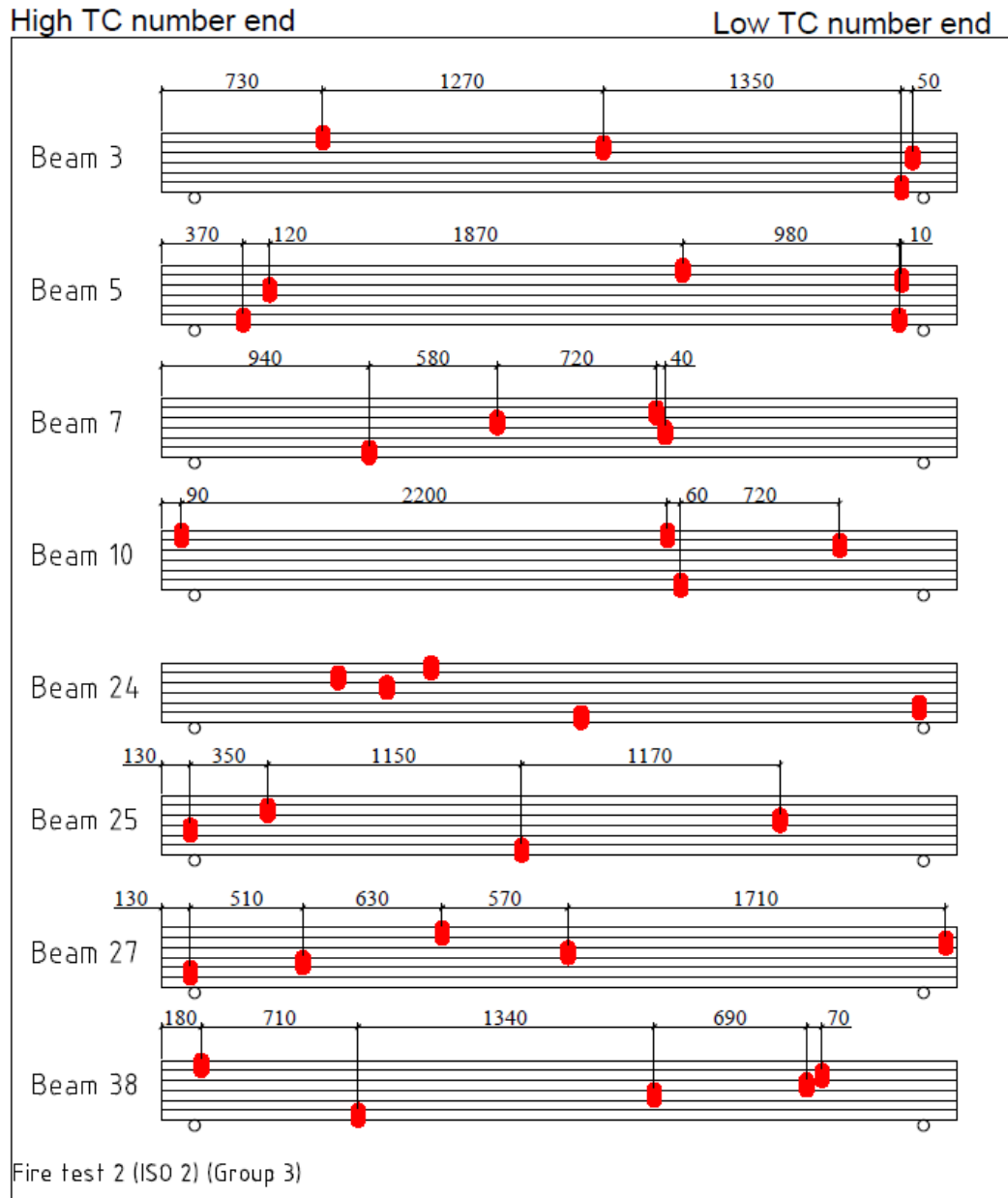


Figure 13.2, finger joint layout in fire test 2. All distances are marked in mm from the East ends of the beams, as described in the test setup

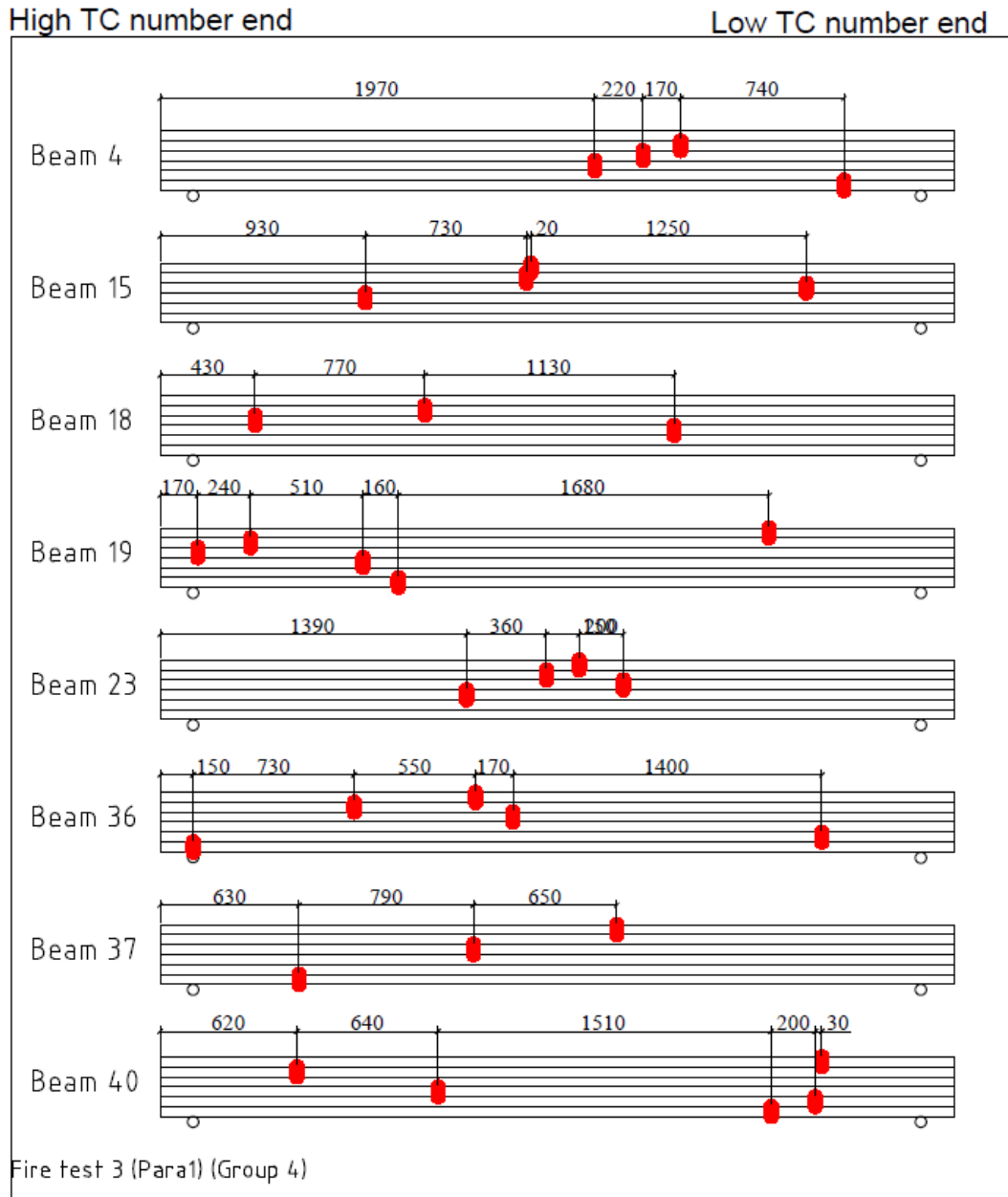


Figure 13.4, finger joint layout in fire test 3. All distances are marked in mm from the East ends of the beams, as described in the test setup

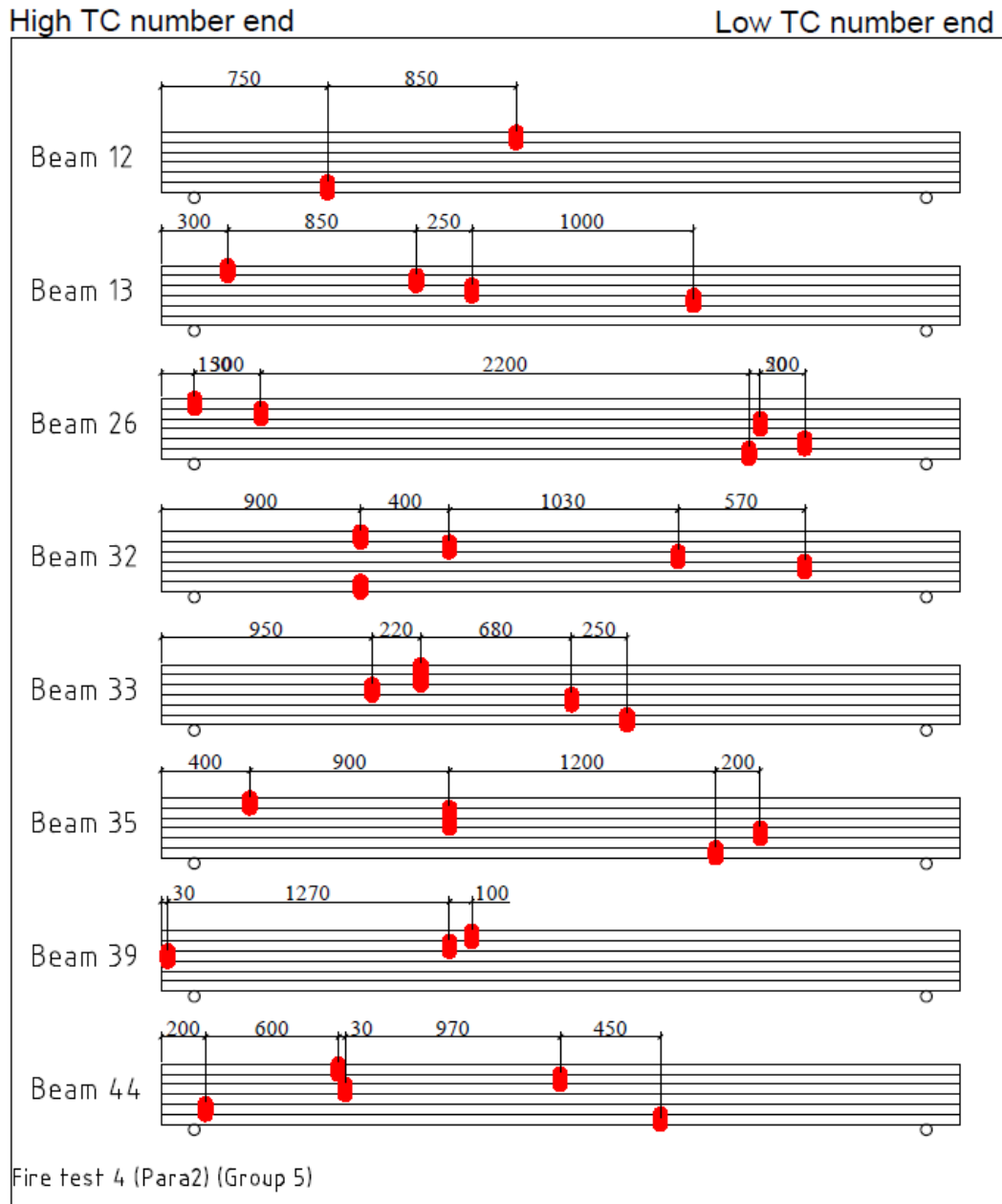


Figure 13.4, finger joint layout in fire test 4. All distances are marked in mm from the west ends of the beams, as described in the test setup

14 Appendix 3 – cross-sectional analysis

In this appendix, the results of the resulting sectional analysis are presented. This is the data which was used to derive the distributions of the charring rate and the sectional properties presented in section 7. One table is provided for each test. As described in the report, 3 pieces of length ca. 20 cm were taken from each beam following each test and the sectional analysis was repeated for each end of these pieces. There are therefore 6 sectional analyses carried out for each beam, where there was adequate timber remaining to perform the analysis. In the tables, the sections are numbered according to the following convention: *beam number (group) location*, where location indicates if the section is from the end of the beam with the high (H) or low (L) thermocouple numbers or from the centre (C).

In the tables below, the lowest remaining lamella was excluded from the analysis and is highlighted red. Any sections coloured orange indicate that not enough of that section remained to carry out the analysis.

Table 14.1, sectional analysis summary from fire test 1

section	Lamella	section width (mm)	char depth (mm)	Residual depth (mm)	Area (mm ²)	Second moment of area (mm ⁴)	Section modulus (mm ³)
1(2)H	1	64	38	213	1.21E+04	4.23E+07	3.85E+05
	2	57	41				
	3	63	38				
	4	60	40				
	5		70				
	1	60	40	207	1.18E+04	4.33E+07	3.90E+05
	2	59	40				
	3	58	41				
	4	57	41				
	5		70				
1(2)C	1	58	41	216	1.23E+04	4.35E+07	3.92E+05
	2	54	43				
	3	65	37				
	4	62	39				
	5		70				
	1	53	44	220	1.12E+04	3.50E+07	3.12E+05
	2	52	44				
	3	59	40				
	4	61	39				
	5		70				
1(2)L	1	60	40	221	1.22E+04	4.49E+07	3.87E+05
	2	55	42				
	3	62	39				
	4	58	41				
	5		70				

section	Lamella	section width (mm)	char depth (mm)	Residual depth (mm)	Area (mm ²)	Second moment of area (mm ⁴)	Section modulus (mm ³)
	1	60	40	224	1.27E+04	4.81E+07	4.15E+05
	2	58	41				
	3	61	39				
	4	62	39				
	5		70				
6(2)H	1	58	41	216	1.11E+04	4.12E+07	3.58E+05
	2	56	42				
	3	48	46				
	4	50	45				
	5		70				
6(2)C							
6(2)L	1	63	38	216	1.27E+04	4.74E+07	4.19E+05
	2	63	38				
	3	56	42				
	4	59	40				
	5		70				
8(2)H	1	64	38	212	1.19E+04	4.34E+07	3.87E+05
	2	58	41				
	3	54	43				
	4	56	42				
	5		70				
8(2)H	1						
	2						
	3						
	4						
	5						
8(2)H	1						
	2						
	3						
	4						
	5						

section	Lamella	section width (mm)	char depth (mm)	Residual depth (mm)	Area (mm ²)	Second moment of area (mm ⁴)	Section modulus (mm ³)
	2						
	3						
	4						
	5						
8(2)C	1	54	43				
	2	53	44				
	3	45	47				
	4	49	46				
	5		70	210	1.02E+04	3.72E+07	3.34E+05
	1	52	44				
	2	50	45				
	3	54	43				
	4	49	46				
	5		70	213	1.05E+04	3.72E+07	3.39E+05
8(2)L	1	62	39				
	2	58	41				
	3	51	45				
	4	57	42				
	5		70	213	1.16E+04	4.20E+07	3.71E+05
	1	61	40				
	2	62	39				
	3	56	42				
	4	54	43				
	5		70	209	1.16E+04	3.98E+07	3.59E+05
9(2)H	1	58	41				
	2	52	44				
	3	52	44				
	4	46	47				
	5		70	214	1.08E+04	3.95E+07	3.44E+05
	1	60	40				
	2	52	44				
	3	50	45				
	4	50	45				
	5		70	215	1.09E+04	4.09E+07	3.57E+05
9(2)C	1	59	41				
	2	51	44				
	3	47	47				
	4	49	46				
	5		70	213	1.04E+04	3.85E+07	3.37E+05
	1	63	38				
	2	51	45	213	1.06E+04	3.98E+07	3.46E+05

section	Lamella	section width (mm)	char depth (mm)	Residual depth (mm)	Area (mm ²)	Second moment of area (mm ⁴)	Section modulus (mm ³)
	3	44	48				
	4	50	45				
	5		70				
9(2)L	1	59	40	212	1.02E+04	3.73E+07	3.24E+05
	2	52	44				
	3	46	47				
	4	45	47				
	5		70				
	1	68	36	212	1.13E+04	4.11E+07	3.51E+05
	2	57	42				
	3	48	46				
	4	41	49				
	5		70				
11(2)H	1	60	40	213	1.12E+04	3.77E+07	3.23E+05
	2	63	39				
	3	57	41				
	4	48	46				
	5		70				
	1	55	43	216	1.06E+04	3.66E+07	3.18E+05
	2	58	41				
	3	54	43				
	4		70				
	5		70				
11(2)C	1	59	41	216	1.18E+04	4.17E+07	3.65E+05
	2	61	39				
	3	54	43				
	4	58	41				
	5		70				
	1	55	42	210	1.06E+04	3.56E+07	3.17E+05
	2	56	42				
	3	51	45				
	4	50	45				
	5		70				
11(2)L	1	61	40	210	1.17E+04	4.03E+07	3.59E+05
	2	63	39				
	3	53	44				
	4	57	42				
	5		70				
	1	59	40	217	1.19E+04	4.31E+07	3.73E+05
	2	63	38				
	3	57	42				

section	Lamella	section width (mm)	char depth (mm)	Residual depth (mm)	Area (mm ²)	Second moment of area (mm ⁴)	Section modulus (mm ³)
	4	50	45				
	5		70				
30(2)H	1	58	41	215	1.05E+04	3.88E+07	3.89E+05
	2	56	42				
	3	48	46				
	4	50	45				
	5		70				
	1	57	41	210	1.07E+04	3.90E+07	4.00E+05
	2	60	40				
	3	51	44				
	4	56	42				
	5		70				
30(2)C	1	57	41	213	1.05E+04	3.88E+07	3.89E+05
	2	50	45				
	3	45	48				
	4	54	43				
	5		70				
	1	54	43	214	1.03E+04	3.94E+07	3.64E+05
	2	46	47				
	3	45	48				
	4	57	42				
	5		70				
30(2)L	1	58	41	214	1.07E+04	3.87E+07	3.39E+05
	2	49	45				
	3	49	46				
	4	54	43				
	5		70				
	1	53	44	217	1.07E+04	3.94E+07	3.47E+05
	2	51	44				
	3	50	45				
	4	52	44				
	5		70				
42(2)H	1	54	43	217	1.06E+04	3.72E+07	3.20E+05
	2	57	42				
	3	52	44				
	4	47	47				
	5		70				
	1	68	36	219	1.12E+04	4.43E+07	3.68E+05
	2	53	43				
	3	49	46				
	4	47	47				

section	Lamella	section width (mm)	char depth (mm)	Residual depth (mm)	Area (mm ²)	Second moment of area (mm ⁴)	Section modulus (mm ³)
	5		70				
42(2)C	1	64	38	210	1.07E+04	3.78E+07	3.29E+05
	2	55	43				
	3	49	46				
	4	50	45				
	5		70				
	1	57	42	212	1.03E+04	3.50E+07	3.03E+05
	2	53	43				
	3	50	45				
	4	48	46				
	5		70				
42(2)L	1	60	40	210	1.03E+04	3.33E+07	2.74E+05
	2	61	40				
	3	48	46				
	4	44	48				
	5		70				
	1	66	37	203	1.09E+04	3.36E+07	2.96E+05
	2	59	41				
	3	56	42				
	4	51	44				
	5		70				
43(2)H	1	61	40	210	1.19E+04	4.09E+07	3.74E+05
	2	60	40				
	3	60	40				
	4	57	42				
	5		70				
	1	58	41	219	1.19E+04	4.38E+07	3.86E+05
	2	59	41				
	3	57	42				
	4	57	42				
	5		70				
43(2)C	1	58	41	217	1.22E+04	4.53E+07	4.12E+05
	2	62	39				
	3	56	42				
	4	56	42				
	5		70				
	1	57	41	215	1.18E+04	4.23E+07	3.79E+05
	2	59	41				
	3	57	41				
	4	56	42				
	5		70				

section	Lamella	section width (mm)	char depth (mm)	Residual depth (mm)	Area (mm ²)	Second moment of area (mm ⁴)	Section modulus (mm ³)
43(2)L	1	53	44	213	1.12E+04	3.83E+07	3.42E+05
	2	59	41				
	3	59	41				
	4	49	46				
	5	70	70				
	1	56	42	210	1.13E+04	3.79E+07	3.40E+05
	2	65	38				
	3	53	43				
	4	55	42				
	5	70	70				

Table 14.2, sectional analysis summary from fire test 2

section	Lamella	section width (mm)	char depth (mm)	Residual depth (mm)	Area (mm ²)	Second moment of area (mm ⁴)	Section modulus (mm ³)
3(3)H	1	71	34	220	1.45E+04	5.54E+07	4.79E+05
	2	69	35				
	3	67	37				
	4	68	36				
	5	70	70				
	1	73	34	223	1.48E+04	5.74E+07	4.88E+05
	2	71	35				
	3	67	36				
	4	68	36				
	5	70	70				
3(3)C							
3(3)L	1	71	34	222	1.46E+04	5.67E+07	4.88E+05
	2	68	36				
	3	68	36				
	4	66	37				
	5	70	70				
	1	71	34	218	1.42E+04	5.34E+07	4.71E+05
	2	66	37				
	3	65	37				
	4	70	35				
	5	70	70				
5(3)H	1	75	33	228	1.47E+04	6.21E+07	5.81E+05
	2	70	35				
	3	60	40				
	4	66	37				
	5	5	5				
	1	71	35	229	1.45E+04	5.99E+07	5.62E+05
	2	74	33				
	3	63	38				
	4	61	40				
	5	5	5				

section	Lamella	section width (mm)	char depth (mm)	Residual depth (mm)	Area (mm ²)	Second moment of area (mm ⁴)	Section modulus (mm ³)	
5(3)C	1	71	35	227	1.52E+04	6.26E+07	5.69E+05	
	2	73	33					
	3	66	37					
	4	65	38					
	5	5	5					
	5(3)L	1	68	36	224	1.42E+04	5.67E+07	5.30E+05
		2	70	35				
		3	64	38				
		4	62	39				
		5	5	5				
5(3)L	1	74	33	219	1.45E+04	5.50E+07	5.39E+05	
	2	75	33					
	3	65	37					
	4	64	38					
	5	5	70					
	7(3)H	1	70	35	221	1.41E+04	5.37E+07	5.12E+05
		2	72	34				
		3	64	38				
		4	65	38				
		5	5	70				
7(3)H	1	68	36	220	1.32E+04	4.96E+07	4.81E+05	
	2	62	39					
	3	62	39					
	4	61	39					
	5	5	70					
	7(3)L	1	63	39	220	1.31E+04	4.82E+07	4.61E+05
		2	65	38				
		3	65	38				
		4	58	41				
		5	5	70				
7(3)C	1	62	39	216	1.29E+04	3.33E+07	3.26E+05	
	2	62	39					
	3	69	36					
	4	63	39					
	5	5	70					
	7(3)L	1	63	39	220	1.34E+04	4.95E+07	4.67E+05
		2	65	38				
		3	68	36				
		4	60	40				
		5	5	70				
7(3)L	1	63	38	221	1.36E+04	5.05E+07	4.77E+05	

section	Lamella	section width (mm)	char depth (mm)	Residual depth (mm)	Area (mm ²)	Second moment of area (mm ⁴)	Section modulus (mm ³)				
	2	62	39	224	1.39E+04	5.50E+07	5.35E+05				
	3	70	35								
	4	60	40								
	5		70								
	1	71	35								
	2	66	37								
	3	63	38								
	4	61	40								
	5		70								
	10(3)H	1	67					36	218	1.30E+04	5.06E+07
2		58	41								
3		59	40								
4		63	39								
5			70								
1		66	37	219	1.32E+04	5.01E+07	4.79E+05				
2		63	38								
3		61	39								
4		61	39								
5			70								
10(3)C	1	67	37	222	1.32E+04	5.16E+07	4.94E+05				
	2	59	40								
	3	62	39								
	4	61	39								
	5		70								
	1	70	35					221	1.41E+04	5.44E+07	5.19E+05
	2	62	39								
	3	69	36								
	4	66	37								
	5		70								
10(3)L	1	63	39	218	1.23E+04	4.59E+07	4.44E+05				
	2	58	41								
	3	58	41								
	4	58	41								
	5		70								
	1	64	38					218	1.30E+04	4.80E+07	4.63E+05
	2	63	38								
	3	61	40								
	4	61	40								
	5		70								
24(3)H	1	68	36	221	1.33E+04	5.01E+07	4.46E+05				
	2	65	37								

section	Lamella	section width (mm)	char depth (mm)	Residual depth (mm)	Area (mm ²)	Second moment of area (mm ⁴)	Section modulus (mm ³)
	3	68	36	218	1.39E+04	5.46E+07	4.69E+05
	4	68	36				
	5		70				
	1	66	37				
	2	64	38				
	3	65	38				
	4	67	36				
	5		70				
24(3)C	1	61	40	219	1.33E+04	5.01E+07	4.46E+05
	2	61	40				
	3	64	38				
	4	64	38				
	5		70				
	1	68	36				
	2	62	39				
	3	66	37				
	4	64	38				
	5		70				
24(3)L	1	52	44	218	1.12E+04	4.24E+07	3.88E+05
	2	48	46				
	3	54	43				
	4	53	43				
	5		70				
	1	57	41				
	2	57	41				
	3	59	40				
	4	59	40				
	5		70				
25(3)H	1	70	35	222	1.35E+04	5.48E+07	5.19E+05
	2	59	41				
	3	59	40				
	4	63	39				
	5		70				
	1	70	35				
	2	60	40				
	3	55	43				
	4	59	40				
	5		70				
25(3)C	1	58	41	215	1.35E+04	5.50E+07	5.18E+05
	2	56	42				
	3	48	46				

section	Lamella	section width (mm)	char depth (mm)	Residual depth (mm)	Area (mm ²)	Second moment of area (mm ⁴)	Section modulus (mm ³)
	4	50	45	210	1.34E+04	5.41E+07	5.07E+05
	5		70				
	1	57	41				
	2	60	40				
	3	51	44				
	4	56	42				
	5		70				
25(3)L	1	69	35	219	1.36E+04	5.40E+07	5.10E+05
	2	61	40				
	3	61	40				
	4	64	38				
	5		70				
	1	65	37	220	1.27E+04	5.16E+07	4.87E+05
	2	56	42				
	3	52	44				
	4	60	40				
5		70					
27(3)H	1	54	43	217	1.06E+04	3.72E+07	3.20E+05
	2	57	42				
	3	52	44				
	4	47	47				
	5		70				
	1	68	36	219	1.12E+04	4.43E+07	3.68E+05
	2	53	43				
	3	49	46				
	4	47	47				
	5		70				
27(3)C	1	64	38	210	1.07E+04	3.78E+07	3.29E+05
	2	55	43				
	3	49	46				
	4	50	45				
	5		70				
	1	57	42	212	1.03E+04	3.50E+07	3.03E+05
	2	53	43				
	3	50	45				
	4	48	46				
	5		70				
27(3)L	1	60	40	210	1.03E+04	3.33E+07	2.74E+05
	2	61	40				
	3	48	46				
	4	44	48				

section	Lamella	section width (mm)	char depth (mm)	Residual depth (mm)	Area (mm ²)	Second moment of area (mm ⁴)	Section modulus (mm ³)
	5		70	203	1.09E+04	3.36E+07	2.96E+05
	1	66	37				
	2	59	41				
	3	56	42				
	4	51	44				
	5		70				
38(3)H	1	47	46	221	1.47E+04	5.67E+07	5.42E+05
	2	68	36				
	3	68	36				
	4	70	35				
	5		70				
	1	71	35	222	1.45E+04	5.63E+07	5.34E+05
	2	71	34				
	3	64	38				
	4	71	35				
	5		70				
38(3)C	1	68	36	219	1.47E+04	5.41E+07	5.12E+05
	2	73	34				
	3	70	35				
	4	70	35				
	5		70				
	1	69	35	219	1.40E+04	5.23E+07	5.07E+05
	2	70	35				
	3	64	38				
	4	67	37				
	5		70				
38(3)L	1	66	37	216	1.31E+04	4.86E+07	4.72E+05
	2	64	38				
	3	61	40				
	4	61	39				
	5		70				
	1	62	39	227	1.39E+04	5.55E+07	5.15E+05
	2	67	37				
	3	67	37				
	4	60	40				
	5		70				

Table 14.3, sectional analysis summary from fire test 3

section	Lamella	section width (mm)	char depth (mm)	Residual depth (mm)	Area (mm ²)	Second moment of area (mm ⁴)	Section modulus (mm ³)
4(4)H	1	97	21	228	1.95E+04	8.10E+07	7.51E+05
	2	87	26				
	3	89	26				
	4	85	27				
	5	78	31				
	1	90	25	228	1.90E+04	7.63E+07	6.99E+05
	2	83	29				
	3	93	23				
	4	86	27				
	5	80	30				
4(4)C		87	27	226	1.86E+04	7.50E+07	6.89E+05
		85	28				
		85	27				
		85	28				
		78	31				
		88	26	226	1.87E+04	7.35E+07	6.84E+05
		84	28				
		91	24				
		84	28				
		75	33				
4(4)L	1	90	25	231	1.95E+04	8.12E+07	7.33E+05
	2	82	29				
	3	95	22				
	4	59	41				
	5	80	30				
	1	89	26	221	1.88E+04	7.24E+07	6.78E+05
	2	87	26				
	3	90	25				
	4	87	27				
	5	77	32				
15(4)H	1	84	28	226	1.79E+04	7.36E+07	6.71E+05
	2	79	30				
	3	82	29				
	4	80	30				
	5	80	5				
	1	82	29	233	1.82E+04	8.02E+07	7.06E+05
	2	80	30				
	3	81	30				
	4	75	33				
	5	83	5				

section	Lamella	section width (mm)	char depth (mm)	Residual depth (mm)	Area (mm ²)	Second moment of area (mm ⁴)	Section modulus (mm ³)				
15(4)C	1		70								
	2		70								
	3		70								
	4		70								
	5		5								
	1		70								
	2		70								
	3		70								
	4		70								
	5		5								
15(4)L	1		70								
	2		70								
	3		70								
	4		70								
	5		70								
	1		70								
	2		70								
	3		70								
	4		70								
	5		70								
18(4)H	1	80	30								
	2	75	32								
	3	82	29								
	4	82	29								
	5	76	32					232	1.79E+04	7.48E+07	6.64E+05
	1	86	27								
	2	80	30								
	3	84	28								
	4	81	29								
	5	77	32								
18(4)C	1	82	29								
	2	87	27								
	3	85	27								
	4	82	29								
	5	78	31					236	1.90E+04	8.21E+07	7.23E+05
	1	80	30								
	2	83	28								
	3	87	26								
	4	81	30								
	5	83	28								
18(4)L	1	80	30	234	1.80E+04	7.67E+07	6.87E+05				

section	Lamella	section width (mm)	char depth (mm)	Residual depth (mm)	Area (mm ²)	Second moment of area (mm ⁴)	Section modulus (mm ³)				
	2	80	30	230	1.84E+04	7.77E+07	6.84E+05				
	3	84	28								
	4	78	31								
	5	76	32								
	1	81	30								
	2	78	31								
	3	84	28								
	4	82	29								
	5	85	28								
	19(4)H	1	82					29	229	1.81E+04	7.29E+07
2		85	27								
3		85	28								
4		86	27								
5		75	33								
1		90	25	235	1.96E+04	8.65E+07	7.64E+05				
2		84	28								
3		90	25								
4		85	28								
5		81	29								
19(4)C	1	85	27					232	1.87E+04	7.89E+07	7.13E+05
	2	87	27								
	3	87	26								
	4	78	31								
	5	81	30								
	1	77	31	231	1.82E+04	7.66E+07	6.73E+05				
	2	82	29								
	3	85	27								
	4	78	31								
	5	84	28								
19(4)L	1	87	27					234	1.96E+04	8.53E+07	7.51E+05
	2	86	27								
	3	88	26								
	4	86	27								
	5	84	28								
	1	84	28	232	1.83E+04	7.68E+07	6.90E+05				
	2	81	30								
	85	85	28								
	79	79	31								
	78.7	79	31								
23(4)H	1	91	25					225	1.92E+04	8.09E+07	7.24E+05
	2	83	29								

section	Lamella	section width (mm)	char depth (mm)	Residual depth (mm)	Area (mm ²)	Second moment of area (mm ⁴)	Section modulus (mm ³)
	3	84	28	235	1.96E+04	8.40E+07	7.46E+05
	4	88	26				
	5	88	26				
	1	89	26				
	2	85	27				
	3	87	26				
	4	88	26				
	5	82	29				
23(4)C	1	84	28	230	1.89E+04	8.00E+07	7.07E+05
	2	82	29				
	3	88	26				
	4	83	29				
	5	86	27				
	1	84	28				
	2	83	29				
	3	86	27				
	4	85	27				
	5	88	26				
23(4)L	1	96	22	236	2.11E+04	9.69E+07	8.32E+05
	2	87	27				
	3	89	25				
	4	91	25				
	5	96	22				
	1	90	25				
	2	84	28				
	3	85	28				
	4	86	27				
	5	87	26				
36(4)H	1		70	235	1.96E+04	8.72E+07	7.64E+05
	2		70				
	3		70				
	4		70				
	5		70				
	1		70				
	2		70				
	3		70				
	4		70				
	5		70				
36(4)C	1	76	32	235	1.70E+04	7.52E+07	6.56E+05
	2	73	34				
	3	76	32				

section	Lamella	section width (mm)	char depth (mm)	Residual depth (mm)	Area (mm ²)	Second moment of area (mm ⁴)	Section modulus (mm ³)
	4	72	34				
	5	77	32				
	1		70				
	2		70				
	3		70				
	4		70				
	5		70				
36(4)L	1	80	30	239	1.92E+04	8.70E+07	7.39E+05
	2	84	28				
	3	85	28				
	4	81	30				
	5	84	28				
	1	86	27	234	1.86E+04	8.09E+07	7.21E+05
	2	85	28				
	3	83	28				
	4	76	32				
	5	80	30				
37(4)H	1		70				
	2		70				
	3		70				
	4		70				
	5		70				
	1		70				
	2		70				
	3		70				
	4		70				
	5		70				
37(4)C	1		70				
	2		70				
	3		70				
	4		70				
	5		70				
	1		70				
	2		70				
	3		70				
	4		70				
	5		70				
37(4)L	1		70				
	2		70				
	3		70				
	4		70				

section	Lamella	section width (mm)	char depth (mm)	Residual depth (mm)	Area (mm ²)	Second moment of area (mm ⁴)	Section modulus (mm ³)
	5		70				
	1		70				
	2		70				
	3		70				
	4		70				
	5		70				
40(4)H	1	92	24	227	1.93E+04	8.04E+07	7.37E+05
	2	89	26				
	3	86	27				
	4	84	28				
	5	80	30				
	1	80	30	227	1.85E+04	7.66E+07	7.14E+05
	2	90	25				
	3	82	29				
	4	78	31				
	5	79	31				
40(4)C	1		70				
	2		70				
	3		70				
	4		70				
	5		70				
	1		70				
	2		70				
	3		70				
	4		70				
	5		70				
40(4)L	1	97	22	236	2.10E+04	9.35E+07	8.30E+05
	2	94	23				
	3	91	24				
	4	85	28				
	5	87	27				
	1	94	23	234	2.01E+04	8.96E+07	8.02E+05
	2	91	25				
	3	86	27				
	4	83	29				
	5	84	28				

Table 14.4, sectional analysis summary from fire test 4

section	Lamella	section width (mm)	char depth (mm)	Residual depth (mm)	Area (mm ²)	Second moment of area (mm ⁴)	Section modulus measured
12(5)H	1	81	30	221	1.52E+04	5.74E+07	5.62E+05
	2	72	34				
	3	70	35				
	4	72	34				
	5	52	44				
	1	79	31	227	1.61E+04	6.31E+07	6.00E+05
	2	74	33				
	3	80	30				
	4	70	35				
	5	59	40				
12(5)C							
12(5)L	1	86	27	225	1.77E+04	7.09E+07	6.55E+05
	2	79	30				
	3	83	28				
	4	81	30				
	5	70	35				
	1	87	26	225	1.74E+04	6.69E+07	6.43E+05
	2	83	28				
	3	82	29				
	4	79	31				
	5	63	39				
13(5)H	1	69	35	225	1.44E+04	5.78E+07	5.35E+05
	2	64	38				
	3	67	37				
	4	66	37				
	5	60	5				
	1	79	31	220	1.47E+04	5.87E+07	5.62E+05
	2	65	38				
	3	63	39				
	4	67	36				

	5	60	5				
13(5)C	1		70				
	2		70				
	3		70				
	4		70				
	5		5				
	1		70				
	2		70				
	3		70				
	4		70				
	5		5				
13(5)L	1	79	31				
	2	74	33				
	3	77	32				
	4	87	27				
	5	66	37	228	1.69E+04	6.68E+07	6.13E+05
	1	83	29				
	2	75	33				
	3	79	31				
	4	78	31				
	5	59	41	222	1.66E+04	6.32E+07	6.05E+05
26(5)H	1	70	35				
	2	66	37				
	3	66	37				
	4	66	37				
	5	55	42	219	1.41E+04	5.35E+07	5.09E+05
	1	71	35				
	2	68	36				
	3	69	36				
	4	67	37				
	5	48	46	218	1.41E+04	5.18E+07	5.07E+05
26(5)C	1		70				
	2		70				
	3		70				
	4		70				
	5		70				
	1		70				
	2		70				
	3		70				
	4		70				
	5		70				
26(5)L	1	81	29				
	2	75	32				
	3	74	33				
	4	75	32	217	1.47E+04	5.30E+07	5.13E+05

	5	49	46				
	1	73	34				
	2	70	35				
	3	72	34				
	4	71	34				
	5	46	47	220	1.56E+04	5.63E+07	5.52E+05
32(5)H	1	72	34				
	2	70	35				
	3	64	38				
	4	61	40				
	5	45	48	217	1.35E+04	4.86E+07	4.87E+05
	1	80	30				
	2	68	36				
	3	62	39				
	4	61	40				
	5	45	48	218	1.38E+04	5.16E+07	5.28E+05
32(5)C	1	76	32				
	2	68	36				
	3	70	35				
	4	72	34				
	5	48	46	214	1.46E+04	5.27E+07	5.18E+05
	1	75	33				
	2	71	35				
	3	73	34				
	4	69	35				
	5	55	42	224	1.52E+04	5.80E+07	5.55E+05
32(5)L	1	64	38				
	2	65	37				
	3	72	34				
	4	76	32				
	5	54	43	221	1.43E+04	5.24E+07	4.84E+05
	1	63	39				
	2	61	40				
	3	73	34				
	4	73	33				
	5	60	40	223	1.45E+04	5.46E+07	4.95E+05
33(5)H	1	62	39				
	2	63	38				
	3	63	39				
	4	61	39				
	5	54	43	222	1.33E+04	5.12E+07	4.80E+05
	1	66	37				
	2	59	41				
	3	55	43				
	4	61	40	222	1.29E+04	5.09E+07	4.85E+05

	5	50	45				
33(5)C	1		70				
	2		70				
	3		70				
	4		70				
	5		70				
	1		70				
	2		70				
	3		70				
	4		70				
	5		70				
33(5)L	1	76	32				
	2	80	30				
	3	79	30				
	4	81	29				
	5	58	41	222	1.65E+04	6.13E+07	5.76E+05
	1	79	31				
	2	75	32				
	3	73	34				
	4	66	37				
	5	63	38	223	1.57E+04	6.12E+07	5.84E+05
35(5)H	1	79	31				
	2	73	34				
	3	69	36				
	4	67	37				
	5	52	44	221	1.47E+04	5.44E+07	5.35E+05
	1	72	34				
	2	65	38				
	3	62	39				
	4	63	39				
	5	46	47	217	1.35E+04	5.05E+07	5.01E+05
35(5)C	1		70				
	2		70				
	3		70				
	4		70				
	5		70				
	1		70				
	2		70				
	3		70				
	4		70				
	5		70				
35(5)L	1	73	33				
	2	66	37				
	3	71	35				
	4	75	33	222	1.51E+04	5.86E+07	5.47E+05

	5	59	41				
	1	74	33				
	2	67	37				
	3	68	36				
	4	74	33				
	5	61	40	224	1.52E+04	6.01E+07	5.57E+05
39(5)H	1	78	31				
	2	69	35				
	3	64	38				
	4	65	38				
	5	38	51	211	1.37E+04	4.81E+07	4.94E+05
	1	76	32				
	2	68	36				
	3	65	37				
	4	64	38				
	5	38	51	214	1.36E+04	4.76E+07	4.86E+05
39(5)C	1		70				
	2		70				
	3		70				
	4		70				
	5		70				
	1		70				
	2		70				
	3		70				
	4		70				
	5		70				
39(5)L	1		70				
	2		70				
	3		70				
	4		70				
	5		70				
	1		70				
	2		70				
	3		70				
	4		70				
	5		70				
44(5)H	1	84	28				
	2	83	29				
	3	82	29				
	4	83	28				
	5	71	34	231	1.80E+04	7.30E+07	6.67E+05
	1	82	29				
	2	82	29				
	3	82	29				
	4	78	31	229	1.77E+04	7.17E+07	6.60E+05

	5	73	33								
44(5)C	1		70								
	2		70								
	3		70								
	4		70								
	5		70								
	1		70								
	2		70								
	3		70								
	4		70								
	5		70								
44(5)L	1	78	31	221	1.56E+04	6.01E+07	5.67E+05				
	2	71	35								
	3	75	33								
	4	73	34								
	5	61	40								
	1	76	32					227	1.58E+04	6.34E+07	5.92E+05
	2	73	33								
	3	73	34								
	4	70	35								
	5	63	38								

15 Appendix 4 – Q-Q plots

In this appendix, the normal Q-Q plots are shown following the sectional analysis detailed in §7.

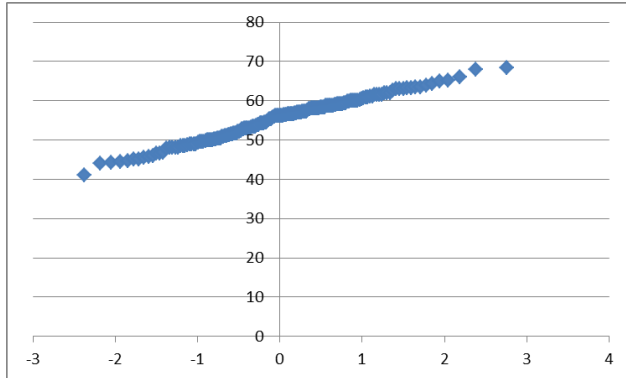


Figure 15.1, Q-Q plot of lamella width from fire test 1

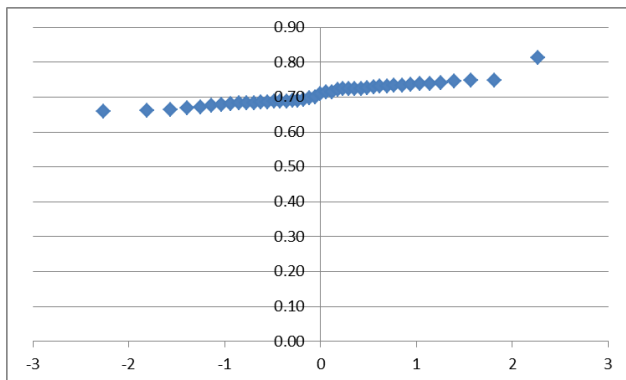


Figure 15.2, Q-Q plot of mean 1-dimensional charring rate over 60 minutes based on lamella width after fire test 1

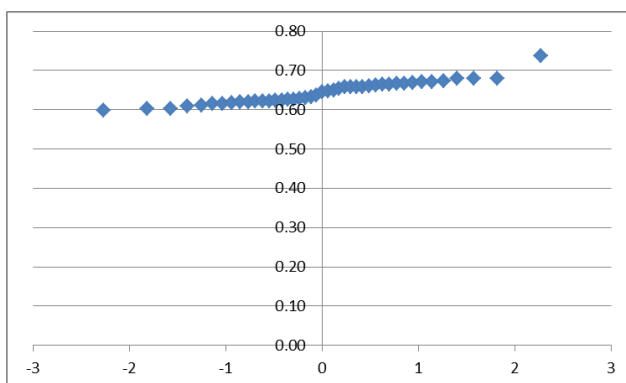


Figure 15.3, Q-Q plot of mean 1-dimensional charring rate over 66 minutes based on lamella width after fire test 1

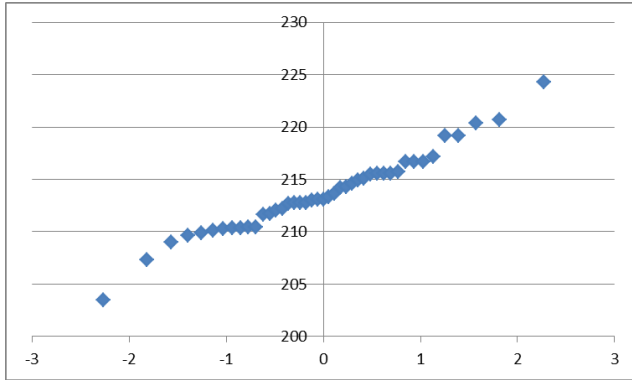


Figure 15.4, Q-Q plot of residual section depth after fire test 1

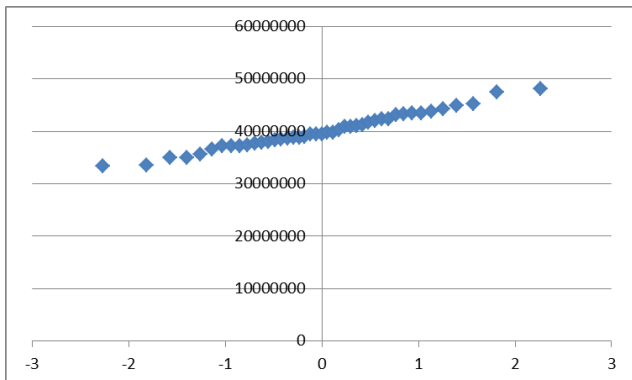


Figure 15.5, Q-Q plot of second moment of area of residual section after fire test 1

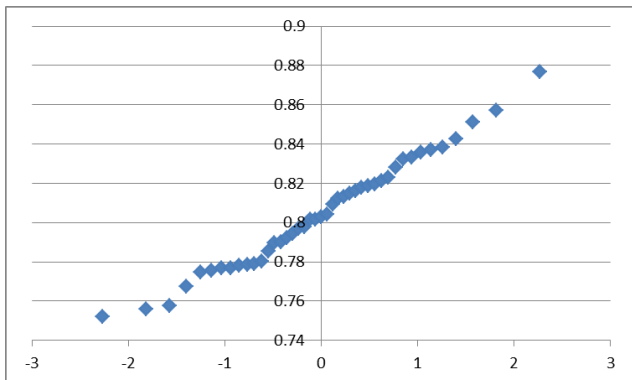


Figure 15.6, Q-Q plot of notional charring rate based on residual section after 60 minutes following fire test 1

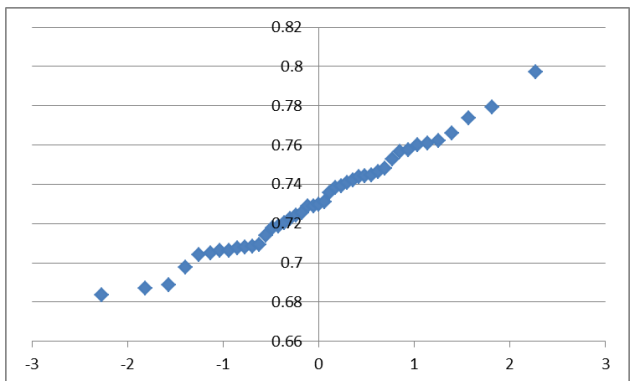


Figure 15.7, Q-Q plot of notional charring rate based on residual section after 66 minutes following fire test 1

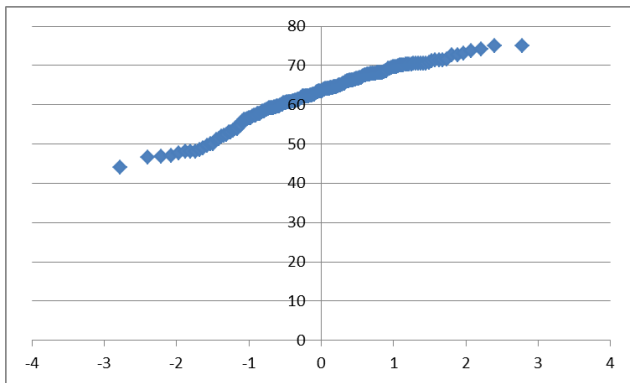


Figure 15.8, Q-Q plot of lamella width from fire test 2

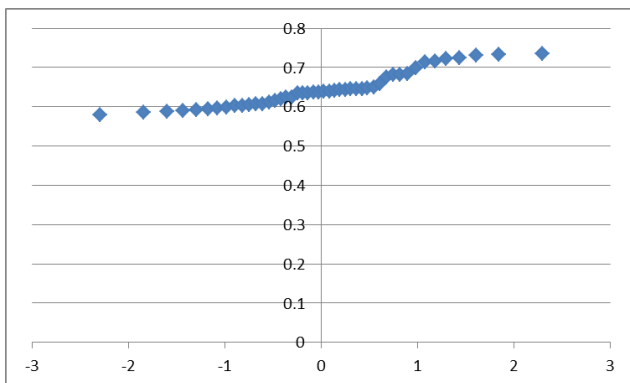


Figure 15.9, Q-Q plot of mean 1-dimensional charring rate over 60 minutes based on lamella width after fire test 2

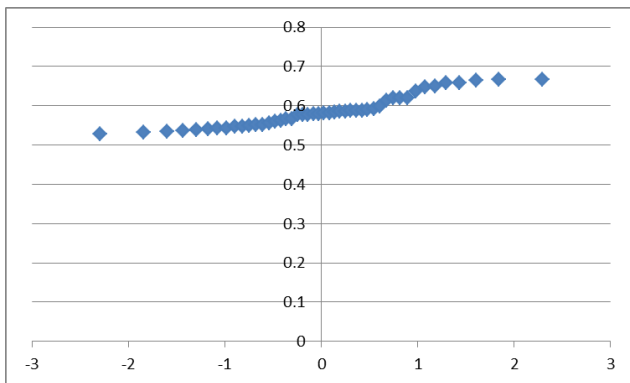


Figure 15.10, Q-Q plot of mean 1-dimensional charring rate over 66 minutes based on lamella width after fire test 2

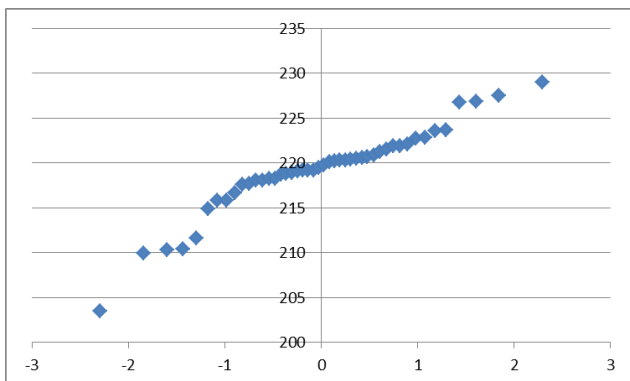


Figure 15.11, Q-Q plot of residual section depth after fire test 2

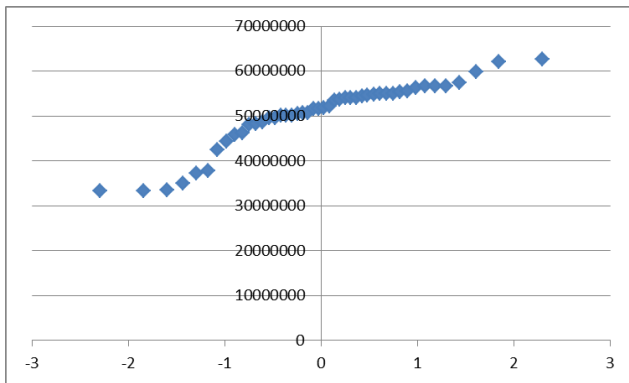


Figure 15.12, Q-Q plot of second moment of area of residual section after fire test 2

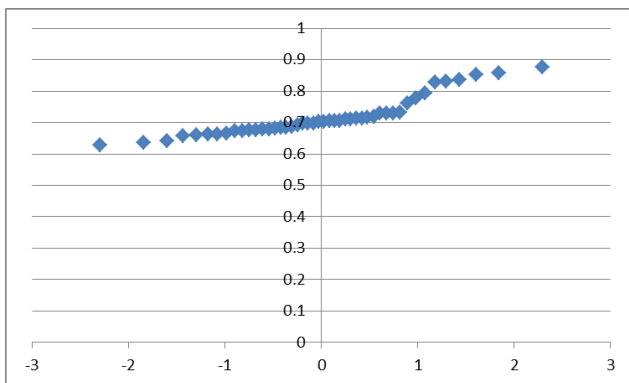


Figure 15.13, Q-Q plot of notional charring rate based on residual section after 60 minutes following fire test 2

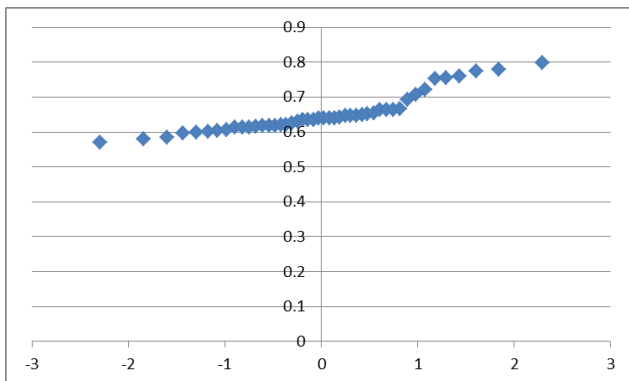


Figure 15.14, Q-Q plot of notional charring rate based on residual section after 66 minutes following fire test 2

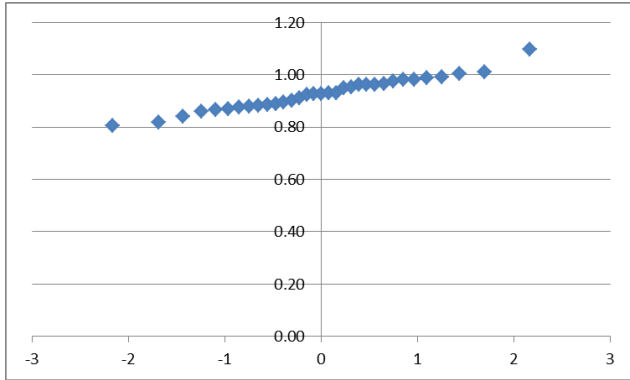


Figure 15.15, Q-Q plot of lamella width from fire test 3

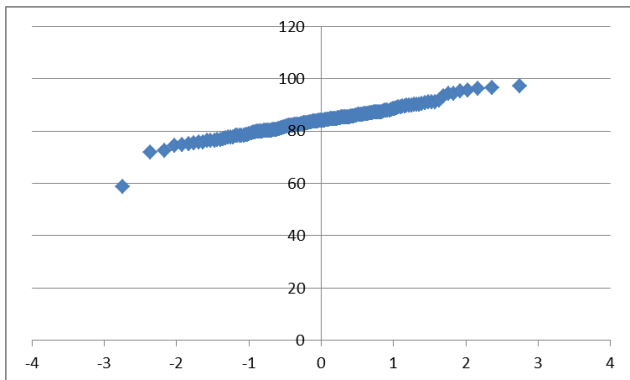


Figure 15.16, Q-Q plot of mean 1-dimensional charring rate over 30 minutes based on lamella width after fire test 3

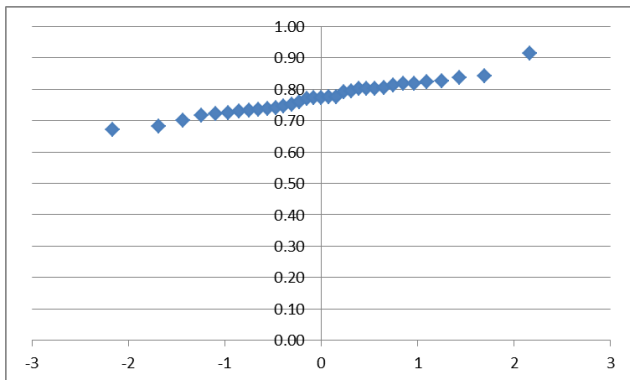


Figure 15.17, Q-Q plot of mean 1-dimensional charring rate over 36 minutes based on lamella width after fire test 3

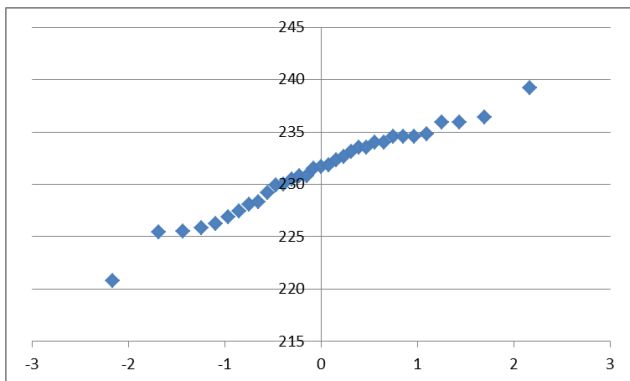


Figure 15.18, Q-Q plot of residual section depth after fire test 3

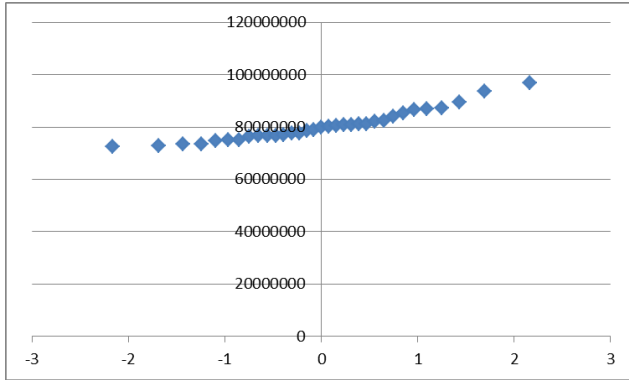


Figure 15.19, Q-Q plot of second moment of area of residual section after fire test 3

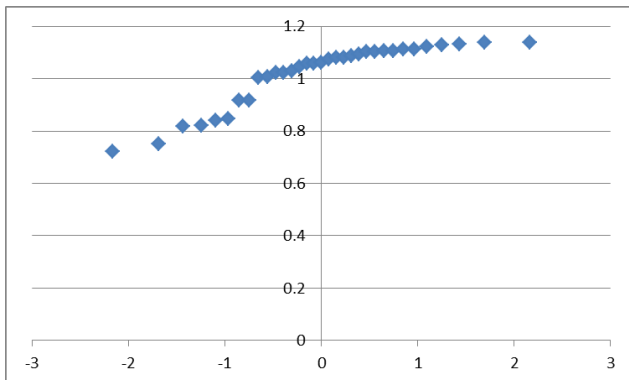


Figure 15.20, Q-Q plot of notional charring rate based on residual section after 30 minutes following fire test 3

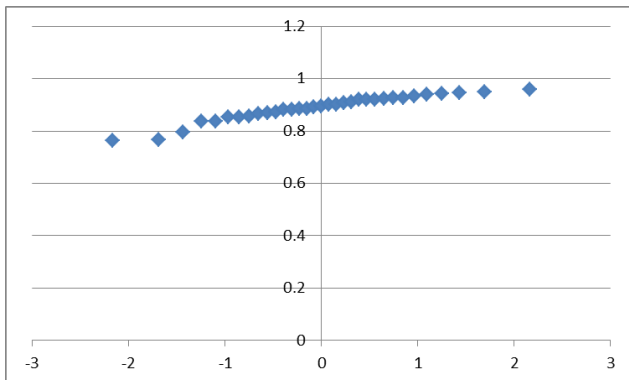


Figure 15.21, Q-Q plot of notional charring rate based on residual section after 36 minutes following fire test 3

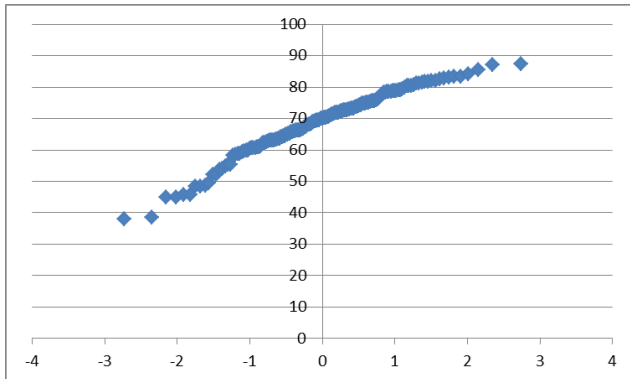


Figure 15.22, Q-Q plot of lamella width from fire test 4

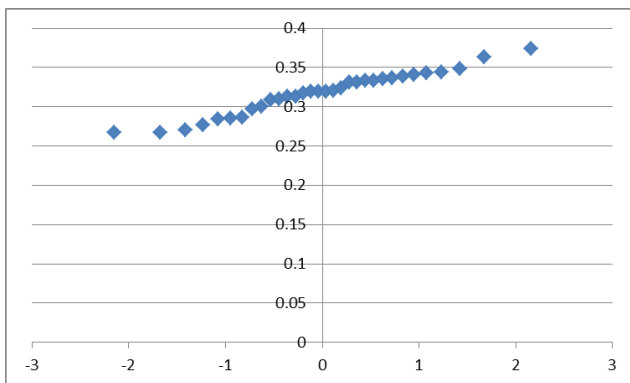


Figure 15.23, Q-Q plot of mean 1-dimensional charring rate over 107 minutes based on lamella width after fire test 4

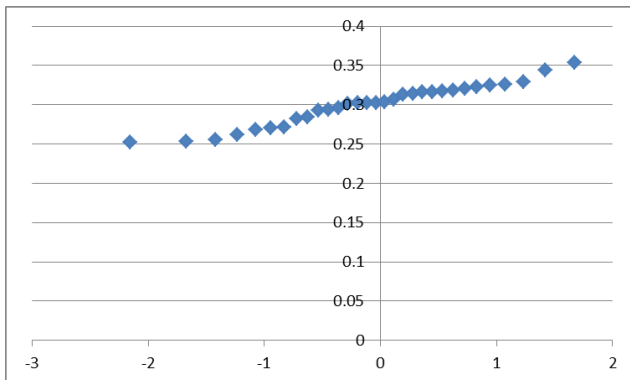


Figure 15.24, Q-Q plot of mean 1-dimensional charring rate over 113 minutes based on lamella width after fire test 4

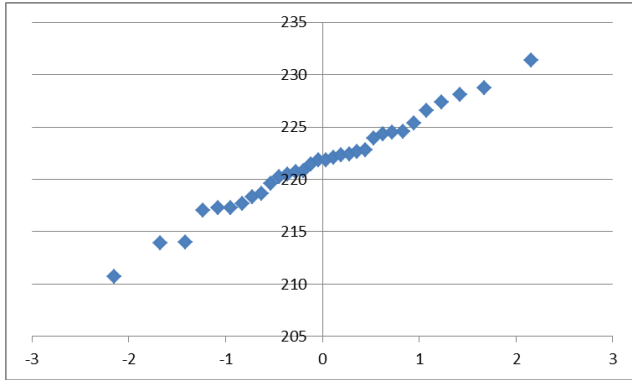


Figure 15.26, Q-Q plot of residual section depth after fire test 4

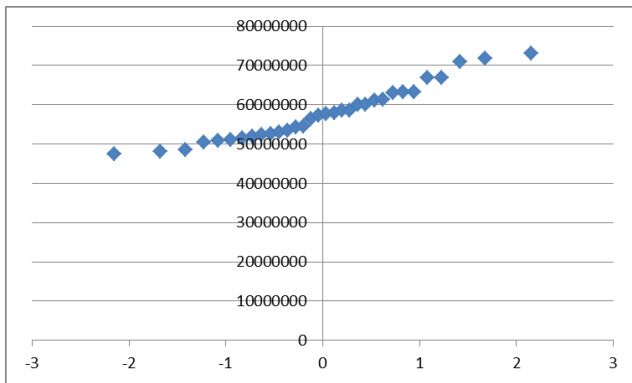


Figure 15.27, Q-Q plot of second moment of area of residual section after fire test 4

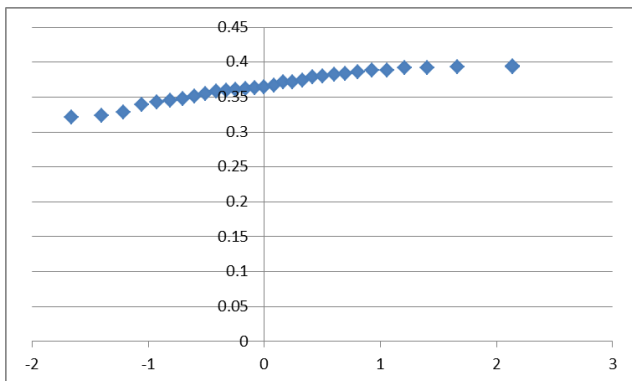


Figure 15.28, Q-Q plot of notional charring rate based on residual section after 107 minutes following fire test 4

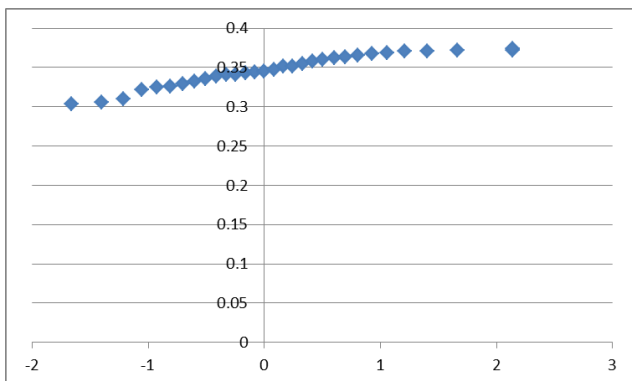
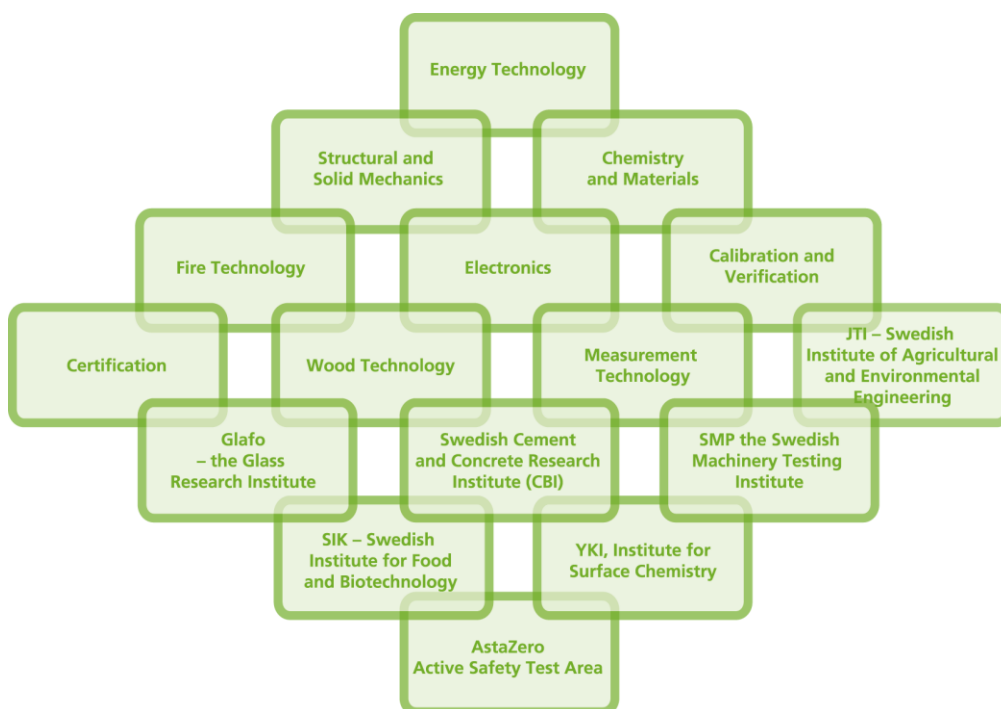


Figure 15.29, Q-Q plot of notional charring rate based on residual section after 113 minutes following fire test 4

SP Technical Research Institute of Sweden

Our work is concentrated on innovation and the development of value-adding technology. Using Sweden's most extensive and advanced resources for technical evaluation, measurement technology, research and development, we make an important contribution to the competitiveness and sustainable development of industry. Research is carried out in close conjunction with universities and institutes of technology, to the benefit of a customer base of about 10000 organisations, ranging from start-up companies developing new technologies or new ideas to international groups.



SP Technical Research Institute of Sweden

Box 857, SE-501 15 BORÅS, SWEDEN

Telephone: +46 10 516 50 00, Telefax: +46 33 13 55 02

E-mail: info@sp.se, Internet: www.sp.se

www.sp.se

Fire Technology

SP Report 2014:35

ISBN 978-91-87461-78-1

ISSN 0284-5172

More information about publications published by SP: www.sp.se/publ